

A NOVEL ALGORITHM FOR PREDICTION OFF-LINE STATOR LEAKAGE
INDUCTANCE AND ON-LINE STATOR RESISTANCE OF INDUCTION
MOTORS

A THESIS SUBMITTED TO
THE GRADUATE SCHOOL OF NATURAL AND APPLIED SCIENCES
OF
MIDDLE EAST TECHNICAL UNIVERSITY

BY

VOLKAN SEZGİN

IN PARTIAL FULFILMENT OF THE REQUIREMENTS
FOR
THE DEGREE OF MASTER OF SCIENCE
IN
ELECTRICAL AND ELECTRONICS ENGINEERING

JANUARY 2009

Approval of the thesis

**A NOVEL ALGORITHM FOR PREDICTION OFF-LINE STATOR
LEAKAGE INDUCTANCE AND ON-LINE STATOR RESISTANCE OF
INDUCTION MOTORS**

Submitted by **VOLKAN SEZGİN** in partial fulfillment of the requirements for
the degree of **Master of Science in Electrical and Electronics Engineering,**
Middle East Technical University by,

Prof. Dr. Canan ÖZGEN
Dean, Graduate School of **Natural and Applied Sciences** _____

Prof. Dr. İsmet ERKMEN
Head of Department, **Electrical and Electronics Engineering** _____

Prof. Dr. H. Bülent ERTAN
Supervisor, **Electrical and Electronics Engineering, METU** _____

Examining Committee Members:

Prof. Dr. Muammer ERMİŞ
Electrical and Electronics Engineering, METU _____

Prof. Dr. H. Bülent ERTAN
Electrical and Electronics Engineering, METU _____

Prof. Dr. Kemal LEBLEBİCİOĞLU
Electrical and Electronics Engineering, METU _____

Assist. Prof. Dr. M. Timur AYDEMİR
Electrical and Electronics Engineering, Gazi University _____

Dr. Erbil NALÇACI
EPDK (Retired) _____

Date: 02.01.2009

I hereby declare that all information in this document has been obtained and presented in accordance with academic rules and ethical conduct. I also declare that, as required by these rules and conduct, I have fully cited and referenced all material and results that are not original to this work.

Name, Last name: Volkan Sezgin

Signature :

ABSTRACT

A NOVEL ALGORITHM FOR PREDICTION OFF-LINE STATOR LEAKAGE INDUCTANCE AND ON-LINE STATOR RESISTANCE OF INDUCTION MOTORS

SEZGİN, Volkan

M.Sc., Department of Electrical and Electronics Engineering

Supervisor: Prof. Dr. H. Bülent ERTAN

January 2009, 162 pages

In vector control of induction motors it is essential to know the parameters of the motor. Known approaches to this problem have some drawbacks. This thesis work is planned to develop solutions to the existing problems. The proposed solutions will be implemented and tested.

Keywords: Field oriented control, parameter estimation, induction motor drive.

ÖZ

ENDÜKSİYON MOTORLARINDA ÇEVİRİMDİŐİ OLARAK STATOR KAÇAK ENDÜKTANSININ VE ÇEVİRİMİÇİ OLARAK STATOR DİRENCİNİN TAHMİN EDİLMESİ İÇİN YENİ BİR YÖNTEM

SEZGİN, Volkan

Yüksek Lisans, Elektrik Elektronik MühendisliĐi Bölümü

Tez Danışmanı: Prof. Dr. H. Bülent ERTAN

Ocak 2009, 162 sayfa

Endüksiyon motorlarının vektör kontrol yöntemi ile sürülmesinde, motor parametrelerini bilmek zorunludur. Bu problemi çözmek için üretilen bilinen yaklaşımların bazı sakıncaları vardır. Bu tez çalışmasında, bu varolan sorunlara çözümler geliştirilmesi planlanmaktadır. Öngörülen çözümler uygulanacak ve test edilecektir.

Anahtar Kelimeler: Alan yönlendirmeli kontrol, parametre tahmini, asenkron motor sürücü

To my Family

ACKNOWLEDGEMENTS

I would like to express my sincere gratitude to Prof. Dr. H. Bülent ERTAN for his guidance, patient supervision and support that made this study possible.

I would like to thank Ozan KEYSAN, Akın ACAR, Ahmet C. DURGUN for their precious suggestions, encouragement and willingness for help in all phases of this study.

I would like to thank my family and fiancée S. Pınar Aydın for their continuous support, confidence and reassurance.

TABLE OF CONTENTS

ABSTRACT.....	iv
ÖZ	v
ACKNOWLEDGEMENTS.....	vii
TABLE OF CONTENTS.....	viii
LIST OF TABLES.....	xi
LIST OF FIGURES	xii
LIST OF SYMBOLS	xv
CHAPTERS	
1 INTRODUCTION	1
1.1. Introduction.....	1
2 HARDWARE & SOFTWARE ENVIRONMENT	3
2.1. Introduction.....	3
2.2. Principles of Vector Control Theory	3
2.2.1. Sensorless Vector Control of Induction Machines	5
2.3. Hardware.....	11
2.3.1. Pulse Processing Stage.....	13
2.3.1.1. XOR Gate	16
2.3.1.2. Dead Time Generator.....	17
2.3.2. Isolation Module and IPM Stage	19
2.3.2.1. Power Supply of the Isolation Module and IPM Stage	22
2.3.2.2. Input Signals of the IPM Stage	23
2.3.2.3. Fault Signals of the IPM Stage	24
2.3.3. Power Stage	25
2.3.4. Measurement Stage.....	27

2.4.	Software Environment	30
2.4.1.	Flowchart of the Software.....	31
2.4.1.1.	Variable Definitions, Initializations Module	33
2.4.1.2.	Motor Parameters Module	34
2.4.1.3.	Obtaining Rated Flux Module [4].....	35
2.4.1.4.	Voltage and Current Measurements Module	36
2.4.1.5.	Dynamic Braking Initialization Module	37
2.4.1.6.	ab to dq Transformations Module.....	37
2.4.1.7.	PI Controller Module	40
2.4.1.8.	d-q to α - β Transformation Module	41
2.4.1.9.	Space Vector Pulse Width Modulation (SVPWM) Module	41
2.4.1.10.	Pulse Skipping Module	46
2.4.1.11.	Sending PWM Signals Module.....	46
2.4.1.12.	Flux and Speed Estimations Module	47
2.4.1.13.	DC Link Compensation Module.....	51
2.4.1.14.	Dynamic Braking Module	59
2.5.	Conclusion	67
3	OFF LINE PREDICTION OF LEAKAGE INDUCTANCE	68
3.1.	Introduction.....	68
3.2.	Theory of Off-Line Prediction of Leakage Inductance.....	69
3.3.	Experimental Results of Off – Line Prediction of Leakage Inductance	73
3.3.1.	Off Line Leakage Inductance Measurement for Test Motor #1	79
3.3.2.	Off Line Leakage Inductance Measurement for Test Motor #2	82
3.3.3.	Off Line Leakage Inductance Measurement for Test Motor #3	84
3.4.	Conclusion	86
4	ON-LINE STATOR RESISTANCE ESTIMATION METHOD	88
4.1.	Introduction.....	88
4.2.	The Field Orientation Control Method	89
4.3.	Online Stator Resistance Estimation Method	93
4.4.	Experimental Results where Sinusoidal Source is used	95

4.4.1. R_s Estimation at 50 Hz Supply Voltage.....	96
4.4.2. R_s Estimation at 30 Hz Supply Voltage.....	100
4.5. Experimental Results with a PWM Drive.....	107
4.5.1. R_s Estimation at 30 Hz, with a PWM Drive	109
4.5.2. R_s Estimation at 10 Hz with a PWM Drive	114
4.5.3. R_s Estimation at 10 Hz with 2 nd Test Motor	119
4.5.4. R_s Estimation at 10 Hz with 3 rd Test Motor.....	123
4.6. Stator Resistance Variation with Temperature under Load.....	127
4.7. Conclusion	131
5 CONCLUSION.....	133
5.1. General.....	133
5.2. Future Work.....	134
REFERENCES	136
APPENDICES	
A Calculation of PI Controller Parameters	140
B DATASHEET of IPM.....	149
C PARAMETERS OF TEST MOTORS	159
C.1. Parameters of Test Motor #1	159
C.2. Parameters of Test Motor #2	160
C.3. Parameters of Test Motor #3	161

LIST OF TABLES

Table 2. 1 – Truth table of XOR	16
Table 3. 1 - The Test Motor Data	69
Table 3. 2 – Parameters used in the estimation of 1 st machine’s leakage Inductance	80
Table 3. 3 - Parameters used in the estimation of 2 nd machine’s leakage Inductance	83
Table 3. 4 - Parameters used in the estimation of 3 rd machine’s leakage Inductance	85
Table 3. 5 – Comparison of Conventional and Proposed Leakage Inductance Measurement Results	86
Table 4. 1 - Stator resistance estimation results at the specified interval given at figure 4.5	98
Table 4. 2 - Stator resistance estimation results after compensating the errors in ψ_{sa} calculation	100
Table 4. 3 – Stator resistance estimation results related with figure 4.9	103
Table 4. 4 - Stator resistance estimation results wrt corrected ψ_{sa}	104
Table 4. 5 - Stator resistance estimation results related with figure 4.11	106
Table 4. 6 - Stator resistance estimation results wrt corrected ψ_{sa}	107
Table 4. 7 - Parameters of 1 st motor used in the on- line R_s estimation.....	109
Table 4. 8 – Stator resistance estimation results at the specified interval given at figure 4.15	112
Table 4. 9 – Updated version of table 4.7 after compensating the errors in calculating the ψ_{sa}	112
Table 4. 10 - Stator resistance estimation results at the specified interval given at figure 4.14	113
Table 4. 11 - Stator resistance estimation results at 10 Hz, experiment is done with PWM drive.....	116
Table 4. 12 – Another stator resistance estimation results at 10 Hz, experiment is done with driver	118
Table 4. 13 - Parameters of 2 nd motor used in the on- line R_s estimation.....	119
Table 4. 14 - Parameters of 3 rd motor used in the on- line R_s estimation	123
Table 4. 15 – Measured and Estimated R_s and temperature, while the motor is running under load	128

LIST OF FIGURES

FIGURES

Figure 2. 1 – Schematic diagram of separately excited dc-machine with currents orientation	4
Figure 2. 2 – Vector-controlled induction machine	5
Figure 2. 3 – abc and α - β stationary reference frame vector diagram	7
Figure 2. 4 – Stationary (α - β) and rotating (d-q) reference frames	9
Figure 2. 5 – Sensorless vector control of induction motor scheme	11
Figure 2. 6- Block Diagram of the hardware used in this thesis	12
Figure 2. 7 – PWM Signals with inverter IGBTs and Braking IGBT	13
Figure 2. 8 – Required and produced pulses to obtain the reference voltage given as an example	14
Figure 2. 9 – Block diagram of pulse processing stage	15
Figure 2. 10 – XOR gate with inputs, X1 and X2	16
Figure 2. 11 – Block diagram of Dead time generator	18
Figure 2. 12 – Isolation stage of the Hardware	19
Figure 2. 13 – Circuitry of opto-coupler in the isolation module	20
Figure 2. 14 – Application example of Mitsubishi IPM	21
Figure 2. 15 –Block diagram of the 4-output 15V DC Power Supply for Isolation Board.....	22
Figure 2. 16 – Functional Diagram of the IPM.....	24
Figure 2. 17 – Fault Signals Isolation Schematics.....	25
Figure 2. 18 – Power Stage of the Driver	26
Figure 2. 19 – Typical dc-link voltage supplied from 3-phase 380 V grid source.	27
Figure 2. 20 – Measurement block diagram of the driver	28
Figure 2. 21 – Detailed measurement circuitry for one signal.....	29
Figure 2. 22 – Circuit diagram of low-pass filter	29
Figure 2. 23 – Magnitude and Phase response of Low-Pass filter used in the measurements.....	30
Figure 2. 24 – Flowchart of the vector control software	32
Figure 2. 25 – Module to drive the motor until its rated flux	36
Figure 2. 26 – Projection of stator current vector to α - β coordinate system	37
Figure 2. 27 – Projection of stator current vector from a-b coordinate system to d-q coordinate system	38
Figure 2. 28 – Block diagram of the PI controllers used for obtaining reference d-q voltages	40
Figure 2. 29 - Representation of the sectors in the stationary reference frame	42
Figure 2. 30 – Switching times if the reference voltage is in sector 1.....	44
Figure 2. 31 – Flowchart of the module used for calculating the duty cycles	44
Figure 2. 32 – Calculation of duty cycles for sector 1.....	45
Figure 2. 33 – Calculation of duty cycles	45
Figure 2. 34 – Module used to send PWM signals	47

Figure 2. 35 – Block diagram of digital Filter	48
Figure 2. 36 – Schematic representation of integrator	49
Figure 2. 37 – Block diagram of two cascade filters as an integrator.....	50
Figure 2. 38 – Experimental setup to observe the dc-link compensation	52
Figure 2. 39 – DC-link voltage measurement diagram.....	53
Figure 2. 40 – DC-link voltage, modulation constant K and Torque variations when the K is taken constant.	54
Figure 2. 41 - DC –link voltage, phase A and B voltages and currents and torque waveforms during the modulation constant is taken as a constant value.	56
Figure 2. 42 – DC-link voltage, K modulation constant and Torque variations with updated K value.	57
Figure 2. 43 – DC –link voltage, phase A and B voltages and currents and torque waveforms during the modulation constant is updated	58
Figure 2. 44 – DC-link voltage variations while dynamic braking module is deactivated.	60
Figure 2. 45 – Theoretical DC-link voltage variations during the dynamic braking module is working with hysteresis band; 580 V-600 V.....	61
Figure 2. 46 – Schematic diagram of Inverter with Braking IGBT	63
Figure 2. 47 – Recorded dc-link voltage during the dynamic braking module is active.....	63
Figure 2. 48 – Current waveform on the dynamic braking resistance.....	64
Figure 3. 1 – Equivalent Circuit of Induction Machine	70
Figure 3. 2 – Rotor flux change during the sub-transient period.	72
Figure 3. 3 – Experimental Setup to estimate the off line leakage inductance.....	74
Figure 3. 4 – Inverter connected to the induction machine	75
Figure 3. 5 – Equivalent circuit of induction machine when lower side IGBTs are shorted.....	76
Figure 3. 6 – Low-pass filter used to clear noises on the measurements.....	77
Figure 3. 7 – Setup used in the Simulink to simulate the transfer function characteristic	78
Figure 3. 8 – Step response of low-pass filter used in the measurements	79
Figure 3. 9 – Measured data for Leakage Inductance Prediction for test motor #1.	80
Figure 3. 10 – Estimated leakage inductance in the measurement period for the test motor # 1.	81
Figure 3. 11 - Measured data for Leakage Inductance Prediction for test motor #2.	82
Figure 3. 12 - Estimated leakage inductance in the measurement period for the test motor # 2.....	83
Figure 3. 13 - Measured data for Leakage Inductance Prediction for test motor #3.	84
Figure 3. 14 - Estimated leakage inductance in the measurement period for the test motor # 3.....	85
Figure 4. 1- Vector Diagram for Field Orientation of Induction Motor	90

Figure 4. 2- Field Oriented Control (FOC) Scheme for the Motor Drive under Test	92
Figure 4. 3 – Experimental setup used for R_s estimation using 3-phase sinusoidal source.....	96
Figure 4. 4 – The variables used in the estimation of R_s at 50 Hz.....	97
Figure 4. 5 – Stator resistance estimation at zero cross of $\psi_{s\alpha}$ at 50 Hz	98
Figure 4. 6 – Stator resistance estimation after compensating the errors in $\psi_{s\alpha}$ calculation.....	99
Figure 4. 7 - Measured Variables; V_{sac} , V_{sbc} , I_{sa} , I_{sb} and transformed variables $V_{s\alpha}$, $V_{s\beta}$, $I_{s\alpha}$, $I_{s\beta}$, $\psi_{s\alpha}$, $\psi_{s\beta}$ at 30 Hz.....	101
Figure 4. 8 – Variables that are used in the R_s estimation at 30 Hz.....	102
Figure 4. 9 - Stator resistance estimation at zero cross of $\psi_{s\alpha}$ at 30 Hz.....	103
Figure 4. 10 - Stator resistance estimation where the $\psi_{s\alpha}$ is corrected at 30 Hz.	104
Figure 4. 11 – Stator resistance estimation at another zero cross instant of $\psi_{s\alpha}$ at 30 Hz.....	105
Figure 4. 12 - Stator resistance estimation where the $\psi_{s\alpha}$ is corrected at 30 Hz for another zero cross instant of $\psi_{s\alpha}$	106
Figure 4. 13 – Experimental setup of stator resistance estimation with driver... ..	108
Figure 4. 14 - Variables that are used in the R_s estimation at 30 Hz with driver.....	110
Figure 4. 15 - Stator resistance estimation at zero cross of $\psi_{s\alpha}$ at 30 Hz with driver.....	111
Figure 4. 16 - Stator resistance estimation at another zero cross of $\psi_{s\alpha}$ at 30 Hz with driver.....	113
Figure 4. 17 - Variables that are used in the R_s estimation at 10 Hz with PWM drive.....	115
Figure 4. 18 - Stator resistance estimation at zero cross of $\psi_{s\alpha}$ at 10 Hz with PWM drive.....	116
Figure 4. 19 – Another stator resistance estimation interval at 10 Hz with driver.....	117
Figure 4. 20 – Variables of 2 nd machine which will be used to estimate the R_s at 10 Hz.....	120
Figure 4. 21 – Stator resistance estimation at zero cross of $\psi_{s\alpha}$ at 10 Hz with PWM drive, for 2 nd machine.....	121
Figure 4. 22 – Another interval for 2 nd machine to estimate the R_s at 10 Hz.....	122
Figure 4. 23 - Variables of 3 rd machine which will be used to estimate the R_s at 10 Hz.....	124
Figure 4. 24 - Stator resistance estimation at zero cross of $\psi_{s\alpha}$ at 10 Hz with driver, for 3 rd machine.....	125
Figure 4. 25 – Another interval to estimate the stator resistance for 3 rd machine at 10 Hz.....	126
Figure 4. 26 – Experimental setup used to observe stator resistance change under load.....	128
Figure 4. 27 – Measured and estimated R_s variation while motor is running under load.....	129

LIST OF SYMBOLS

i_{sa}	: Stator a phase current
i_{sb}	: Stator b phase current
i_{sc}	: Stator c phase current
i_{sd}	: d component of stator current
i_{sq}	: q component of stator current
i_{rd}	: d component of rotor current
i_{rq}	: q component of rotor current
$I_{s\alpha}$: α component of stator current
$I_{s\beta}$: β component of stator current
\vec{I}_s	: Stator current space phasor
$\vec{\Psi}_r$: Rotor flux space phasor
i_{sdref}	: reference value of d axis stator current
i_{sqref}	: reference value of q axis stator current
V_{sdref}	: reference value of d axis stator voltage
V_{sqref}	: reference value of q axis stator voltage
P_{core}	: Core loss power
R_{eq}	: Equivalent resistance
f	: Frequency
L_r	: Rotor self inductance
L_s	: Stator self inductance
L_{ls}	: Stator leakage inductance
L_{lr}	: Rotor leakage inductance
L_s'	: Stator transient inductance
R_s	: Stator winding resistance
R_r'	: Referred rotor resistance
L_m	: Mutual inductance

\vec{i}_{mr}	: Rotor magnetizing current space phasor in the rotor flux oriented reference frame
$\Psi_{s\alpha}$: α component of the stator flux
$\Psi_{s\beta}$: β component of the stator flux
$\Psi_{r\alpha}$: α component of the rotor flux
$\Psi_{r\beta}$: β component of the rotor flux
σ	: Leakage factor
$V_{s\alpha}$: α component of the stator voltage
$V_{s\beta}$: β component of the stator voltage
T_e	: Motor torque
ω_e	: Angular synchronous speed
τ	: Digital filter time constant
τ_s'	: stator time
G	: Gain block
V_{ref}	: Magnitude of the reference voltage
UP	: U phase upper IGBT switching signal
VP	: V phase upper IGBT switching signal
WP	: W phase upper IGBT switching signal
UN	: U phase lower IGBT switching signal
VN	: V phase lower IGBT switching signal
WN	: W phase lower IGBT switching signal
B	: Braking IGBT switching signal
θ	: Angle of rotor flux space phasor with respect to α axis
P	: Number of pole pairs
I_{so}	: Initial value of stator phase current in leakage inductance measurement
k_p	: Proportional coefficient of PI controller
k_i	: Integral coefficient of PI controller
V_m	: Motor back emf

Ψ_{\min} : Minimum value of rotor flux magnitude
 Ψ_{\max} : Maximum value of rotor flux magnitude
 Ψ_{mean} : Mean value of rotor flux magnitude
 Ψ_{ref} : Reference value of rotor flux magnitude

CHAPTER 1

INTRODUCTION

1.1. Introduction

It is very important that to know motor parameters accurately in vector control drives. There are many studies about parameter estimation of induction machines in literature. However, most of them have some problems or disadvantages. Those parameter estimation techniques in literature are explained in Chapter 4 of this thesis.

In this thesis work, a novel off-line leakage inductance and on-line stator resistance estimation methods of induction machines are developed and some experiments are performed to verify the accuracy of the proposed estimation methods. To carry out the experiments, a previous sensorless vector control drive is first improved; dynamic braking and dc-link compensation modules are added.

In chapter 2, hardware and software environment of the vector control drive will be explained in detail. In hardware, there are some stages named; pulse processing stage, isolation module and intelligent power module (IPM) stage, power stage and measurement stages will be explained with their block diagrams. Software of the vector control drive is written in C-programming language and it is developed in modular form. All those modules will be explained in detail in chapter 2.

In chapter 3, off-line leakage inductance estimation technique will be introduced. Theory behind the proposed method will be given and experimental results to verify the off-line leakage inductance estimation method will be presented.

In sensorless vector control drives knowing the stator resistance value accurately directly affects the performance of the drive. In chapter 4, a novel approach about on-line stator resistance estimation of induction machines in vector control drive is introduced. The theory behind the proposed method and the related literature will be explained in this chapter. Some experiments performed to support the online stator resistance estimation method proposed in this thesis work are also given in this chapter. In the last part of this chapter, it is shown that test motor's temperature may be accurately predicted by using the estimated stator resistance values.

Finally, chapter 5 presents conclusions of this thesis work.

CHAPTER 2

HARDWARE & SOFTWARE ENVIRONMENT

2.1. Introduction

In this thesis work a motor drive hardware which already existed is improved and redesigned. The new hardware is implemented and tested and used in thesis work. This hardware along with a DSP card is used to drive a given induction motor in scalar control (V/f) mode or vector control mode.

Firstly, a brief explanation about vector control theory will be given. This will be followed by explanation of hardware improvements and the drive software.

2.2. Principles of Vector Control Theory

Vector control method of AC machines is very important invention about performance of motor drives. The main principle of vector control method is to control the ac motors like a separately excited dc motors. In a dc machine, neglecting the armature reaction effect and the field saturation, the developed torque is given by,

$$T_e = K_t' \cdot I_a \cdot I_f \quad (2.1)$$

where I_a is armature current and I_f is a field current. The construction of a dc machine is such that the field flux ψ_f produced by field current I_f is orthogonal to

the armature flux ψ_a produced by armature current I_a . The schematic diagram of a separately excited dc-machine and current orientation are given in Figure 2. 1.

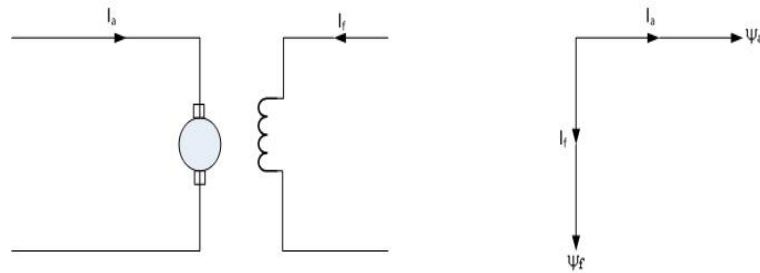


Figure 2. 1 – Schematic diagram of separately excited dc-machine with currents orientation

These I_f and I_a current vectors are orthogonal or decoupled in nature. As a result of that orthogonality, the torque is controlled by controlling the I_a , and it doesn't affect the field flux. On the other hand, field flux is directly depends on field current and changing the field current doesn't change the armature current. Because of decoupling of these currents in dc-machines torque can be controlled by controlling the armature current where the field flux is set to desired level by adjusting the field current. The operation of these two currents has no affect on each other since they are spatial in space. The aim in vector control is to control ac machines' torque and flux variables independently.

DC machine-like performance can also be adapted to an induction machine if the motor control is considered in a synchronously rotating frame, where the sinusoidal variables appear as dc quantities in steady state. In Figure 2. 2, the induction machine with vector controlled inverter is shown with two control current inputs, i_{ds}^* , i_{qs}^* . These currents are the direct axis component and quadrature axis component of stator current, respectively, in a synchronously rotating reference frame.

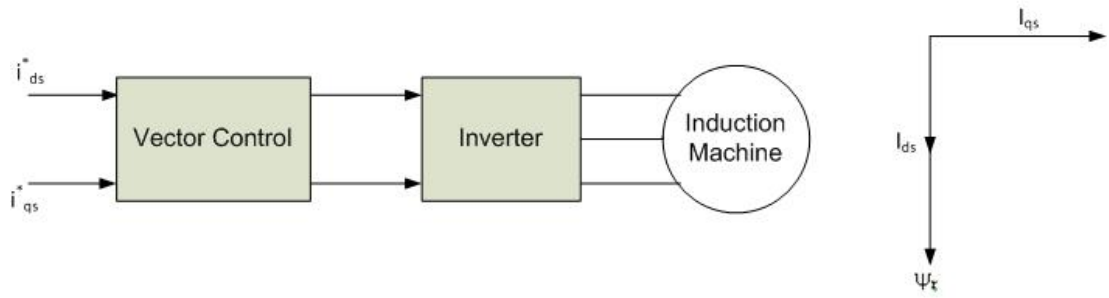


Figure 2. 2 – Vector-controlled induction machine

In vector control of induction machines, i_{ds} is analogous to field current I_f and i_{qs} is analogous to armature current I_a of a dc-machine. Therefore, the torque can be expressed as;

$$T_e = K_t' \cdot i_{ds} \cdot i_{qs} \quad (2.2)$$

That dc machine –like performance is only possible if i_{ds} is oriented in the direction of rotor flux ψ_r and i_{qs} is established orthogonal to it, as shown in Figure 2. 2. This means that when i_{qs}^* is controlled, it affects the actual i_{qs} current only, but does not affect the flux ψ_r . Similarly, when i_{ds}^* is controlled, it controls the rotor flux only and does not affect the i_{qs} component of stator current. Decoupling of currents like that is essential under all operating conditions in a vector-controlled drive.

2.2.1. Sensorless Vector Control of Induction Machines

In this thesis work sensorless operation of vector control of induction machines is implemented. Sensorless vector control of an induction motor drive means vector control without any speed sensors. Speed or position encoder is required for close speed or position control in both vector and scalar controlled drives. However, a speed encoder is not desired in a drive since it increases the cost and negatively

affects the reliability of the drive. It is possible to estimate the speed of the machine by using motor terminal voltages and currents with the help of a DSP microcontroller. However, this speed estimation directly depends on the motor parameters. As mentioned before, in this study novel estimation algorithms are developed for some motor parameters like stator leakage inductance and stator resistance which are very important parameters in sensorless vector control of induction machines.

Speed Estimation Methods:

The induction motor speed estimation techniques proposed in the literature can generally be classified as follows [1]:

- Slip calculation
- Direct synthesis from state equations
- Model referencing adaptive system (MRAS)
- Speed adaptive flux observer (Luenberger observer)
- Extended Kalman Filter (EKF)
- Slot harmonics
- Injection of auxiliary signal on salient rotor

Detailed descriptions of all these methods [25] are beyond the scope of this thesis work. Here slip calculation which is used in this thesis will be explained.

Slip Calculation:

Rotor speed can be calculated from the slip frequency w_{sl} by using the relation $w_r = w_s - w_{sl}$, where w_s is stator frequency and w_r is frequency or speed of rotor in rad/sec.

Before proceeding the calculation of speed, how the sensorless vector control is achieved in this thesis will be explained. We have two induction motor stator terminal voltages and currents named respectively; V_{sac} , V_{sbc} , i_{sa} and i_{sb} . Firstly, the current in the a-axis is aligned with the α -axis of the stationary reference frame (α - β).

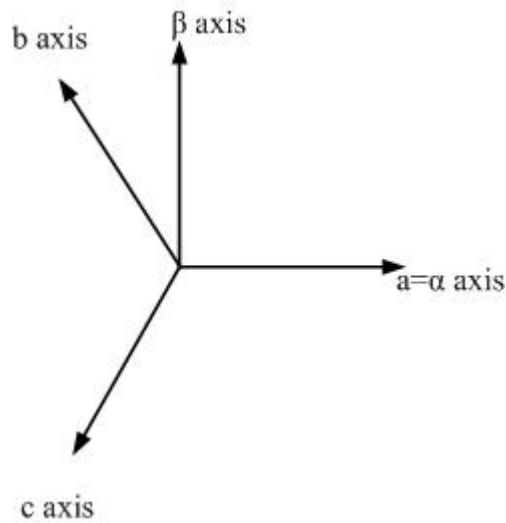


Figure 2. 3 – abc and α - β stationary reference frame vector diagram

Transformations from measured variables to desired quantities are made by the light of Clarke and Park transformations [1].

If the measured variables are phase measurements transformations will be like follow:

$$I_{s\alpha} = \frac{2}{3}i_{sa} - \frac{1}{3}i_{sb} - \frac{1}{3}i_{sc} = i_{sa} \quad (2.3)$$

where $i_{sc} = -(i_{sa} + i_{sb})$

$$I_{s\beta} = \frac{1}{\sqrt{3}}i_{sb} - \frac{1}{\sqrt{3}}i_{sb} = \frac{1}{\sqrt{3}}(i_{sa} + 2i_{sb}) \quad (2.4)$$

On the other hand if the measurements are line measurements transformations will be as follows:

$$V_{s\alpha} = \frac{2}{3}V_{sa} - \frac{1}{3}V_{sb} - \frac{1}{3}V_{sc} = \frac{2}{3}(V_{sa} - V_{sc}) - \frac{1}{3}(V_{sb} - V_{sc}) = \frac{2}{3}V_{sac} - \frac{1}{3}V_{sbc} \quad (2.5)$$

$$V_{s\beta} = \frac{1}{\sqrt{3}}V_{sb} - \frac{1}{\sqrt{3}}V_{sc} = \frac{1}{\sqrt{3}}V_{sbc} \quad (2.6)$$

Now we have stationary reference frame currents and voltages. By using the voltage model [1], stationary reference frame stator flux components can be obtained by using the following equations:

$$\psi_{s\alpha} = \int (V_{s\alpha} - R_s I_{s\alpha}) dt \quad (2.7)$$

$$\psi_{s\beta} = \int (V_{s\beta} - R_s I_{s\beta}) dt \quad (2.8)$$

After obtaining stationary reference frame stator flux components it becomes possible to calculate the stationary reference frame rotor flux components $\psi_{r\alpha}$ and $\psi_{r\beta}$ by the help of following equations:

$$\psi_{r\alpha} = \frac{L_r}{L_m}(\psi_{s\alpha} - \sigma L_s i_{s\alpha}) \quad (2.9)$$

$$\psi_{r\beta} = \frac{L_r}{L_m}(\psi_{s\beta} - \sigma L_s i_{s\beta}) \quad (2.10)$$

$$\psi_r = \sqrt{(\psi_{s\alpha}^2 + \psi_{s\beta}^2)} \quad (2.11)$$

where L_r is rotor self inductance, L_m is magnetizing inductance and σL_s is stator transient inductance where the off-line prediction of this term is achieved in this thesis.

Finally we can obtain the angle between the stationary reference frame and rotating reference frame by using the rotor flux components,

$$\theta = \tan^{-1}\left(\frac{\psi_{r\beta}}{\psi_{r\alpha}}\right) \quad (2.12)$$

so electrical speed becomes;

$$\omega_s = \frac{d\theta}{dt} = \dot{\theta} = \frac{(\psi_{r\alpha} \cdot \dot{\psi}_{r\beta} - \psi_{r\beta} \cdot \dot{\psi}_{r\alpha})}{\psi_r^2} \quad (2.13)$$

where the dotted terms indicate the derivatives of variables involved.

Since the angle between rotating reference frame and stationary reference frame is obtained, rotating reference frame currents can be obtained.

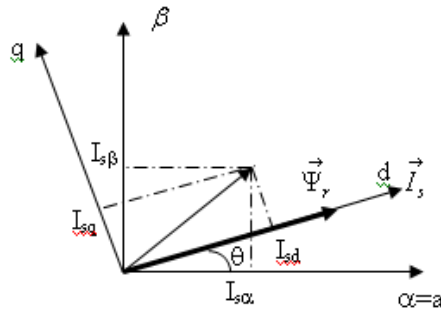


Figure 2. 4 – Stationary (α - β) and rotating (d-q) reference frames

$$I_{sd} = I_{s\alpha} \cos \theta + I_{s\beta} \sin \theta \quad (2.14)$$

$$I_{sq} = -I_{s\alpha} \sin \theta + I_{s\beta} \cos \theta \quad (2.15)$$

After obtaining those d-q axis current components, these are compared with the reference current signals and the required reference voltages are produced to drive the motor at desired flux and torque level.

How those mathematical transformations and calculations are solved in the algorithm will be explained in the software environment part of this chapter.

Finally slip frequency is obtained by using the following relation which is explained in detail [2].

$$w_{sl} = \frac{R_r}{L_r} = \frac{I_{qs}}{I_{ds}} \quad (2.16)$$

So speed of the rotor can be obtained by using equation (2.17);

$$w_r = w_s - w_{sl} \quad (2.17)$$

As a result, Figure 2. 5 shows the general schematics of the sensorless vector control method applied in this thesis.

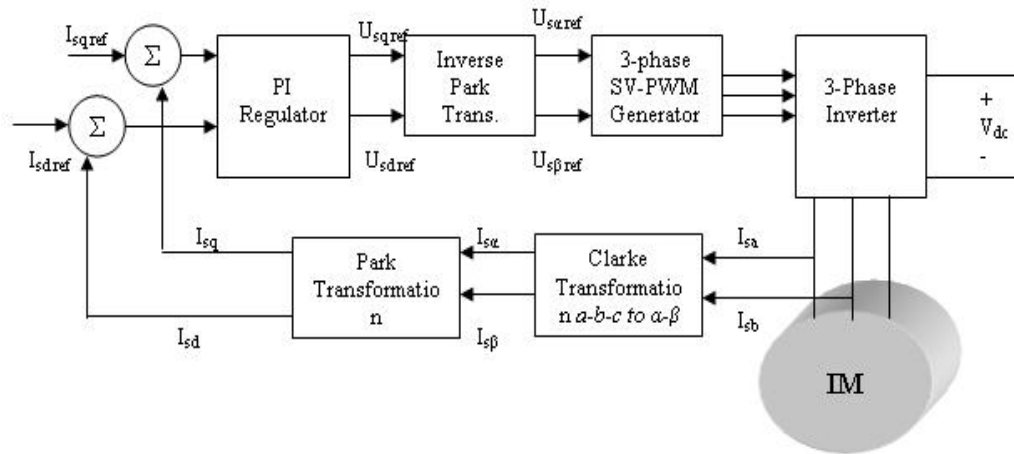


Figure 2. 5 – Sensorless vector control of induction motor scheme

Now, the hardware and software environment of the developed drive will be explained in the following section of this chapter.

2.3. Hardware

This section describes the hardware in detail. Figure 2. 6 shows the block diagram of the setup which is used in this thesis. Hardware starts with the DSP card where the all calculations made and the required pulses, for intelligent power module (IPM) to drive motor for desired conditions, are produced. However, IPM needs symmetrical pulses for its upper and lower IGBTs. But the DSP card used in this work has no capability to produce symmetrical pulses. At this point, pulse processing stage is introduced. This stage converts the signals to desired pwm signals by the help of XOR IC (Integrated Circuit) and dead time generator. Since the voltage level at the IPM stage is so high with respect to the pulse processing stage, there must be an isolation module to separate those stages from each other. In addition to previous hardware, in this thesis work also dynamic braking is introduced. In the isolation stage the pwm signals coming from pulse processing

As you can see from the Figure 2. 6, there are some stages named; power stage, pulse processing stage, isolation and IPM stage and measurement stage. In the following sections those stages will be explained in detail.

2.3.1. Pulse Processing Stage

In this stage, it is aimed to send calculated PWM signals to isolation board as symmetrical signals with dead time added. There are 6 pwm channels at the DSP card and all of them are for IGBTs at the inverter stage. For braking IGBT one of the input output (I/O) pins of DSP card is utilized. In Figure 2. 7, the relation between produced pwm signals at the end of this stage and inverter is shown.

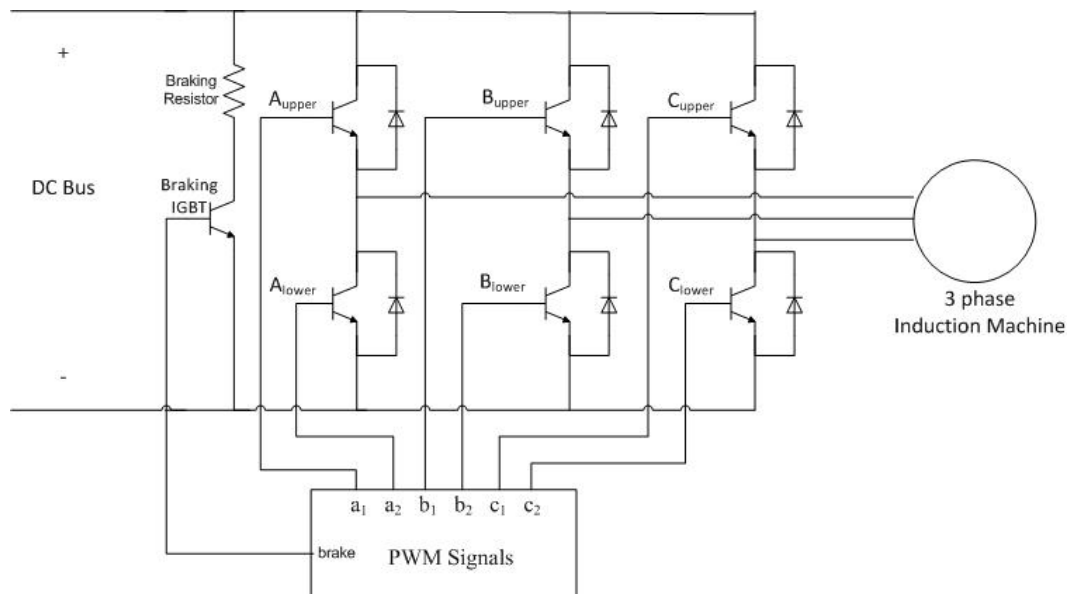


Figure 2. 7 – PWM Signals with inverter IGBTs and Braking IGBT

Now, let examine the required and produced pulses at the inverter side to obtain the line voltage waveform of V_{sac} shown in Figure 2. 8 (a) together with the

pulses produced by the DSP card, where the reference voltages as phase quantities are; $V_{sref} = 129.3$ V $V_{sref\alpha} = 112$ V and $V_{sref\beta} = 64.66$ V. For line-line measurement $V_{sref} = 224$ V.

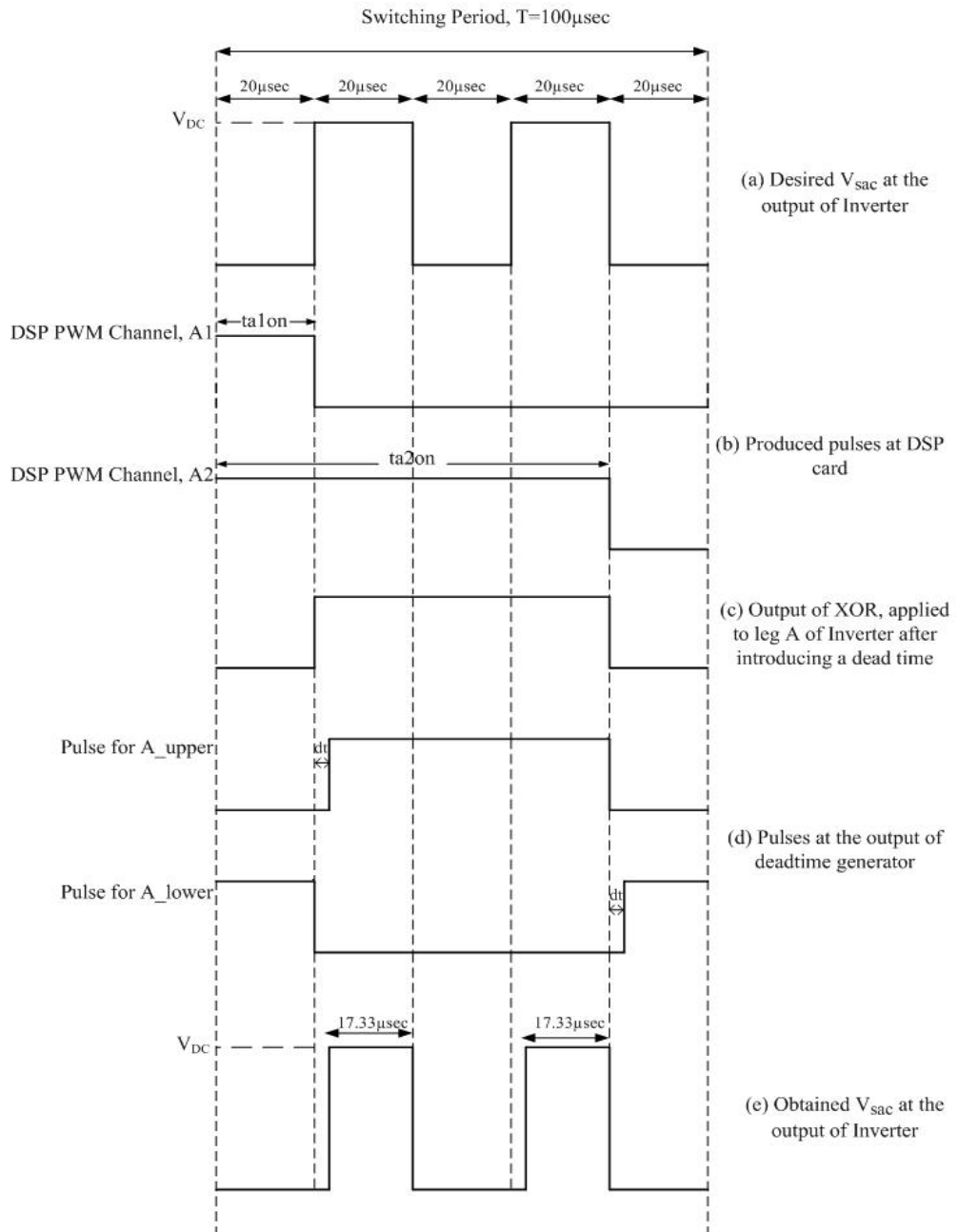


Figure 2. 8 – Required and produced pulses to obtain the reference voltage given as an example

Figure 2. 8 (b) presents the produced pulses at DSP card for the upper and lower IGBTs of phase A of inverter to obtain the voltage waveform shown in Figure 2. 8 (a). Since dsp card used in this thesis work has no capability to produce symmetrical pulses, XOR gates are used to obtain symmetrical pulses. Figure 2. 8 (c) presents the output of XOR gate where the inputs of XOR gate are shown in Figure 2. 8 (b). Figure 2. 8 (d) shows the produced pulses at the output of dead time generator for the same IGBTs to obtain the voltage waveform shown in Figure 2. 8 (a). In the application notes of IPM, it suggests that there must be at least 2.5 μsec dead time between the pulses sent to upper and lower side IGBTs which are at the same leg of inverter. In this thesis work, 2.67 μsec dead time is implemented. That produced pulses at the output of dead time generator are sent to the inverter's A_{upper} and A_{lower} transistors. Finally, at the output side of the inverter, V_{sac} shown in Figure 2. 8 (e) is obtained.

Desired V_{sac} pulse has 40 μsec (20 μsec + 20 μsec) duty cycle over 100 μsec switching period. On the other hand, output V_{sac} pulse is 5.34 μsec (= 2.67 μsec + 2.67 μsec) shorter than the desired V_{sac} pulse.

To obtain symmetrical pulses with dead time implemented for transistor at the inverter, a pulse processing stage is utilized. This stage is shown in Figure 2. 9.

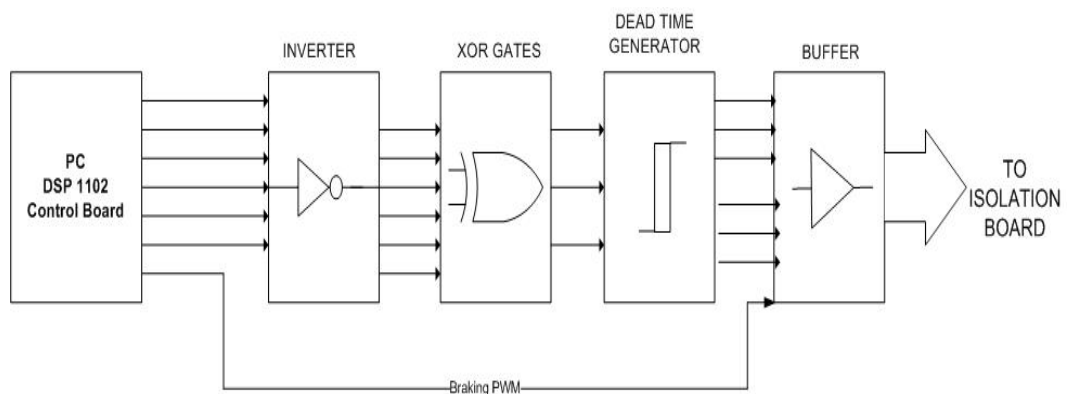


Figure 2. 9 – Block diagram of pulse processing stage

The conversion process of the asymmetrical DSP pulses to symmetrical shape is explained in the following sections.

2.3.1.1. XOR Gate

In this thesis symmetric PWM was used to drive inverter. The DSP card, which is used to obtain required duty cycles, can only generate asymmetric pulses shown in previous section. In order to generate a symmetric duty cycle, XOR gates will be used. The truth table is given in Table 2.1. Schematic presentation of XOR with inputs X1 and X2 is shown in Figure 2. 10.

Table 2. 1 – Truth table of XOR

X1	X2	Output
0	0	0
0	1	1
1	0	1
1	1	0

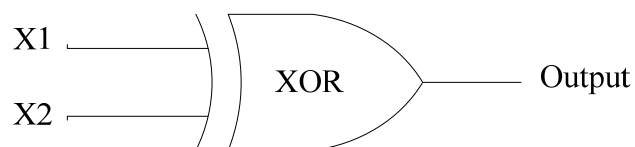


Figure 2. 10 – XOR gate with inputs, X1 and X2

From the truth table when X1 and X2 are same, the output is logic zero and when the X1 and X2 are different, output is logic high. Figure 2. 8 (c) shows the output of XOR gate for the inputs given in Figure 2. 8 (b).

As a result of that XOR operation, symmetrical PWM is obtained at the output of XOR gate. In the system six PWM outputs are generated at the DSP card and after XOR gate operation three symmetric pulses are obtained. Those three pulses are sent to dead time generator where the six pulses will be generated with 2.67 μ sec dead time is implemented between the pulses which will be sent to the same phase of inverter's upper and lower IGBTs.

Since braking switch is consisting of only one IGBT there is no need to make that pulse symmetric. For this reason braking pulse directly goes to the related opto-coupler in the isolation board.

2.3.1.2. Dead Time Generator

Dead time is required to avoid short circuit between upper and lower IGBTs at the same leg of the inverter. IXDP631 chip is used to implement the dead time between the pulses for the upper and lower side of IGBTs at the same leg. This chip generates 2.67 μ sec dead time for the input pulse and generates 2 output pulses where these 2 pulses are for the upper and lower IGBTs on the inverter. To show how this dead time generator works, the output of the XOR gate is processed and the outputs are shown at Figure 2. 8 (d) for one phase.

Figure 2. 11 presents the block diagram of the dead time generator where the U, V and W represents the input of dead time generator. U_{upper} and U_{lower} represent the output pulses for the related phase. Similarly, other outputs are related with remaining two phases.

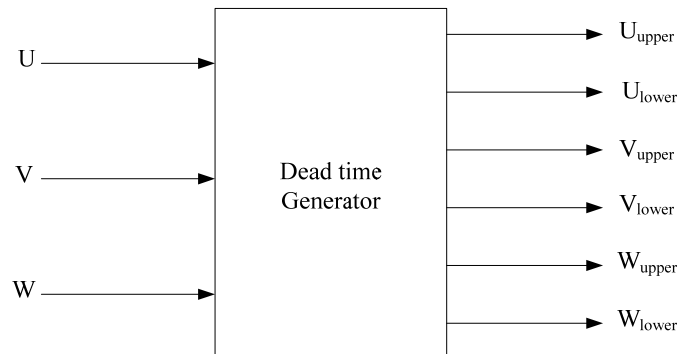


Figure 2. 11 – Block diagram of Dead time generator

In Figure 2. 8 (d), dt represents the dead-time which is $2.67 \mu\text{sec}$. It can be observed that, when the input signal raises to logic high the pulse for the lower side transistor drops to logic zero at the same time. After $2.67 \mu\text{sec}$ the pulse for the upper side transistor goes logic high and it drops to logic zero at instant where the input pulse drops to logic zero. Finally, the pulse for the lower side transistor goes up to logic high after $2.67 \mu\text{sec}$ from the pulse for upper side transistor drops to logic zero. As a result, the upper and lower side transistors of same phase can not remain in the “on” state at the same time by the help of this dead time generator. However, pulses become $2.67 \mu\text{sec}$ shorter due to that dead time. As mentioned in pulse processing stage, section 2.3.1 output pulse at the inverter becomes $5.34 \mu\text{sec}$ shorter than the desired output voltage pulse. In literature there are some studies about dead time compensation but in this thesis work dead time compensation is not considered.

Dead time procedure here is shown for just one phase; the procedure is same for the other 2 phases. As a consequence 6 dead-time implemented PWM signals become available and are sent to the isolation stage of the driver.

2.3.2. Isolation Module and IPM Stage

The isolation module was developed in [12]. The aim of this module is to provide isolation between the intelligent power module (IPM) and the pulse processing module. Isolation module circuit is built up with opto-couplers. HP4504 IC is used as an opto-coupler. This module isolates the PWM signals (UN, UP, VN, VP, WN, WP signals) coming from dead-time generator from input side of the IPM [6]. In addition to that isolation, the isolation module also isolates fault output signals (FO, UFO, VFO, WFO signals) of the IPM from the pulse processing stage, too. Schematic diagram of the isolation module and IPM stage is given in Figure 2. 12.

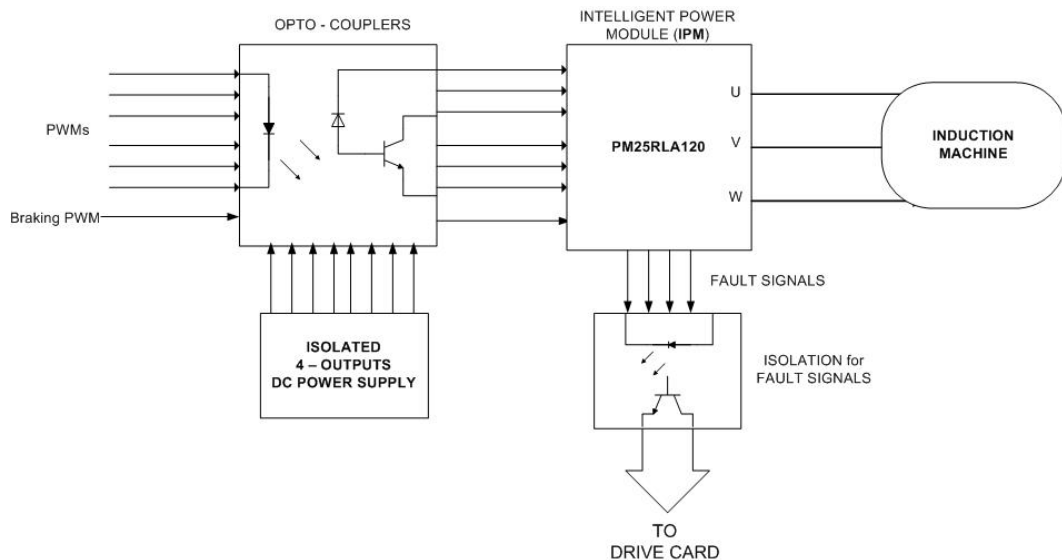


Figure 2. 12 – Isolation stage of the Hardware

In Figure 2. 13, how the opto-couplers are used in the isolation module is shown. As it is seen from Figure 2. 12, opto-coupler isolates input and output signals

from each other. If there is a short circuit or any other fault on the IPM stage, it damages only IPM part, other parts of the driver will be safe by means of isolation stage.

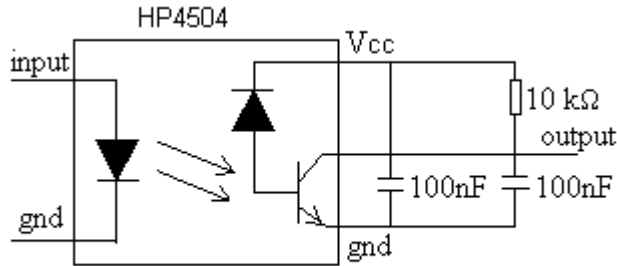


Figure 2. 13 – Circuitry of opto-coupler in the isolation module

However input logic level of IPM is 15 volts and the voltage level of produced pulses at the pulse processing stage is about 5 volts, HP4504 isolates that logic level difference. As a propagation delay, that opto-couplers have 0.3 μ sec typical delay which can be neglected in drive operations since switching period is about 150 μ sec; 0.3 μ sec delay has no important effect on the pulses.

In the application notes of Mitsubishi IPM it is suggested that there must be 4 isolated 15 volts dc power supplies. 3 of them are required for upper IGBTs opto-couplers and remaining one is for lower IGBTs and braking IGBT. In Figure 2. 14, application example of Mitsubishi for PM25RLA120 IPM is shown. V_D represents the power supply for opto-couplers and it is seen there 4 separate V_D is required. In order to supply that 4 isolated 15 volts dc supply M5740 IC is used. How that IC is integrated to isolation board will be explained in the following section.

Apart from the inverter IGBT's opto-couplers, for the braking issue, the IPM application notes suggests a different opto-coupler which has high current transformation ratio. The connection diagram is same as the other opto-couplers, only difference is its current transformation ratio.

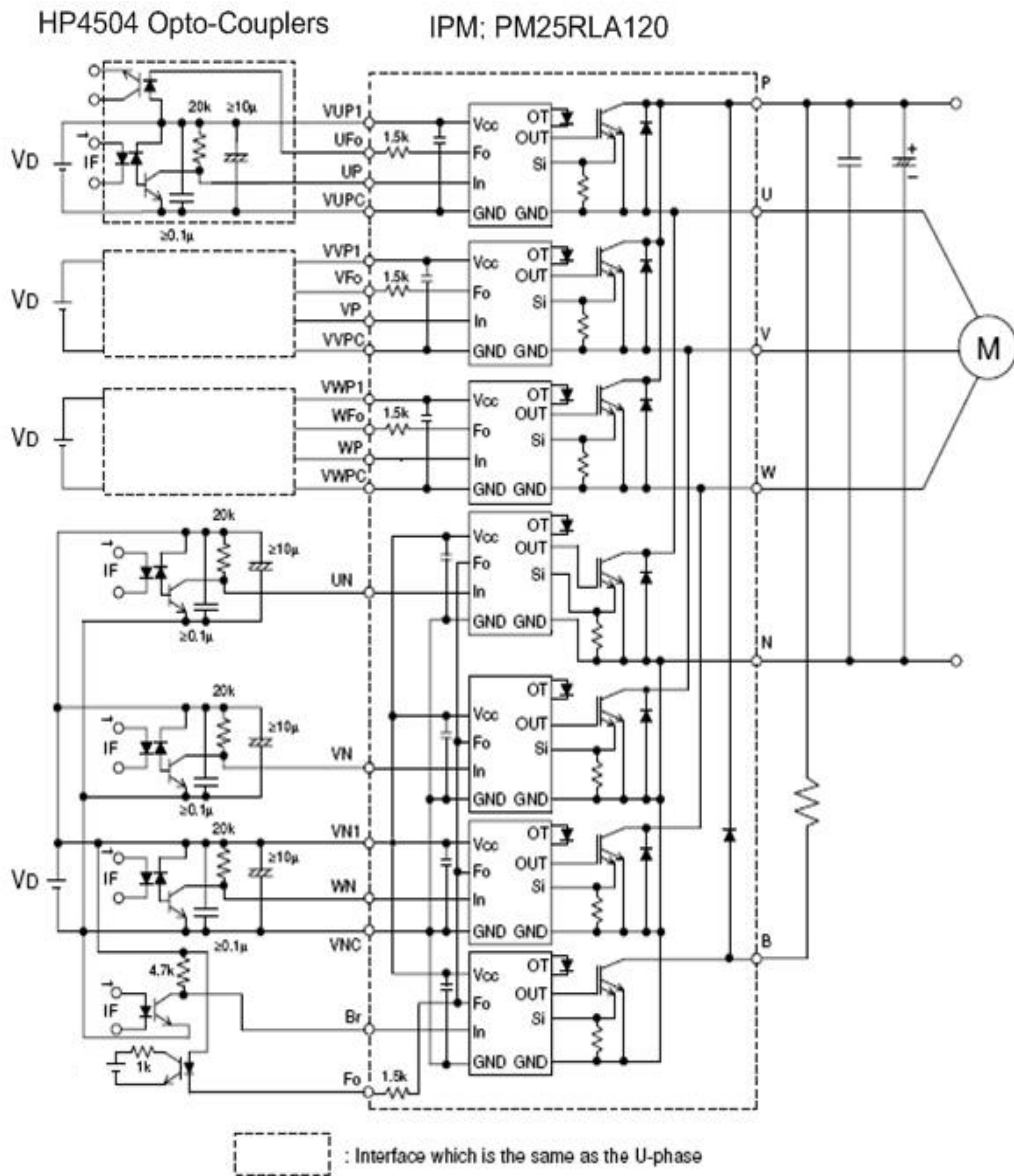


Figure 2. 14 – Application example of Mitsubishi IPM

2.3.2.1. Power Supply of the Isolation Module and IPM Stage

Power supply of the isolation module is placed on the same board. The isolation module requires 4 isolated 15V DC supplies. M57140 hybrid IC is used to provide isolated 15V DC supplies. Below, schematic of the power supply stage is given at Figure 2. 15.

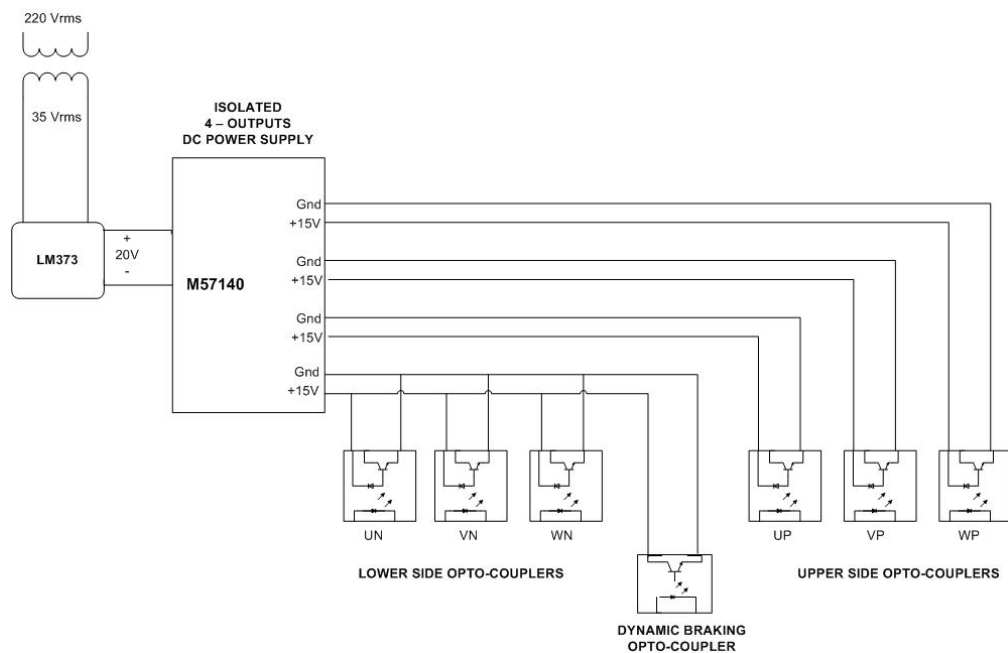


Figure 2. 15 –Block diagram of the 4-output 15V DC Power Supply for Isolation Board

Upper opto-couplers are supplied with 3 outputs of this IC and lower opto-couplers are supplied with the remaining output of M57140. Since the ground connection of upper side transistors are not common 4 output isolated power supply must be used. Three of them are for the upper side transistors and the remaining one is for the lower side transistors and braking transistor. There is no need to use 4 separate power supplies for the lower side transistors and braking transistor since their grounds are all common.

In this thesis work, contrary to previous studies [4, 5, 6, 7] on vector control induction motor drive, dynamic braking capability is also added to drive. It is seen from Figure 2. 15 that there is an opto-coupler for dynamic braking and it is different from other opto-couplers. In the application datasheet of IPM it is mentioned that, the opto-coupler for braking must have high current transformation ratio so opto-coupler for braking is selected as 4N46 IC and it is also supplied from lower side opto-coupler's 15V DC supply. Where the HCPL 4504 opto-couplers have 32% current transformation ratio, but 4N46 has 1500% current transfer ratio which is required for braking IGBT. Dynamic braking test results will be shown in the software part of this chapter in section 2.4.1.14.

2.3.2.2. Input Signals of the IPM Stage

There are 7 input signals, 6 of those input signals for inverter side named; UP, UN, VP, VN, WP, WN and the remaining input for the braking purpose which is named Br here. The inputs are shown in Figure 2. 16.

UP = Pulse stream for upper IGBT in U-phase (with dead-time delays)

UN = Pulse stream for lower IGBT in U-phase (with dead-time delays)

VP = Pulse stream for upper IGBT in V-phase (with dead-time delays)

VN = Pulse stream for lower IGBT in V-phase (with dead-time delays)

WP = Pulse stream for upper IGBT in W-phase (with dead-time delays)

WN = Pulse stream for lower IGBT in W-phase (with dead-time delays)

Br = Pulse stream for Braking IGBT

The fault signals of the IPM are discussed in the next section. The function of other inputs of the IPM not discussed here can be found in Appendix B.

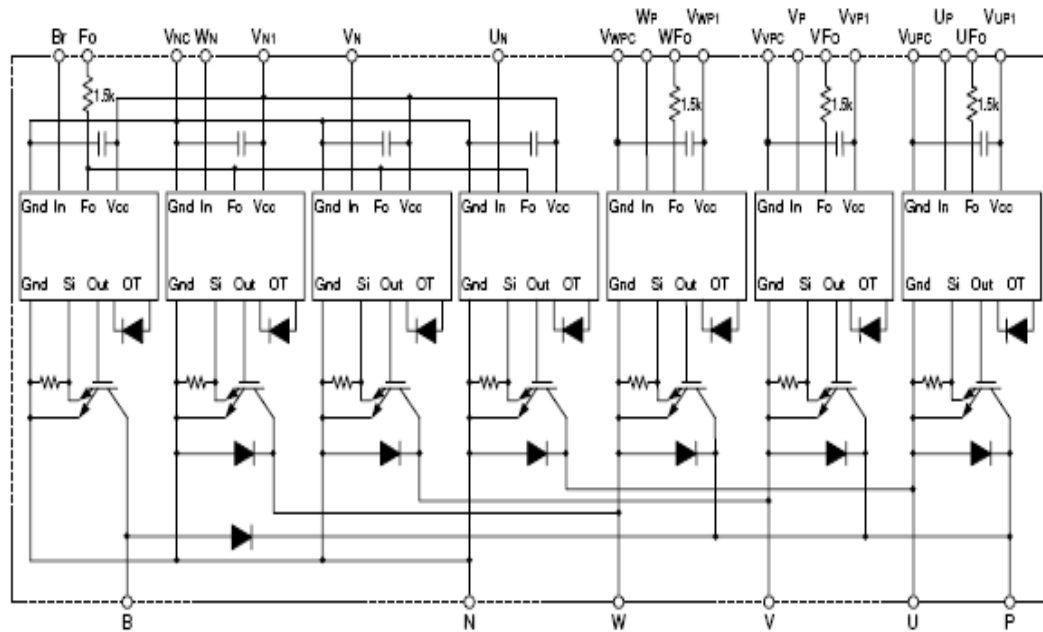


Figure 2. 16 – Functional Diagram of the IPM

2.3.2.3. Fault Signals of the IPM Stage

There are 4 output signals which are called fault signals of PM25RLA120, i.e. the 7-pack IPM used in this thesis. Those fault signals are called: FO, UFO, VFO, WFO, which are shown at previous section in Figure 2. 16.

FO = Fault output from all lower IGBT's and thermal protection of the IPM.

UFO = Fault output from upper IGBT in U phase of IPM

VFO = Fault output from upper IGBT in V phase of IPM

WFO = Fault output from upper IGBT in W phase of IPM

All those 4 fault signals are also isolated from pulse processing stage by using the circuit in Figure 2. 17. The isolation is provided by TLP521 IC which has 4 opto-couplers inside.

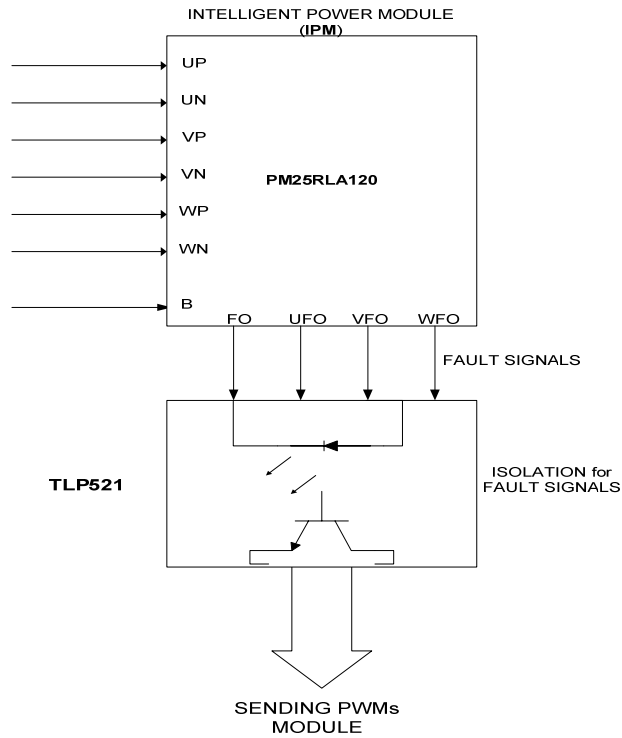


Figure 2. 17 – Fault Signals Isolation Schematics

If there is any fault on the IPM it generates the fault signal and this fault signal is sent to pulse processing stage to stop the driver.

2.3.3. Power Stage

Power stage of the drive is shown in Figure 2. 18. Uncontrolled diode rectifier is supplied with 3 – phase $380V_{rms}$ AC supply to obtain dc-link voltage. There are 2 dc-link capacitors connected in series as dc-link capacitors. Stray inductance of dc-link connections may cause huge peak on the output voltage. To keep that stray inductance minimum, connection between dc-link and inverter is designed so close to each other.

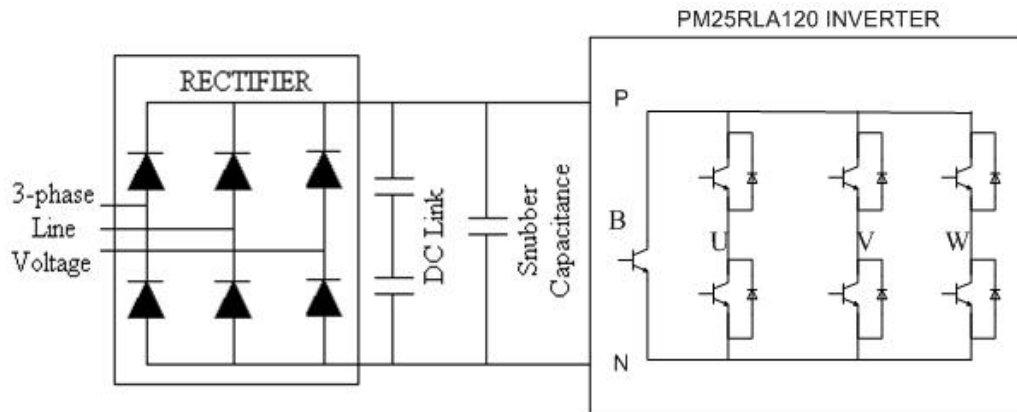


Figure 2. 18 – Power Stage of the Driver

Each dc-link capacitor has 2.4mF, 450 volts capacitance. The reason why 2 capacitors are used instead of using one capacitor at the equivalent rate is that the expense of using one capacitor at ratings 1.2 mF, 900 V is more than using two capacitors having ratings 2.4 mF, 450 V. Since the dc-link voltage is normally about at 550 volts. The resultant capacitor is rated at 1.2 mF, 900 V and can withstand over voltages that may occur during dynamic braking operating condition. In the light of the Mitsubishi IPM application notes, snubber capacitance is used to minimize the surge voltage on the dc-link voltage. It is connected to P-N terminals of the IPM with specifications; 4 μ F, 700V, metalized polypropylene film capacitor.

Typical recorded dc-link voltage at no-load is presented in Figure 2. 19. As mentioned before, it is about 560 volts and it appears that the ripple has peak to peak 2 volts magnitude at no-load condition.

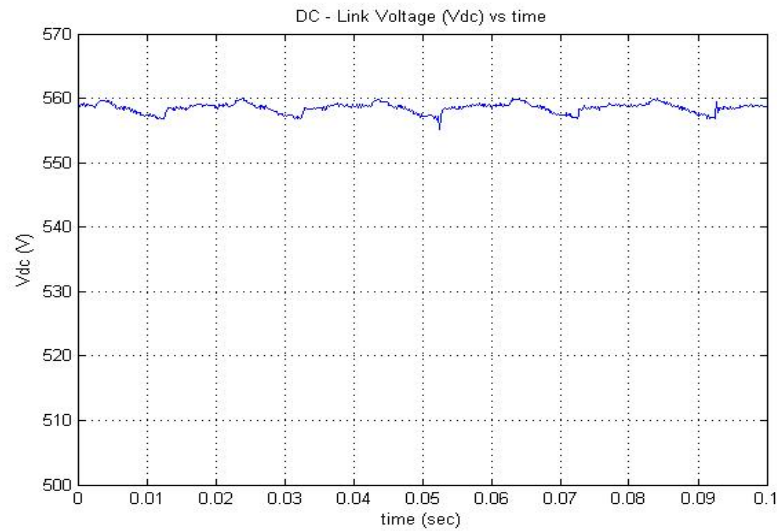


Figure 2. 19 – Typical dc-link voltage supplied from 3-phase 380 V grid source.

In power stage there is an intelligent power module (IPM) named PM25RLA120 is used as an inverter.

The technical specifications of IPM are given below:

- 1200 V, 25 A current-sense, 15 kHz IGBT type inverter
- Monolithic gate drive and protection logic
- Detection, protection and status indication circuits for over current, short circuit, over temperature and under voltage.
- Dead time guarantee 2.5 μ s.

2.3.4. Measurement Stage

Two of the stator currents, voltages and dc-link voltage are sensed with current and voltage transducers. The measured signals are amplified with an OP-AMP amplifier. The output of the amplifier is filtered with an RC filter. The cut-off frequency of the filter is selected to be as 2 kHz. Then filtered outputs are sent to ADCs of the DSP. Since DSP board has just 4 ADC channels, a multiplexer is

used to read 2 variables from one ADC channel. The hardware circuit used for current and voltage measurement is shown in Figure 2. 20.

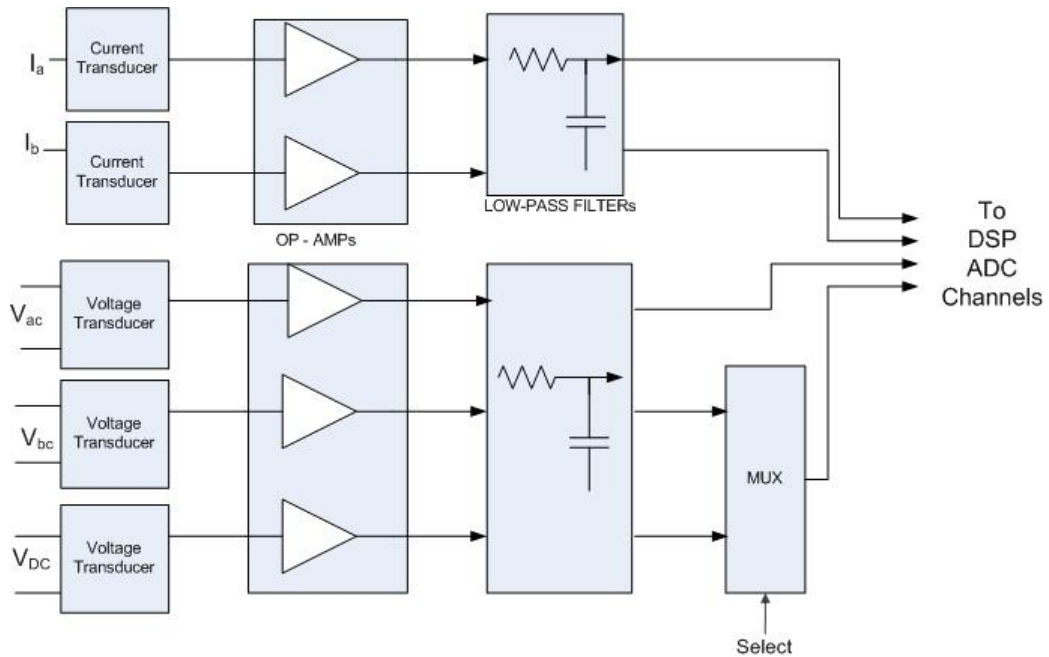


Figure 2. 20 – Measurement block diagram of the driver

Figure 2. 20 shows that two line voltages; V_{ac} and V_{bc} are measured, in addition to that, if the star point of the machine is available, phase voltages; V_{an} and V_{bn} can be also measured. There will be some change at the mathematical expression in the transformation whether the phase voltages or line voltages are measured. In this work line currents are measured. Induction machines used in this thesis are all Y-connected; the measured currents are therefore also phase currents. In Figure 2. 21, detailed measurement diagram is given for one measured variable.

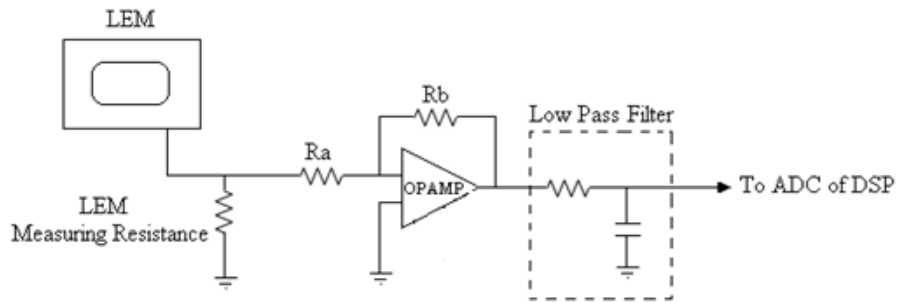


Figure 2. 21 – Detailed measurement circuitry for one signal

The low – pass filter shown in Figure 2. 21 is a typical RC filter where the resistance value is 810 ohms and the capacitance value is 100 nF. The circuit of the filter is shown in Figure 2. 22.

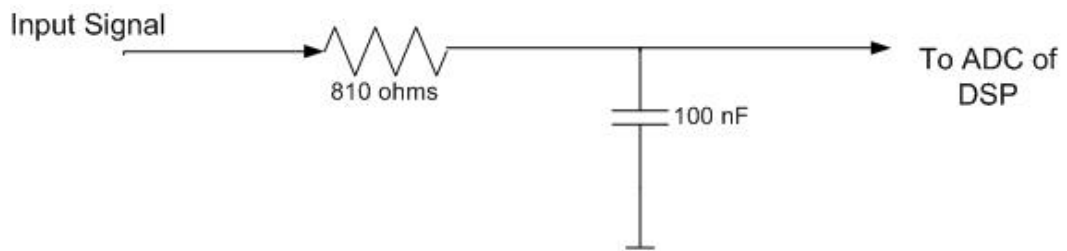


Figure 2. 22 – Circuit diagram of low-pass filter

Transfer function of the filter is given as $H(s)$

$$H(s) = \frac{1}{RC.s + 1} = \frac{1}{8.1 \times 10^{-5}.s + 1} \quad (2.18)$$

The cut-off frequency f_c can be calculated from equation (2.19)

$$2.\pi.f_c = \frac{1}{8.1 \times 10^{-5}} \Rightarrow f_c \cong 2kHz \quad (2.19)$$

The cut-off frequency is determined as 2 kHz with respect to the results of phase and magnitude response of the filter which is shown in Figure 2. 23. It can be seen from Figure 2. 23, that the filter has negligible affect on the input signal's phase and amplitude for the frequencies under 100 Hz. If the frequency of the signal is 100 Hz, then its magnitude is decreased by 0.1% by the filter. Furthermore, the phase of the signal having frequency 100 Hz is delayed about 3 degrees which corresponds to a shift of 0.83% in a period. Since the rated operating frequency is about 50 Hz, the chosen cut-off frequency is meaningful.

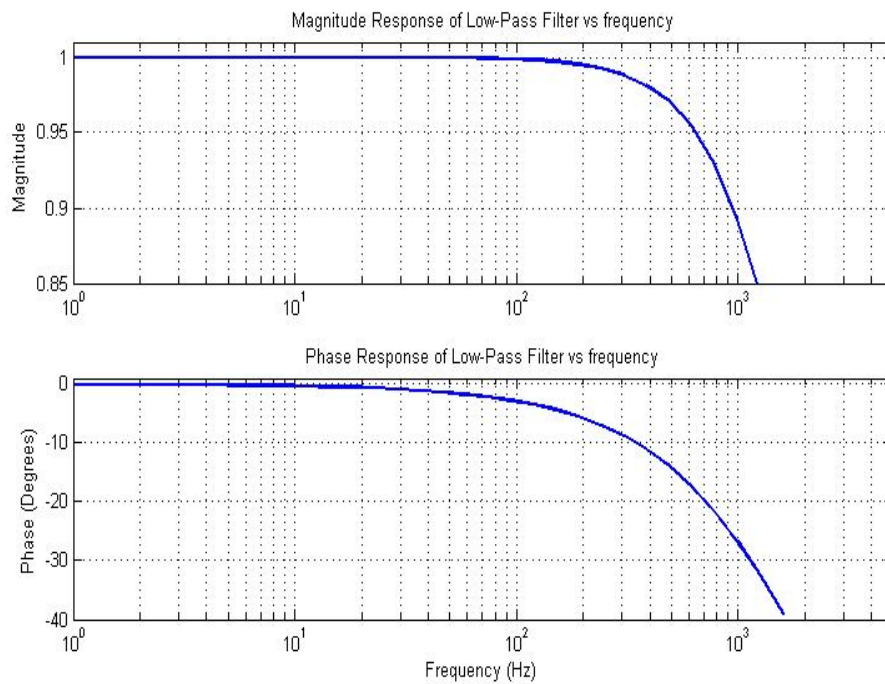


Figure 2. 23 – Magnitude and Phase response of Low-Pass filter used in the measurements

2.4. Software Environment

In this section, the software used for parameter estimation and vector control is explained. Flowchart of the software is given and modules used in this software

are explained with theory background. Also programming language and other programs used in this thesis are described.

First of all the aim of the software is given as; To drive the motor with vector control at a desired torque or speed, motor currents and voltages are sampled simultaneously by the software and required PWM switching signals are generated. Software is written in C programming language, then compiled and downloaded to the DSP with a program called down31. A program LD31 is used to disable the program, which is downloaded and working in controller card, or to restart the disabled program. Both programs, down31 and LD31, came with controller board and work in MsDOS environment. TRACE program is used to observe the variables such as voltage, current, flux etc. in the program. To be able to observe variables in TRACE, a trc file must be formed and put into the same directory with software written in C language. Trc file, which consists of variable names and their types, can be written in notepad or in another editor program. TRACE works in windows environment. While the TRACE program is active, the software cannot be stopped via LD31 program. First TRACE program must be deactivated [4].

2.4.1. Flowchart of the Software

The software is written in modules, since if there is any change at one module there will be no need to change whole module. Flowchart of the software is shown at Figure 2. 24. In the following sections that modules will be described.

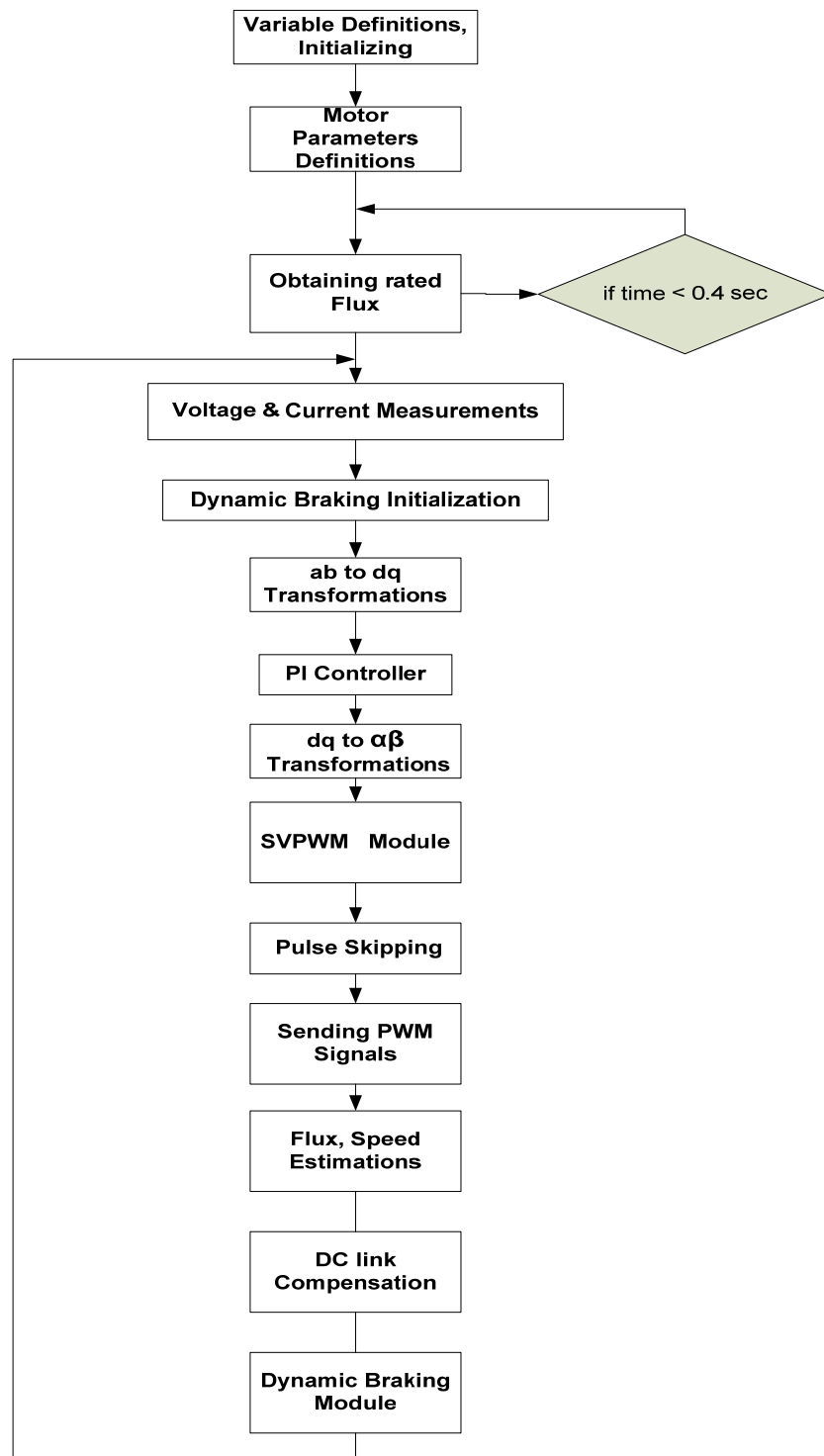


Figure 2. 24 – Flowchart of the vector control software

2.4.1.1. Variable Definitions, Initializations Module

In this module, initialization of all variables used in the whole software is made. In addition to these some required definitions and commands for ds1102 are also made in this module. All of the parameters and variables, used in the modules, are listed below.

Initialization	
TS	: Switching period, control cycle
isa, isb, isc	: a, b, c phase currents of motor
isalfa, isbeta	: α, β components of motor current
isd, isq	: d, q components of motor current
isalfaref, isbetaref	: α, β components of reference current
isdref	: d component of reference current creating rated flux
isqref	: q component of reference current creating desired torque
vsa, vsb	: Motor phase voltages
vsalfa, vsbeta	: α, β components of motor voltage
vsrefalfa, vsrefbeta	: α, β components of reference voltage
vsdref, vsqref	: d, q component of reference voltage
t	: time (second)
fir	: rotor flux
firalfa, firbeta	: α, β components of rotor flux
fisalfa, fisbeta	: α, β components of stator flux
firalfapre, firbetapre	: previous values of α, β components of rotor flux
costeta, sinteta	: sine and cosine of rotor flux position
errorisdref	: error between d component of reference current and d component of motor current
errorisqref	: error between q component of reference current and q component of motor current

errorisdrefint	: integral of error between d component of reference current and d component of motor current
errorisqrefint	: integral of error between q component of reference current and q component of motor current
kiisd, kiisq	: integrator coefficient of PI controller
kpisd, kpisq	: proportional coefficient of PI controller
ws	: synchronous speed
kd	: filter constant
sig	: leakage factor
ls	: stator self inductance
rs	: stator winding resistance
Tz	: half of the zero voltage application period in SVPWM
Tk	: half of the application period of voltage V_k in sector k
Tkk	: half of the application period of voltage V_{k+1} in sector k
ta1on, tb1on, tc1on	: on time duration of PWM channels 1,3,5
dutya1, dutya2	: duty cycles of desired PWM signals of inverter leg a
dutyb1, dutyb2	: duty cycles of desired PWM signals of inverter leg b
dutyc1, dutyc2	: duty cycles of desired PWM signals of inverter leg c
dynbrkflag	: dynamic braking flag
udcolc	: measured dc-link voltage

2.4.1.2. Motor Parameters Module

In this module initial motor parameters like; stator resistance, stator inductance, mutual inductance and sigma value which is equal to $(\sigma = 1 - \frac{L_m^2}{L_s L_r})$, are entered by the user as an initial motor parameters.

2.4.1.3. Obtaining Rated Flux Module [4]

Motor must be driven until rated flux for normal operation. The required time for the motor to reach rated flux can be calculated by using equation 2.23.

$$V = N \frac{d\psi}{dt} \quad (2.20)$$

$$N\psi = \int V dt \quad (2.21)$$

When DC voltage is applied to motor Equation 2.21 becomes Equation 2.22.

$$N\psi = V\Delta t \quad (2.22)$$

$$V\Delta t = L_r i_r \Rightarrow \Delta t = \frac{L_r i_r}{V} \Rightarrow \Delta t = \frac{L_r}{R_r} \quad (2.23)$$

In equations R_r , V , L_r and i_r represents rotor resistance, rotor voltage, rotor self inductance and rotor current respectively. In the algorithm, software starts with aligning the α -axis of stationary reference frame with the a-axis of a-b-c coordinate system of the induction motor. Then, it is desired to set the flux level of the machine to the rated value. To achieve those conditions, the angle between the α -axis and a-axis is taken zero, and reference current is set to obtain the rated flux level for a time interval taken as nearly 6 times of rotor time constant of the machine which is sufficient time to build up the rated flux.

As mentioned in section 2.2, in vector control d-axis component of current; i_{ds} controls the flux level. As an example, the rated i_{sd} value of test machine #1, where the parameters of this machine are listed in Table 3. 1, is equal to 2.4 A and this value is entered to obtain the rated flux level. In each control cycle, reference

currents are compared with measured currents and PI controller is used to obtain reference voltages. Since current control is performed, motor phase currents cannot reach to a level, which damages the motor itself. During this period dc current flow in the machine and flux is set to its rated value. The content of the module is shown below.

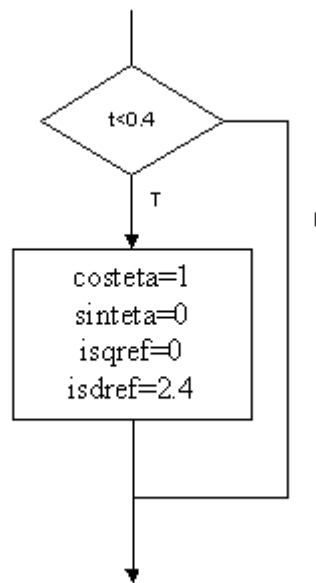


Figure 2. 25 – Module to drive the motor until its rated flux

2.4.1.4. Voltage and Current Measurements Module

In this module measured two line currents and two line voltages are recorded by reading the related ADC (Analog Digital Converters) channels of DSP. Firstly, ADCs are started to capture measurements and then four variables; two line currents and two line voltages are recorded. The conversion of the ADCs must be started by a preceding call to the function `ds1102_ad_start()` [3]. Then ADC channels are read with DSP macro `ds1102_ad` (long channel).

2.4.1.5. Dynamic Braking Initialization Module

This module initializes the variables required for braking. Since there are only 4 ADC channels and we have to measure I_{sa} , I_{sb} , V_{sac} , V_{sbc} and dc-link voltage; one ADC channel must be used to measure two variables, so in this module that pin selection is determined. Operation of ADC takes only 5 μsec to convert the analog measurement to digital platform and we know that the one control cycle of the program is 150 μsec . For this reason, it is possible to read more than one data from the same ADC channel in one control cycle of the software. Here, the ADC channel which reads V_{sbc} voltage is also used to measure the dc-link voltage. In this module once V_{sbc} is measured the select pin of the multiplexer is set to logic high to read the dc-link voltage. At the end of the control cycle, select pin of the multiplexer is set to logic zero again.

2.4.1.6. ab to dq Transformations Module

The aim of the module is to obtain time invariant flux and torque components of the stator currents. In order to obtain these time invariant components, first a projection is required that modifies the three phase system into the (α, β) two dimension orthogonal system.

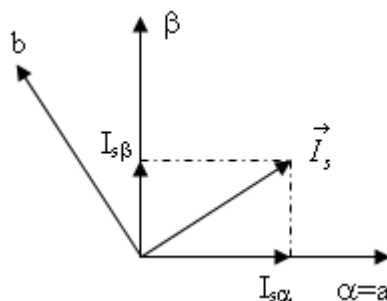


Figure 2. 26 – Projection of stator current vector to α - β coordinate system

Clarke Transformation:

$$I_{s\alpha} = i_{sa} \quad (2.24)$$

$$I_{s\beta} = \frac{1}{\sqrt{3}}i_{sa} + \frac{2}{\sqrt{3}}i_{sb} \quad (2.25)$$

After the projection of stator current vector to two orthogonal (α - β) axis, time variant components of current vector are obtained whose α axis is aligned with the phase a axis rotating with the same synchronous speed. Then, another transformation is required which modifies two phase time variant orthogonal system (α - β) into the d-q time invariant rotating reference frame. The projection of α - β coordinate system to d-q system for rotor flux orientation is shown below. [4, 8]

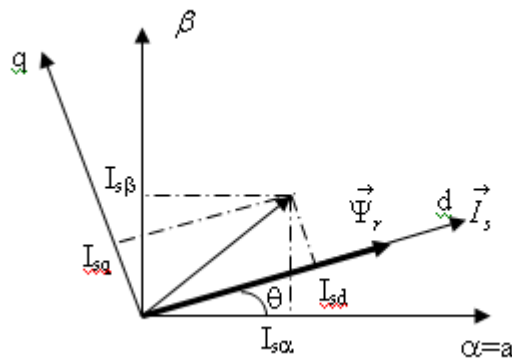


Figure 2. 27 – Projection of stator current vector from a-b coordinate system to d-q coordinate system

Rotor flux orientation, the most popular vector control algorithm in which d axis is aligned with rotor flux linkage vector as shown in Figure 2. 27, where θ is the

rotor flux position with respect to α axis. The flux and torque components of the current vector are determined by the following equations:

Park Transformation:

$$I_{sd} = I_{s\alpha} \cos \theta + I_{s\beta} \sin \theta \quad (2.26)$$

$$I_{sq} = -I_{s\alpha} \sin \theta + I_{s\beta} \cos \theta \quad (2.27)$$

For the measured voltages, transformation procedure is same provided that if those voltages are phase voltages. On the other hand if the measured voltages are line voltages, there will be some change in the transformation from a-b coordinate system to α - β coordinate system. Below, equations 2.28 and 2.29 shows that transformations if the measured voltages are V_{sac} and V_{sbc} [1]

$$V_{s\alpha} = \frac{1}{3}(2.V_{sac} - V_{sbc}) \quad (2.28)$$

$$V_{s\beta} = \frac{1}{\sqrt{3}}(V_{sbc}) \quad (2.29)$$

On the other hand, if the measured voltages are phase voltages, transformations are made by using the following equations; (2.30) and (2.31).

$$V_{s\alpha} = V_{sa} \quad (2.30)$$

$$V_{s\beta} = \frac{1}{\sqrt{3}}V_{sa} + \frac{2}{\sqrt{3}}V_{sb} \quad (2.31)$$

After obtaining α - β components, same procedure is applied to voltages to obtain d-q components.

$$V_{sd} = V_{s\alpha} \cos \theta + V_{s\beta} \sin \theta \quad (2.32)$$

$$V_{sq} = -V_{s\alpha} \sin \theta + V_{s\beta} \cos \theta \quad (2.33)$$

At the end of this module, current and voltage components of d-q frame are calculated.

2.4.1.7. PI Controller Module

In this module, reference voltage values in d-q frame are obtained by using the reference and measured currents. Measured currents are compared with reference values and error signals are obtained. Then PI controller is used to calculate reference voltage values from error signals. Calculation of PI controller parameters is given in Appendix A.

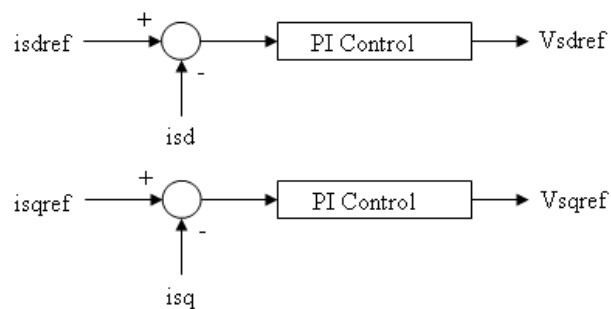


Figure 2. 28 – Block diagram of the PI controllers used for obtaining reference d-q voltages

2.4.1.8. d-q to α - β Transformation Module

Since Space Vector Pulse Width Modulation (SVPWM) module needs α - β reference voltage values to calculate the duty cycles of pwm signals, this module transforms the reference d-q voltages, obtained at PI controller module, to reference α - β voltages. That transformation is done by using the following equations which are named inverse Park transformation.

$$V_{sref\alpha} = V_{sdref} \cdot \cos \theta - V_{sqref} \cdot \sin \theta \quad (2.34)$$

$$V_{sref\beta} = V_{sdref} \cdot \sin \theta + V_{sqref} \cdot \cos \theta \quad (2.35)$$

2.4.1.9. Space Vector Pulse Width Modulation (SVPWM) Module

Space Vector Pulse Width Modulation (SVPWM) Technique is used to calculate the duty cycles of the pwms which are sent to IGBTs of the inverter for the required voltages. Since SVPWM technique is explained in previous thesis [5, 6] in detail, here the theory behind this modulation technique will not be explained.

There are 6 sectors shown in Figure 2. 29 and in this module, firstly in which sector the reference voltage vector is found. Consider a period T_s in the sector. Suppose that T_s is 100 μ sec. As shown in Figure 2. 8 (c), the gate pulses of the IGBTs are symmetrical with respect to the center of period T_s . The software produces channel A1 and channel A2 signals shown in Figure 2. 8 to produce the gate signals of leg A IGBTs. Dead time is introduced between the pulses for the upper and lower gate signals of same leg of inverter at the dead time generator which is explained in section 2.3.1.2. The pulses for other phases are calculated in similar manner. Note that once the gate signal for the upper IGBT is obtained, the

gate signal for the lower IGBT of the same leg is complementary of the upper leg signal.

The task now is to determine the off and on times of the pulses in terms of the reference voltage and space vectors V_0 , V_1 , V_2 and V_7 which are shown in Figure 2. 29.

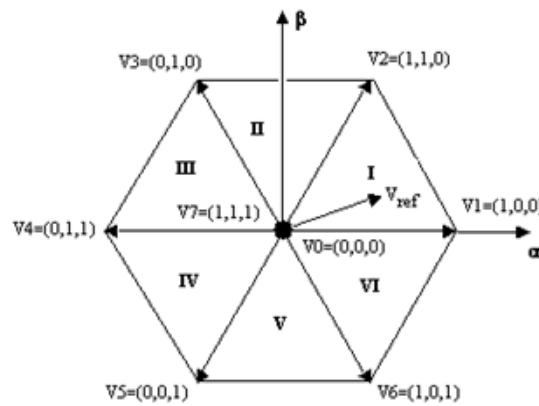


Figure 2. 29 - Representation of the sectors in the stationary reference frame

In calculation of “on” times of the pulses for the upper side IGBTs of the inverter; t_{a1on} , t_{b1on} and t_{c1on} terms are used for the phases A, B and C respectively. On the other hand, “on” times of the pulses for the lower side IGBTs are calculated as a complementary time of the related upper IGBTs’ gate signals. For the reference signal aligned in sector 1, t_{a1on} , t_{b1on} and t_{c1on} calculations are made by using the following equations. In equation 2.36, K represents modulation constant which is directly depends on period of the control cycle and dc-link voltage.

$$K = \frac{\sqrt{3}}{2} \cdot \frac{T_s}{V_{DC}} \quad (2.36)$$

Let us define T_k , $T_{(k+1)}$ and T_z as follows. The subscript k is 1 in sector 1, 2 in sector 2 etc.

$$T_k = \frac{K}{2} \cdot (\sqrt{3}V_{sref\alpha} - V_{sref\beta}) \quad (2.37)$$

$$T_{(k+1)} = K \cdot V_{sref\beta} \quad (2.38)$$

$$T_z = \frac{T_s}{2} - (T_k + T_{(k+1)}) \quad (2.39)$$

Now let us write the relation between the reference voltage vector and space vectors used to obtain that reference voltage as follows.

$$\vec{V}_{sref} \cdot T_s = \vec{V}_0 \frac{T_z}{2} + \vec{V}_k \cdot T_k + \vec{V}_{(k+1)} \cdot T_{(k+1)} + \vec{V}_7 \frac{T_z}{2} \quad (2.40)$$

From equation 2.40, in half of zero time V_0 space vector is applied, then in period of T_k space vector V_k is applied and then in period of $T_{(k+1)}$ space vector $V_{(k+1)}$ is applied and lastly duration of half of zero time V_7 is applied in an one switching period. Duration of time within T_s corresponding to T_k , $T_{(k+1)}$ and T_z may be seen in Figure 2. 30.

The relations between ta_{1on} , ta_{2on} , tc_{1on} and T_1 , T_2 , T_z are given in the following equations.

$$ta_{1on} = \frac{T_z}{2} \quad (2.41)$$

$$tb_{1on} = \frac{T_z}{2} + T_k \quad (2.42)$$

$$t_{c1on} = \frac{T_z}{2} + T_k + T_{(k+1)} \quad (2.43)$$

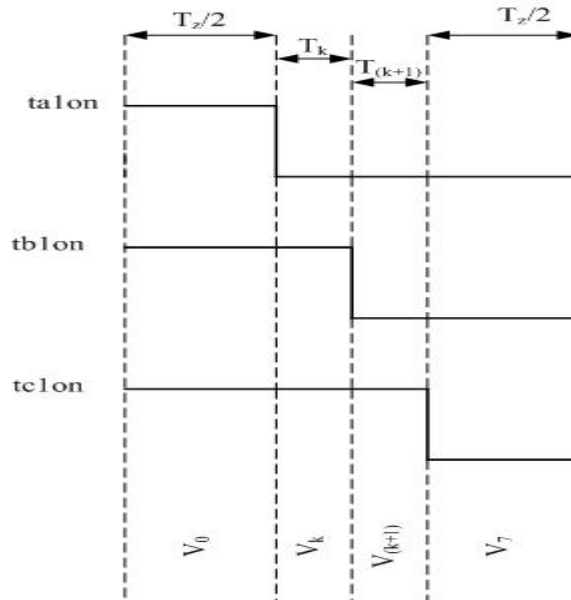


Figure 2. 30 – Switching times if the reference voltage is in sector 1.

Detailed information about calculation of other sectors is given in [6]. The flowchart of the module is given in Figure 2. 31.

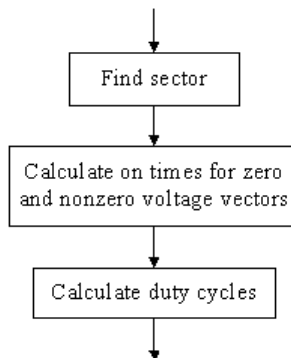


Figure 2. 31 – Flowchart of the module used for calculating the duty cycles

2.4.1.10. Pulse Skipping Module

In the pulse processing stage explained in section 2.3.1, dead time is implemented to signals not to cause short circuit in inverter legs. In this application, dead time is adjusted to 2.67 μs . For this reason signals smaller than 2.67 μs will be lost in dead-time generator circuit. For this purpose, the pulses calculated in previous module having duty cycle less than 3 μs are sent to pulse processing stage as 3 μs pulses.

2.4.1.11. Sending PWM Signals Module

Firstly the necessity for update must be explained. The Space Vector Pulse Width Modulation technique is based on the fact that, as explained in [5] and [6] in detail, every reference voltage vector inside the dashed hexagon, shown in Figure 2. 29, can be expressed as a weighted average combination of the two adjacent active space vectors and the zero-state vectors 0 and 7. Therefore, in each cycle imposing the desired reference vector may be achieved by switching between these four inverter states [9].

In SVPWM module on times of zero and non-zero vectors with respect to sector is calculated by using reference voltage and then duty cycles for inverter legs are calculated. These duty cycles must be updated and sent to inverter legs to constitute the reference voltage. Calculated duty cycles are updated in every 150 μs , which is the control cycle of the program. To update the duty cycles DSP macro `ds1102_p14_pwmvar(long channel, float duty)` is used. With this macro, the PWM duty-cycle of the selected channel is updated and sent to the pulse processing stage.

The content of the module is given in Figure 2. 34.

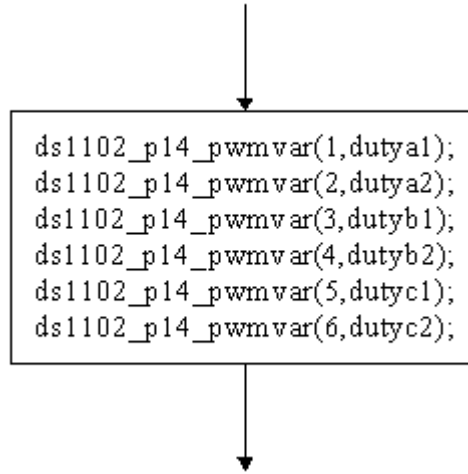


Figure 2. 34 – Module used to send PWM signals

2.4.1.12. Flux and Speed Estimations Module

The aim of this module is to obtain position of the rotor flux needed in field oriented control. For this purpose firstly α , β components of stator flux are obtained by using the voltage model [1]. Then α , β components of rotor flux are obtained from stator flux components and finally rotor flux magnitude and position are calculated.

Voltage model:

$$\psi_{s\alpha} = \int (V_{s\alpha} - R_s I_{s\alpha}) dt \quad (2.44)$$

$$\psi_{s\beta} = \int (V_{s\beta} - R_s I_{s\beta}) dt \quad (2.45)$$

Rotor flux:

$$\psi_{r\alpha} = \frac{L_r}{L_m} (\psi_{s\alpha} - \sigma L_s i_{s\alpha}) \quad (2.46)$$

$$\psi_{r\beta} = \frac{L_r}{L_m} (\psi_{s\beta} - \sigma L_s i_{s\beta}) \quad (2.47)$$

Rotor flux position is simply calculated by using α , β components of rotor flux as follows

$$\psi_r = \sqrt{(\psi_{r\alpha}^2 + \psi_{r\beta}^2)} \quad (2.48)$$

$$\cos \theta = \frac{\psi_{r\alpha}}{\psi_r} \quad (2.49)$$

$$\sin \theta = \frac{\psi_{r\beta}}{\psi_r} \quad (2.50)$$

As seen in equations (2.44) and (2.45) to calculate stator fluxes the integral operation must be performed. In the experiments, two cascaded filters are used as an integrator, since gain and phase response of two cascade filters can be adjusted to be equal to gain and phase response characteristics of integration operation. The reason using two cascade filters as an integrator is that it also clears the noises on the input signals so at the output we have pretty good flux variables. This process can be expressed as follows,

Digital Filter:

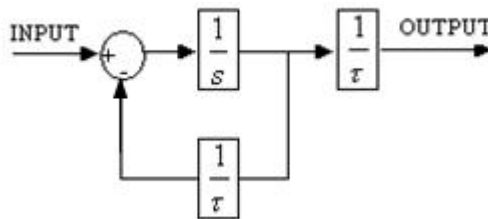


Figure 2. 35 – Block diagram of digital Filter

$$|F(j\omega)| = \frac{1}{\sqrt{1 + (\omega\tau)^2}} \quad (2.51)$$

$$\angle F(j\omega) = \tan^{-1}(\omega\tau) \quad (2.52)$$

Gain and phase shift of the filter are given in equations (2.51) and (2.52). When two filters are cascaded, equation (2.51) becomes (2.53) and (2.52) becomes (2.54).

$$|F(j\omega)| = \frac{1}{1 + (\omega\tau)^2} \quad (2.53)$$

$$\angle F(j\omega) = -2\tan^{-1}(\omega\tau) \quad (2.54)$$

Integrator:

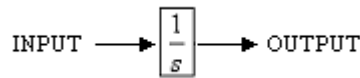


Figure 2. 36 – Schematic representation of integrator

$$|F(j\omega)| = \frac{1}{\omega} \quad (2.55)$$

$$\angle F(j\omega) = -90^\circ \quad (2.56)$$

To be able to use two cascaded filters as an integrator, gain and phase shift must be equal to the gain and phase response of the normal integration operation. For this reason, equation (2.54) and (2.56) must be equal;

$$-2 \tan^{-1}(\omega\tau) = 90 \Rightarrow \tau = \frac{1}{\omega} \quad (2.57)$$

Also gain of two cascaded filters must be equal to integrators gain. To make this possible a gain block ($G=2/w$) is added to the system.

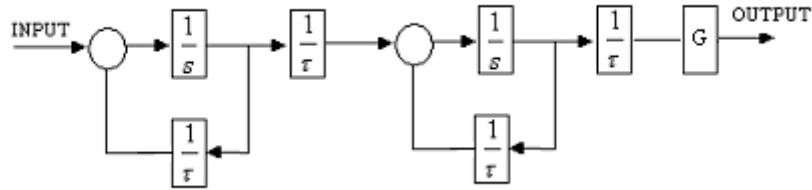


Figure 2. 37 – Block diagram of two cascade filters as an integrator

$\frac{1}{\tau}$ and G are functions of frequency; $w_s \cdot \frac{1}{\tau}$ is the filter coefficient, which is represented as kd in the software and equals to w_s . Gain block (G) and kd are strictly depend on the value of synchronous speed (w_s). Synchronous speed is estimated from rotor flux components as follows.

Rotor flux angle can be calculated from α , β components of rotor flux as shown below:

$$\theta = \tan^{-1} \left(\frac{\psi_{r\beta}}{\psi_{r\alpha}} \right) \quad (2.58)$$

Stator angular velocity can be obtained by taking the differential of rotor flux angle:

$$w = \dot{\theta} = \frac{\left(\psi_{r\alpha} \dot{\psi}_{r\beta} - \psi_{r\beta} \dot{\psi}_{r\alpha} \right)}{\psi_{r\alpha}^2 + \psi_{r\beta}^2} \quad (2.59)$$

The dotted variables in equation (2.59) represent the derivative of related variables. If equation (2.59) is rewritten in terms of sampled data, equation (2.60) is obtained.

$$w(k) = \frac{(\psi_{r\alpha}(k)(\psi_{r\beta}(k) - \psi_{r\beta}(k-1)) - \psi_{r\beta}(k)(\psi_{r\alpha}(k) - \psi_{r\alpha}(k-1)))}{(\psi_{r\alpha}(k)^2 + \psi_{r\beta}(k)^2)T}$$

$$\Rightarrow w(k) = \frac{\psi_{r\alpha}(k-1)\psi_{r\beta}(k) - \psi_{r\alpha}(k)\psi_{r\beta}(k-1)}{(\psi_{r\alpha}(k)^2 + \psi_{r\beta}(k)^2)T} \quad (2.60)$$

In equation (2.60) k represents the state of the variable for the current cycle and $(k-1)$ represents the previous state of the given variable. As it may be seen from the equation (2.60), w depends on the α , β components of rotor flux. Besides, estimation of rotor flux depends on stator voltage and currents. Stator voltage and voltage drop on stator resistance becomes comparable at low speeds. For this reason it is very important to know the stator resistance value accurately to estimate the flux variables correctly.

2.4.1.13. DC Link Compensation Module

As mentioned in section 2.4.1.9, there is a SVPWM constant; K (see equation 2.36) which directly depends on dc-link voltage. Equations; (2.37), (2.38) and (2.39) show the effect of K on duty cycle calculations. In practice, there are some ripples on dc-link voltage and dc-link voltage changes under load conditions. For this reason, it is essential to measure dc-link voltage and update the SVPWM constant K with respect to this measured dc-link voltage instead of taking it as a constant value. In this thesis work, dc-link voltage is measured and the modulation constant K is updated in each control cycle of vector control algorithm. As a result of this, calculation of “on” times of transistors becomes more accurate. Desired reference voltage level can be obtained since the changes on the dc-link voltage are taken into account.

In the following section experimental setup which is used to show the effect of dc-link compensation will be explained.

Experimental Setup:

The schematics of the experimental setup, which is used for DC-link compensation is shown below at Figure 2. 38. As you can see from Figure 2. 38, dc-link voltage is obtained as a output of a 3 phase diode rectifier which charges 1200 μ F, 900V capacitance to 560 V.

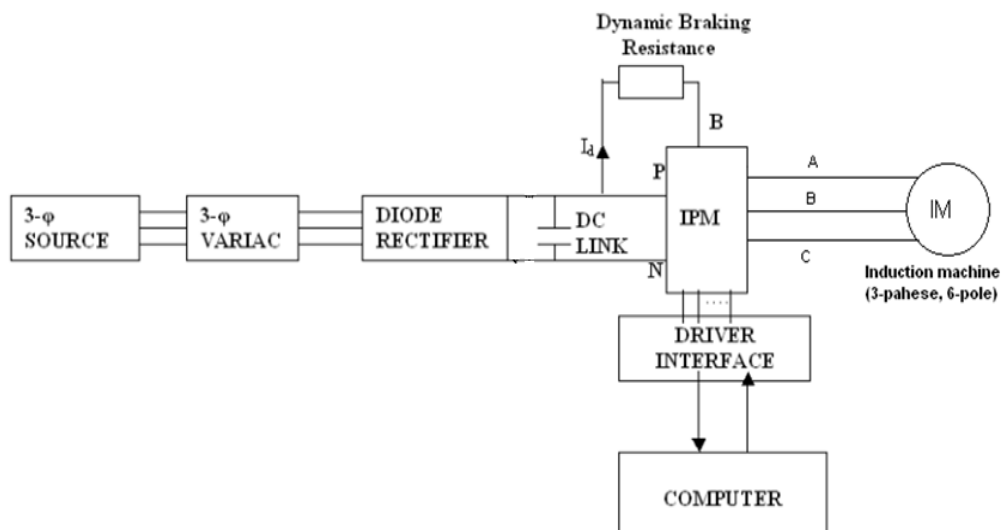


Figure 2. 38 – Experimental setup to observe the dc-link compensation

In Figure 2. 39, it is shown how dc-link voltage is measured by the help of voltage transducer and it is viewed on the computer via trace program of dsp1102 system.

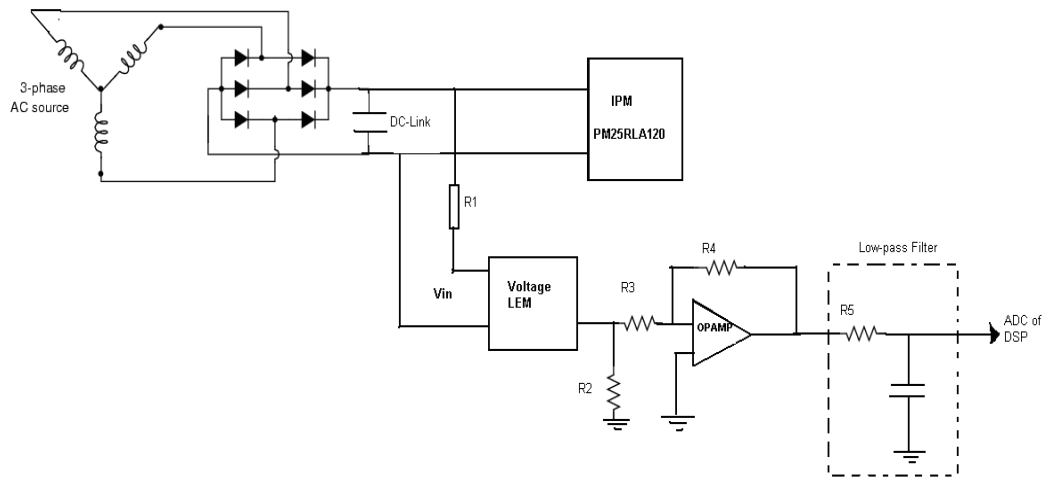


Figure 2. 39 – DC-link voltage measurement diagram

The measurement procedure and low-pass filter characteristics are explained in section 2.4.1.4. The algorithm used for dc-link compensation is as follows.

Software:

```

ds1102_ad_start();
udcolc=-632.15*ds1102_ad(1);    //measures dc-link
K=(kok3/2)*TS/udcolc;          //K is used at SVPWM  $T_k$   $T_{(k+1)}$  calculations.

```

udcolc : measured dc-link voltage variable.

K : variable which is used at the space vector pulse width modulation to calculate the duty cycles.

kok3 : $\sqrt{3}$

TS : control cycle of the software

Results of DC – Link Compensation:

In this part, results of experiments performed while K is taken as a constant value and while K is taken as a function of measured dc-link voltage will be presented.

Modulation Constant K is taken as a constant value:

In this section, the dc-link voltage is measured while the reference torque is changing between +2Nm to -2Nm for test machine #1 under no-load. While the positive reference torque is applied motor accelerates from 600 rpm to 1800 rpm and when the motor reaches 1800 rpm negative reference torque is applied to decelerate the machine to 600 rpm.

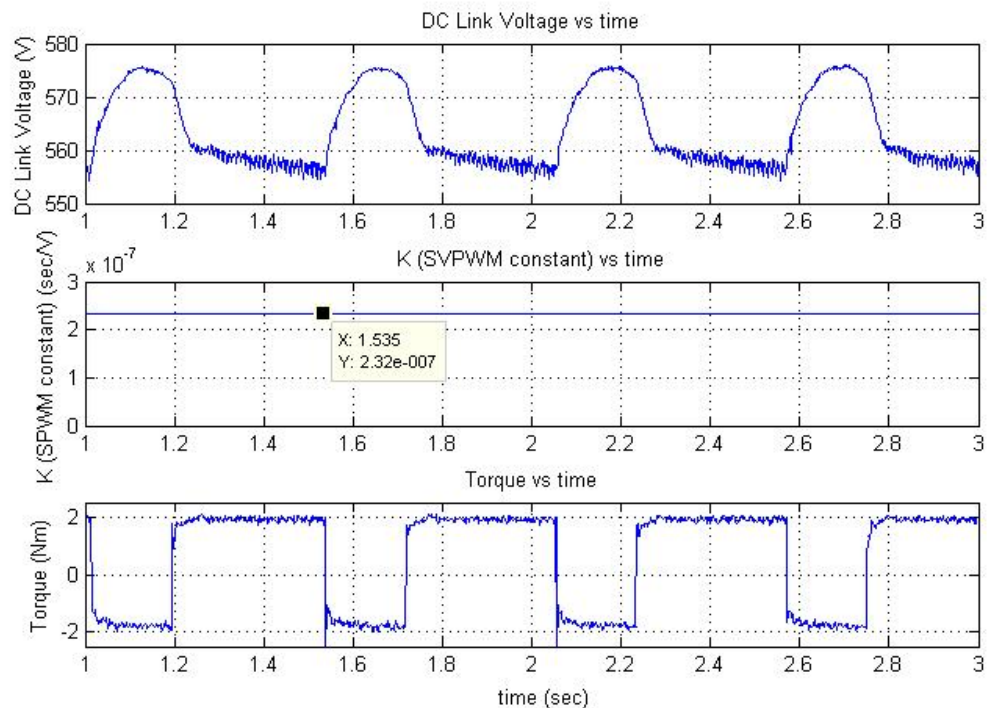


Figure 2. 40 – DC-link voltage, modulation constant K and Torque variations when the K is taken constant.

It is seen from Figure 2. 40, while the positive reference torque is applied dc-link voltage decreases about 3.5 volts. On the other hand, while the negative reference torque is applied for deceleration from 1800 rpm to 600 rpm dc-link voltage increases up to 575 volts from 557 volts. In this experiment, modulation constant K is taken as a constant value for dc-link voltage is equal to 560 volts. However, in this experiment, dc-link voltage is changing about 3% with respect to 560 V. As mentioned in section 2.4.1.9, modulation constant K directly effects the calculation of duty cycles. If the K is calculated for constant dc-link voltage, it is obvious that there will be 3% error in calculation of duty cycles. As a result of this, the error in calculation of duty cycles results in error at the output voltage with respect to given reference voltage. In conclusion, to obtain the reference voltage accurately at the output, it is very important to measure the dc-link voltage and update the modulation constant K with respect to that measured dc-link voltage.

Figure 2. 41 shows the resultant phase A, B voltages and currents waveforms where the modulation constant is calculated with respect to constant dc-link voltage.

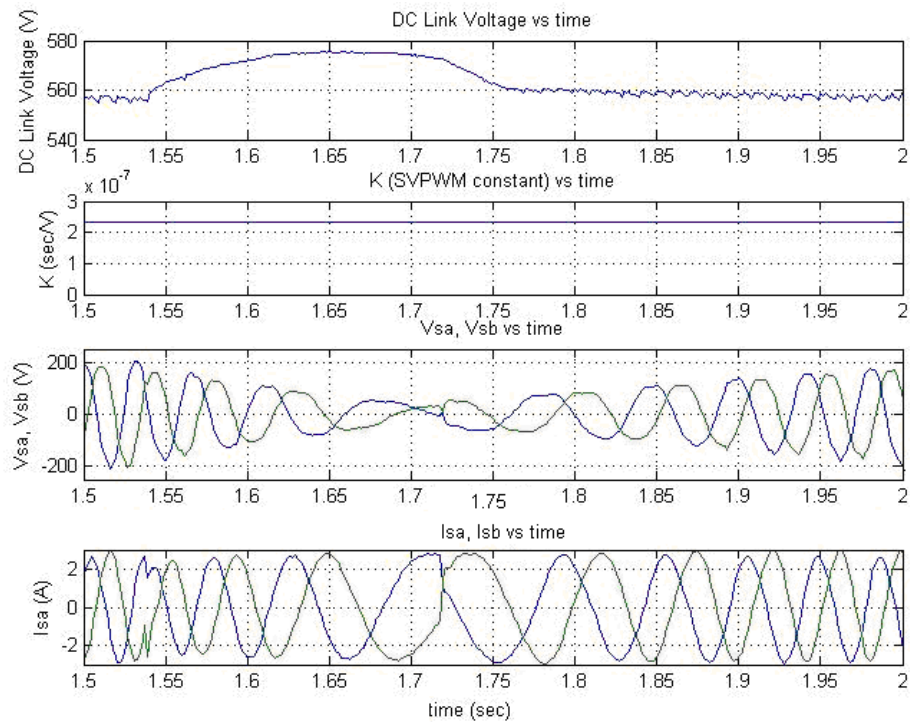


Figure 2. 41 - DC –link voltage, phase A and B voltages and currents and torque waveforms during the modulation constant is taken as a constant value.

Modulation Constant K is a function of DC-link Voltage:

In this section, same experiment is performed where the reference torque is again changed between +2Nm to –2Nm. This time modulation constant K is calculated as a function of measured dc-link voltage. Measured dc-link voltage is shown in Figure 2. 42.

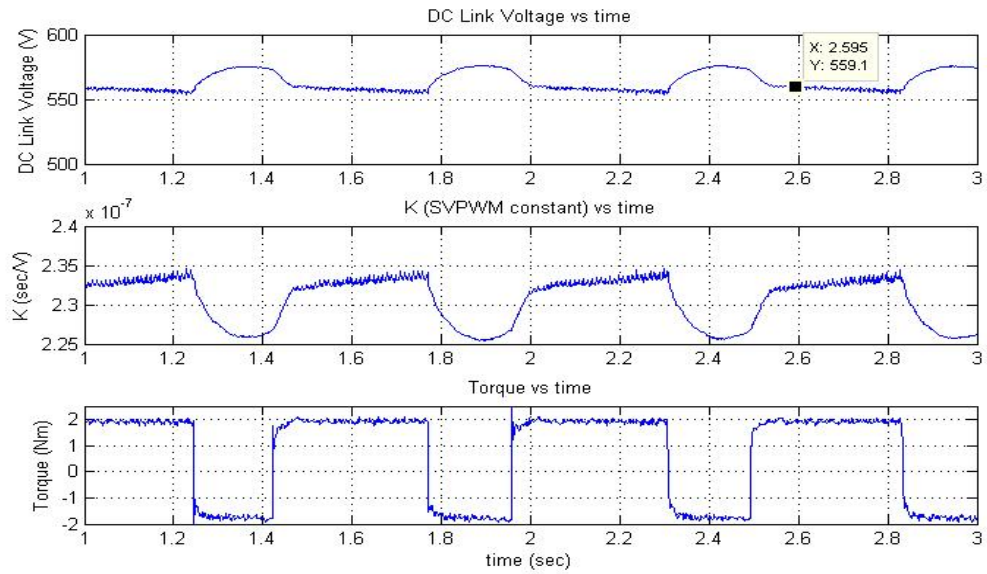


Figure 2. 42 – DC-link voltage, K modulation constant and Torque variations with updated K value.

It is seen from Figure 2. 42, modulation constant is updated at each control cycle with respect to the measured dc-link voltage. K is changing about 3% with respect to the value calculated for constant dc-link voltage.

Measured phase voltages and currents are also recorded during this operation and their waveforms are shown below in Figure 2. 43

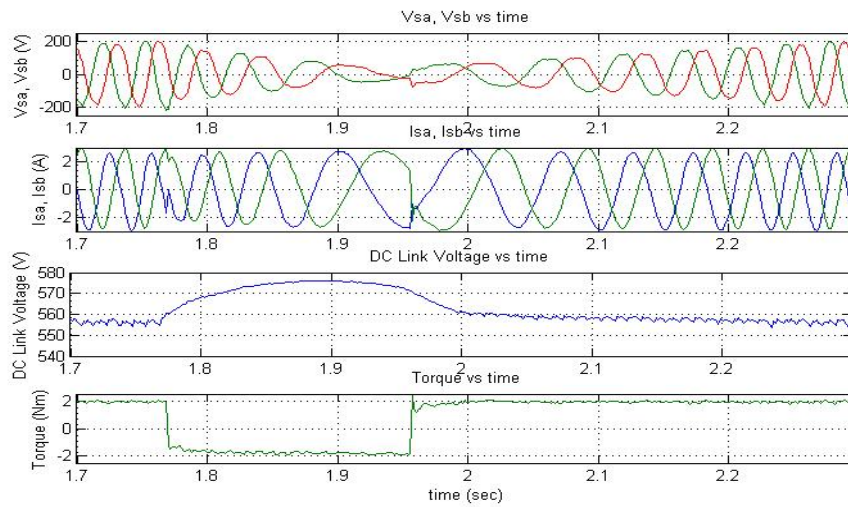


Figure 2. 43 – DC –link voltage, phase A and B voltages and currents and torque waveforms during the modulation constant is updated

If K is updated with respect to the measured dc-link voltage, more accurate duty cycles are obtained. As a result of this, more accurate reference voltages can be obtained.

In conclusion, in practice dc-link voltage is not constant. It changes related to the motor operation and load conditions. Therefore, modulation constant K shouldn't be taken as a constant value where the dc-link voltage is assumed constant. It is shown that dc-link voltage changes with respect to the motor operation, so modulation constant K must be taken as a function of measured dc-link voltage to obtain the reference variables at the output accurately. Dc-link compensation module is one of the important modules that improve the performance of the drive developed here.

Another improvement on the vector control drive is addition of dynamic braking facility to the drive. In the following section dynamic braking module developed in this thesis work will be explained.

2.4.1.14. Dynamic Braking Module

In dynamic tests, motor accelerates or decelerates from one speed to another speed. While motor is accelerating current flow is from driver to motor side, on the other hand when motor starts to decelerate with negative torque reference there will be a current flow from motor to the driver side. While motor is decelerating with negative reference torque stored energy in the motor flows to dc-link capacitors. Therefore, that excessive energy causes increase at the dc-link voltage. Since dc-link capacitors have a voltage limit, this excessive energy should be dissipated and the capacitor voltage should be limited at an acceptable level. Dynamic braking is the most known method to discharge that excessive energy and keep the dc-link voltage at acceptable level.

As an example, let me calculate how much excessive energy is produced while the test machine #1, used in this thesis, is driven to rotate between 600 rpm to 1800 rpm under no-load conditions. Excessive energy can be found by using the equation (2.61).

$$E = \frac{1}{2} J \cdot | (w_{final}^2 - w_{initial}^2) | \quad (2.61)$$

where;

$$w_{initial} = 1800 \text{ rpm} = 188,5 \text{ rad/sec}$$

$$w_{final} = 600 \text{ rpm} = 62,83 \text{ rad/sec}$$

$$J = 2,45 \cdot 10^{-3} \text{ kg.m}^2 \text{ (Inertia of the test motor \#1)}$$

After placing the values in equation (2.61) as follows,

$$E = \frac{1}{2} J \cdot (w_{final}^2 - w_{initial}^2) = \frac{1}{2} (0,00245) \cdot | (62,83^2 - 188,5^2) | \cong 38,69 \text{ Joules}$$

Now, what will be the final voltage level of the dc-link voltage if the motor is decelerating from 1800 rpm to 600 rpm will be calculated.

$$E_{capacitor} = \frac{1}{2} C \cdot (V_{final}^2 - V_{initial}^2) = \frac{1}{2} (0,0012) \cdot (V_{final}^2 - 560^2) \cong 38,69 \text{ Joules}$$

$$\Rightarrow V_{final} \cong 615 \text{ Volts}$$

$$C = 1.2 \text{ mF}$$

To observe the condition given in example, an experiment is performed on test machine #1. As in example given above the test motor #1 is driven to accelerate and decelerate between 600 rpm to 1800 rpm under no-load. While motor is accelerating +2 Nm reference torque is set and while motor decelerating -2 Nm reference torque is set. During this experiment dynamic braking module is kept in “off” state and dc-link voltage is recorded. In Figure 2. 44, recorded dc-link voltage is shown.

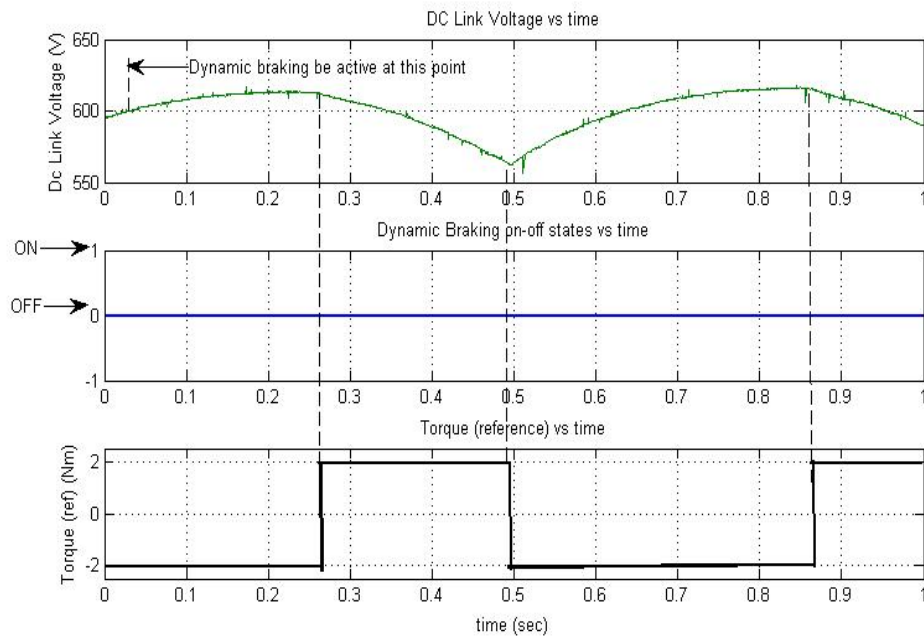


Figure 2. 44 – DC-link voltage variations while dynamic braking module is deactivated.

As you see from Figure 2. 44, while negative reference torque is applied where the motor is rotating from 1800 rpm to 600 rpm, dc-link voltage increases to 615 V as expected. Consequently, it is seen that at dynamic tests while motor is decelerating with negative reference torque, dc-link voltage increases and this increase is related to the system's inertia and decelerating speed range. To keep the dc-link voltage at desired level to be at safe, dynamic braking module is introduced for dynamic tests.

In dynamic braking module, a hysteresis band is selected for dc-link voltage where the dynamic braking module will be active. Lower limit of the hysteresis band is selected as 580 V and upper limit of the band is selected as 600 V so dc-link voltage is not desired to exceed 600 V level. Therefore, if dc-link voltage increases to 600 V dynamic braking will be active and excessive energy on dc-link capacitors will be dissipated on dynamic braking resistor until the dc-link voltage decreases to 580 V. The lower limit is selected as 580 V instead of near value to 560 V to avoid too many switching of braking transistor. Operation of the hysteresis band controller is given in Figure 2. 45.

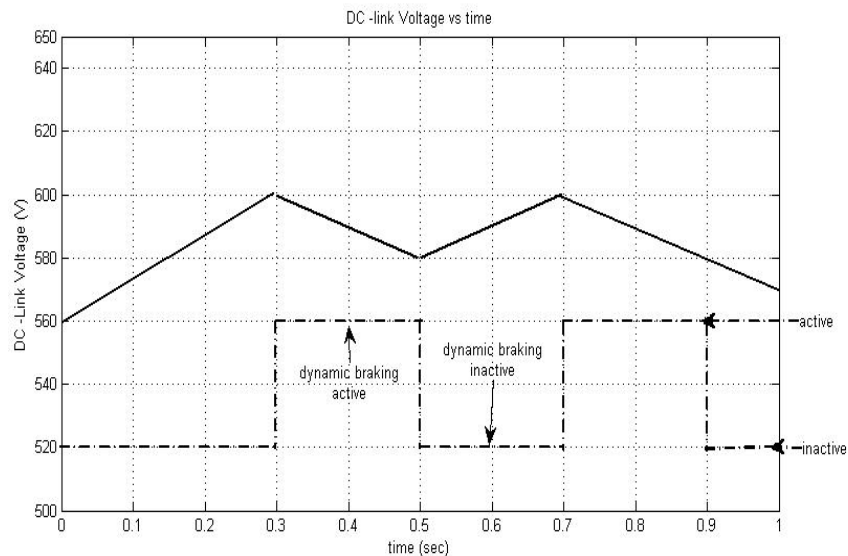


Figure 2. 45 – Theoretical DC-link voltage variations during the dynamic braking module is working with hysteresis band; 580 V-600 V

Selecting Dynamic Braking Resistance:

Rated Current value of Brake pin of IPM is: 10 A. However, in this thesis work braking current is set to about 5 A. It is mentioned that allowed maximum dc-link voltage is 600 V. According to those limitations I determine the value of dynamic braking resistance (R_D) as follows,

$$R_D = \frac{DC-linkVoltage}{DynamicBrakecurrent} = \frac{600}{5} = 120\Omega \quad (2.62)$$

By using that calculation, dynamic braking resistance is chosen as 124 ohms. Power rating of the this braking resistor is calculated as follows;

$$P_{R_D} = \frac{V_{DC}^2}{R_D} = \frac{600^2}{124} = 2903Watts \quad (2.63)$$

By using the result of equation 2.63, we can say that the power rating of the baring resistor should be about 3 kW.

Experimental Results:

An experiment is performed to see the dynamic braking module is working properly. Experiment is performed on test machine #1 under no-load conditions and -2 Nm reference torque is applied to decelerate the motor from 1800 rpm to 600 rpm. Dynamic braking module is wanted to be active when the dc-link voltage reaches to 600 V and decrease this voltage to 580 V level. Figure 2. 47 shows the recorded dc-link voltage with dynamic braking transistor's "on", "off" states. Braking IGBT and dynamic braking resistance is shown in Figure 2. 46

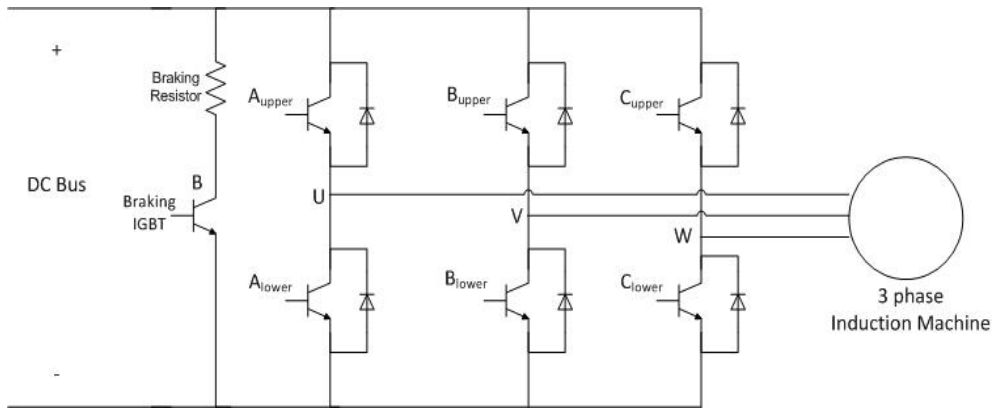


Figure 2. 46 – Schematic diagram of Inverter with Braking IGBT

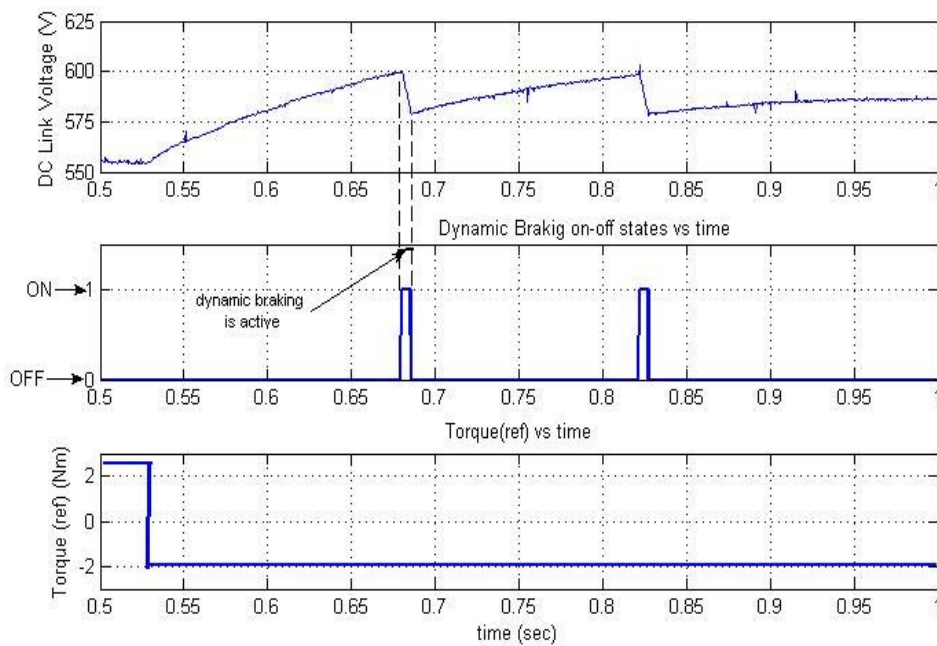


Figure 2. 47 – Recorded dc-link voltage during the dynamic braking module is active

As you see from Figure 2. 47, when the negative reference torque is applied dc-link voltage starts to increase and when it reaches to 600 V dynamic braking

module activates the dynamic braking IGBT so the excessive energy is dissipated on dynamic braking resistance until the dc-link voltage drops to 580 V.

During this experiment, dynamic braking current is recorded by using an oscilloscope. Figure 2. 48 shows that measured dynamic braking current. It is seen from this figure that the braking current is about 4.8 A as expected. Duration of current is about 25 msec.

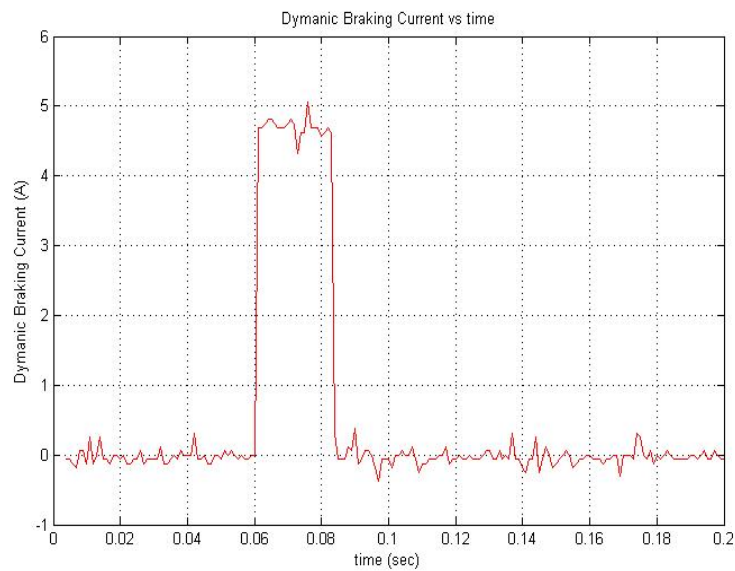


Figure 2. 48 – Current waveform on the dynamic braking resistance.

In the following part content of the software of dynamic braking module is given.

Dynamic braking software:

```
float dynbrkflag= 0;           //initialization of the variable
                                //dynbrkflag; determines the whether
                                //dynamic braking is active(1) or not
                                //(0).

if (dynbrkflag== 1)

ds1102_p14_pin_io_write(32);   // 32=(0000 0000 0010 0000)
else

    ds1102_p14_pin_io_write(32800); // this part makes the dynamic
                                        //resistor as a selective bit; if
                                        //dynbrkflag is active(1) it makes 0 the
                                        //16th bit of the ds1102, otherwise it
                                        //makes 16th pin 1.

ds1102_ad_start();           // starts the dsp analog digital pins

udcolc = -632.15*ds1102_ad(1)-1.13; //dc link is measured by the 2nd input
                                        //of the ad input of the ds1102; -
                                        //632.15 and-1.13 values are for the
                                        //calibration of the dc-link reading
                                        //correctly.

if(udcolc>=600)

{

    dynbrkflag=1;           //damps extra energy on the
                                //dynamic resistor if the dc-link
                                //voltage is more than 600 Volts.

    ds1102_p14_pin_io_write(0000); // makes all pins 0 (0000 0000 0000
                                        //0000), so excessive charges
                                        //dissipated over the energy damping
                                        //resistor.
```

```

}

if((udcolc<600)&&(udcolc>580)&&(dynbrkflag= = 1))

{

    ds1102_p14_pin_io_write(0000);    // dynamic braking is still active
                                        since the dc-link voltage is above the
                                        580 V. which is our desired dc-link
                                        value

}

if((udcolc<600)&&(udcolc>580)&&(dynbrkflag= = 0))

{

    ds1102_p14_pin_io_write(32768);    // If the dynbrkflag is inactive and
                                        the dc-link voltage is between 580
                                        and 600 volts, it continues to stay
                                        like that since the upper limit is 600
                                        volts for our dissipation value.

}

if((udcolc<=580)

{

    ds1102_p14_pin_io_write(32768);    // if the voltage is under the 580
                                        volts, there is no need to use dynamic
                                        braking since we are in the safe
                                        region as an dc-link voltage value.
                                        Finally make the dynbrkflag zero.

    dynbrkflag=0;

}

```

2.5. Conclusion

In conclusion, in chapter 2 the hardware and software environment are explained in detail.

In the hardware section, what kind of pulses required to drive the inverter are shown, then starting from dsp card, it is explained how that pwm signals came to desired shape. Following that, isolation module and power stage of the inverter is explained. Finally how the voltage and current measurements are taken and how they are used in the program are shown in the measurement stage of the hardware part.

As a second part of this chapter, software environment is explained in modules. Each module is explained with theory background them and supported with some graphs. In this thesis work, in addition to previous studies on vector control drives, dc-link compensation and dynamic braking modules are added. Test results of those modules are shown in the related modules of software part.

In future, to improve the drive, there should be new dsp cards producing symmetrical pwm signals and working under MATLAB program. For software part it will be nice to prepare a user interface for those modules.

CHAPTER 3

OFF LINE PREDICTION OF LEAKAGE INDUCTANCE

3.1. Introduction

In this part, we shall concentrate on methods for determination of the leakage inductance of an induction motor for self-commissioning. In the literature quite a number of studies exist which address the self-tuning problem [18-21]. One of the solutions for the offline estimation of the stator leakage inductance is applying a series of voltage pulses to the machine and measuring stator transient time constant [20]. The highest level of current in this method is at most 30% of the rated current; however rated flux or current should be present during estimation process for more realistic results. In [14], a complex voltage waveform is applied to the machine during the estimation of the stator leakage inductance; hence this method requires a powerful microcontroller and complex hardware. There are other methods that require high performance hardware for the calculation of the stator leakage inductance [15, 16] The method in this thesis is much simpler and efficient than the methods mentioned above for stator leakage inductance estimation. In short its advantages are as follows:

- Estimation can be performed at rated flux or current, hence its results are realistic [10];
- The region where the estimation is performed is much longer than the software control cycle to take enough number of current samples, thus enabling the automated estimation [15];
- This method creates little computational burden for the microprocessor; extra hardware is not needed [15, 16];

- Current measurement, used for leakage inductance measurement, is a noise free signal [10, 13] (the phase is short circuited during the measurement and the current measured is DC); this method works even for the motors with low stator phase voltages, for which parameter estimation is particularly difficult [17].

In the following section, first the theory behind the proposed algorithm is introduced. Following this, the offline leakage inductance predictions using the proposed approach on 3-phase induction motors will be given and compared with the conventional measurement findings. The basic label data of the test motors are given in Table 3. 1. To determine the motor parameters and rotor time constants of test motors, standard no-load and locked rotor tests are performed on each motor. These test results are presented in the Appendix C.

Table 3. 1 - The Test Motor Data

Rating	Power rating (kW)	poles	Rated current (A)	Voltage (V)	Rotor time constant (ms)	Rated Rotor Flux (Wb)	Rated I_{sd} (A)
Test Motor							
1	1.0	2	2.7	380 Y	64.3	0.90	2.40
2	1.1	6	3.1	380 Y	44.2	0.77	2.50
3	2.2	2	4.8	380 Y	129.7	0.87	2.26

3.2. Theory of Off-Line Prediction of Leakage Inductance

Stator transient inductance term (σL_s) refers to the inductance value measured from stator winding terminals.

This term is defined by the following equation 3.1[1]:

$$\sigma L_s = \frac{L_{ls} L_{lr} + L_m (L_{ls} + L_{lr})}{L_m + L_{lr}} \quad (3.1)$$

Where, L_{ls} and L_{lr} are stator and rotor leakage inductances, respectively; and L_m is the magnetizing (mutual) inductance. With the assumption of $L_m \gg L_{lr}$, usually, stator transient inductance (σL_s) is considered as the sum of stator and rotor leakage inductances. When the machine is not energized and the initial flux is zero at standstill, reference d-axis current (I_{sd}) is applied to the machine. As a result of this reference current dc current is applied to the phase A, so initial flux is established. During the leakage inductance estimation motor is at standstill, which is the reason why we called this method as off-line leakage inductance estimation.

The proposed stator transient inductance measurement method relies on forcing a user-defined dc current through the stator phase windings for short time duration. This current establishes the flux in the motor. Note that; applying a controlled current assures that the motor and the inverter is not subjected to over currents [12]. After the rotor flux is built up to the desired value; the stator phase windings are short-circuited with the aid of the inverter switches, As soon as the stator phases are short-circuited, stator phase voltages decrease to zero and the stator phase currents start to decrease. At this condition, the stator voltage (V_s) and rotor magnetizing current (I_{mr}) are shown at Figure 3. 1 and related equations are given by the following equations [10]:

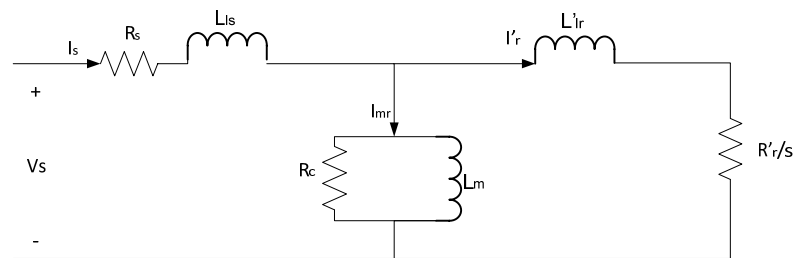


Figure 3. 1 – Equivalent Circuit of Induction Machine

$$I_{mr} = \frac{\psi_r}{L_m} \quad (3.2)$$

$$U_s = R_s I_s + \sigma L_s \frac{dI_s}{dt} + (1 - \sigma) L_s \frac{dI_{mr}}{dt} \quad (3.3)$$

Where, R_s is the stator resistance, I_s is the stator phase current, and ψ_r , is the rotor flux.

A typical variation of the phase current after the short circuit is shown in Figure 3. 2. A short time interval right after short-circuiting a phase is called the "sub-transient region" (this interval is much shorter than the rotor time constant, see Table 3. 1). Since the rotor flux is a slow changing variable, in the sub-transient region, the change in the rotor flux may be neglected and it may be assumed that the flux stays at the value set by the drive [2]. In that case the last term in equation 3.3 may be assumed to be zero.

To prove this point, a simulation is implemented for the test motor #1 whose rated flux is 0.9 Wb, shown at Table 3. 1. Matlab – Simulink simulation program is used to show that rotor flux remains nearly constant during the shorting period. Induction motor model is selected and the parameters of test motor #1 is defined for that simulation model motor. Firstly, dc-voltage is applied to stator terminals of the motor and then it is suddenly shorted. Related phase voltage, current and rotor flux is given at Figure 3. 2. It can be easily seen from that figure the change in the flux is very small and therefore our assumption holds. This situation is the same for other test motors since their rotor time constants (see Table 3. 1) are very large with respect to the measurement period. Therefore, Equation (3.2) may be simplified and take the form shown in (3.4). σL_s (stator transient inductance) may be calculated using this equation, provided that the stator resistance (R_s) is known and the stator current is measured.

In the application here, phase voltages and currents are measured with voltage and current transducers and those measured signals are sent to DSP card after filtered by low-pass filter whose cut off frequency is about 2 kHz (see Figure 3. 6). The measurement process is explained at section 2.3.4 of chapter 2 in detail.

$$U_s = R_s I_s + \sigma L_s \frac{dI_s}{dt} \quad (3.4)$$

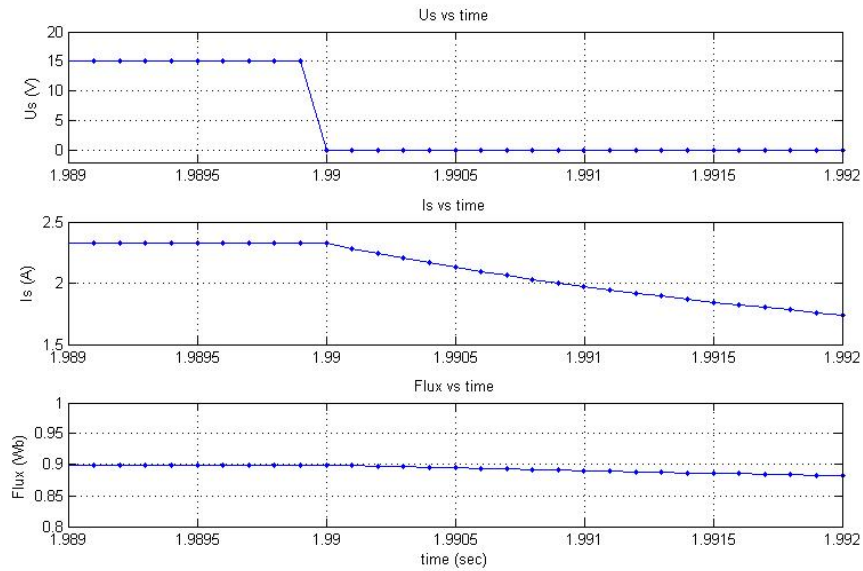


Figure 3. 2 – Rotor flux change during the sub-transient period.

Suppose that the stator current is measured at every Δt seconds. In this case, dI_s may be approximated by the difference of the two consecutive measurements of current, namely between $(n)^{\text{th}}$ and $(n-1)^{\text{th}}$ measurements. Therefore, Equation (3.4) may be written as in (3.5) and each variable is measured or calculated at every Δt seconds.

$$U_s(n) = R_s I_s(n) + \sigma L_s(n) \frac{(I_s(n) - I_s(n-1))}{\Delta t} \quad (3.5)$$

$$\sigma L_s(n) = \frac{(U_s(n) - R_s I_s(n)) \Delta t}{(I_s(n) - I_s(n-1))} \quad (3.6)$$

In the application here, σL_s is calculated "n" times (10 times here), in successive 0.1 ms intervals using (3.6). Since the stator resistance is known (can be measured via some well-known method), L_{ls} is easy to calculate.

As mentioned before, usually $L_m \gg L_{ls}$ and $L_m \gg L_{lr}$, σL_s can be assumed to be sum of L_{ls} and L_{lr} from using the equation (3.1). In addition to this, we know that in squirrel cage induction machines L_{lr} is assumed to be equal to L_{ls} . by using those assumptions equation 3.1 becomes as follows.

$$\sigma L_s(n) = L_{ls} + L_{lr} = 2.L_{ls} \Rightarrow L_{ls} = \frac{\sigma L_s}{2} \quad (3.7)$$

3.3. Experimental Results of Off – Line Prediction of Leakage Inductance

In the Figure 3. 3 you see the experimental setup which is used to drive the motor until its rated flux value and take measurements from motor to estimate the off-line leakage inductance value.

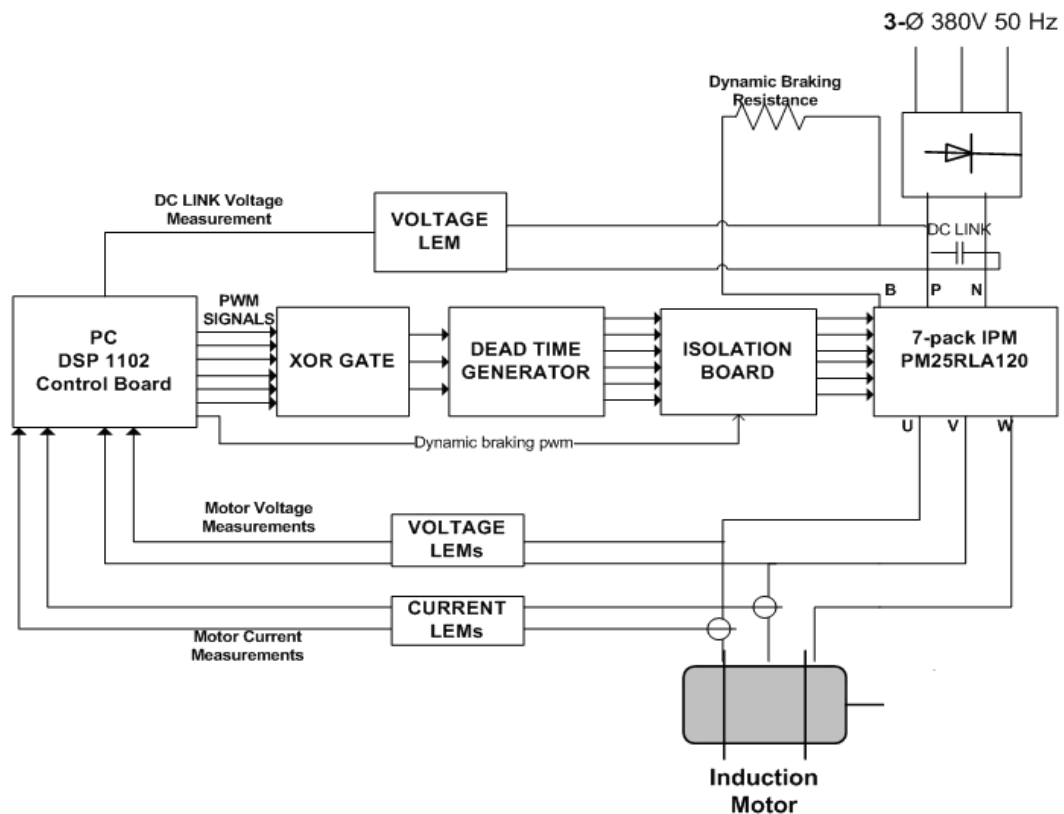


Figure 3. 3 – Experimental Setup to estimate the off line leakage inductance

Experiments are done on 3 different test motors whose parameters are listed at Table 3. 1 which is given at the beginning of this chapter. In the off-line leakage inductance estimation experiments, 2 phase voltages and 2 phase currents are measured, since all test motors are Y-connected and star point is available for all of them. For Δ -connected motors the same prediction is valid; however some transformations are matched to obtain phase values from line-line measurements. Measurements are taken for each 100 μ sec. and all measurements are filtered by a low-pass filter where its cut-off frequency is about 2 kHz. In those experiments dc-link voltage is kept at 300 V. All recorded data captured by using trace31 program which is a signal monitoring recording program of DS1102 environment.

In the off-line leakage inductance estimation algorithm, DC voltage is applied to the motor until the flux reaches rated flux value; in this period only dc voltage is

applied to the machine so it is at standstill. The time to achieve rated flux for each motor is selected as 1 sec. Since the maximum rotor time constant is about 130 msec and it is enough to wait about 5 times rotor time constant to reach the steady state value for rated rotor flux value, 1 sec. is therefore appropriate for all 3 test motors to obtain rated flux value. Once the rated flux level is reached the terminals which are U, V, W of the 7-pack IPM are shorted by sending pulses to lower side switching elements which are shown at Figure 3. 4. By shorting the stator terminals of the machine, dc voltage at stator terminals begins to fall to zero and stator current also begins to fall to zero. The estimation process starts when the phase voltage drops under zero and after making 10 estimations the process stops. The measurement and calculation is made every 100 μ sec so it takes 1 msec to access the final leakage inductance estimation value. The final off-line leakage inductance value is taken as average of those 10 estimated data.

The U, V, W terminals, upper and lower IGBTs are shown at Figure 3. 4. To make the U, V and W terminals shorted lower side IGBTs are made “on” and upper side IGBTs are made “off”, accordingly stator terminals of the induction machine becomes shorted.

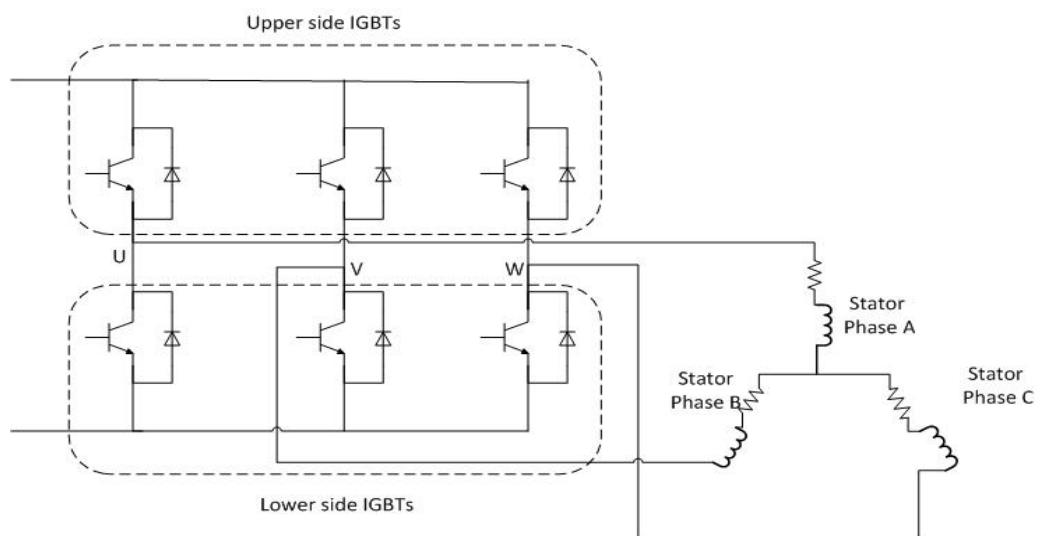


Figure 3. 4 – Inverter connected to the induction machine

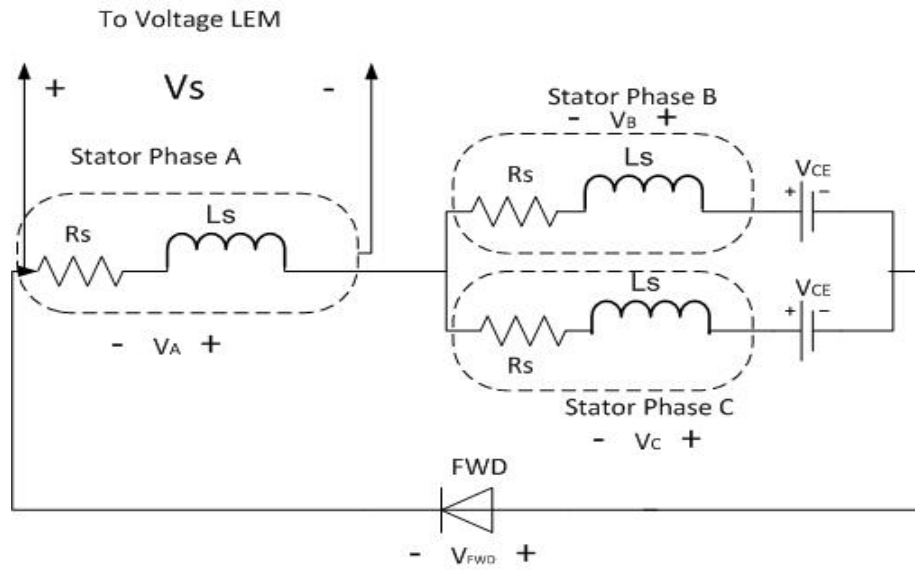


Figure 3. 5 – Equivalent circuit of induction machine when lower side IGBTs are shorted

As you see from the Figure 3. 9 voltage falls under zero about to 2.5 – 3 volts. The reason for that is; when IGBTs at lower side are shorted there will be voltage drop across the free wheeling diode which is shown at Figure 3. 5. The voltage drop at those diodes is typically 2.5 volts for PM25RLA120 which is the intelligent power module (IPM) used in this application. In addition to this, the voltage drop on the collector-emitter terminals of transistors is about 1V for current flow of about 2.5 Amps when they are in the on state. The datasheet of this IPM is presented in the Appendix B. Below it can be seen how much the stator phase voltage goes under zero when the lower side IGBTs are shorted.

$$-V_A - V_B + V_{CE} + V_{FWD} = 0 \quad (3.7)$$

where, $V_B = V_C = V_A/2$ since all phases are identical, so let's say $V_A = V_s$ which is a phase voltage when the lower side IGBTs are shorted, so, $V_B = V_s/2$ in addition to these, $V_{CE} = 1 \text{ V}$ and $V_{FWD} = 2.4 \text{ V}$ from datasheet of PMR25RLA120. When those data are placed in the equation 3.7 it can be found that, the expected phase voltage is about -2.27 volts.

$$-V_s - \frac{V_s}{2} + 1 + 2.4 = 0 \Rightarrow V_s = 2.27 \text{ Volts}$$

Since the polarity of the measurement of phase voltage is reversed for this situation, the measured phase voltage is found to be -2 Volts when the data is recorded.

In recorded data it can be observed that the phase voltage does not drop to zero voltage suddenly, there is a delay about 200-300 μsec . since the motor terminals are shorted suddenly, we know that the phase voltage should become zero just after shorting switching elements. On the other hand, there is a low-pass filter which is used to clear the noise on the measurements. That delay comes from the characteristics of this analog RC filter.

In Figure 3. 8, the step response characteristic of this filter is shown. Results are obtained from Matlab-Simulink simulation program.

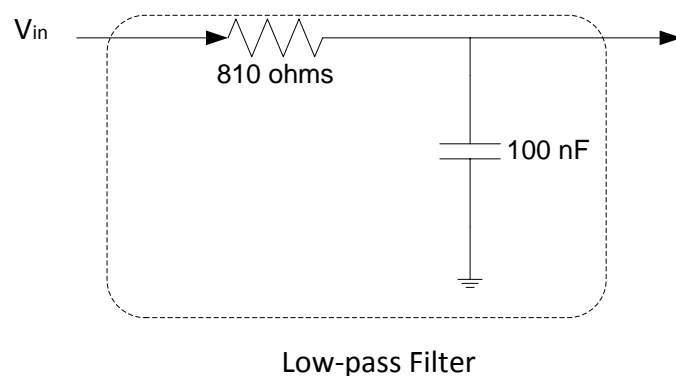


Figure 3. 6 – Low-pass filter used to clear noises on the measurements.

The transfer function of the filter shown at Figure 3. 6 is represented as H(s):

$$H(s) = \frac{V_{in}(s)}{V_{out}(s)} = \frac{1}{8.1 \times 10^{-5} s + 1}$$

In the simulation the step response of this transfer function is simulated, simulation step time is taken as 100 μ sec, which is same as the algorithm's sample time.

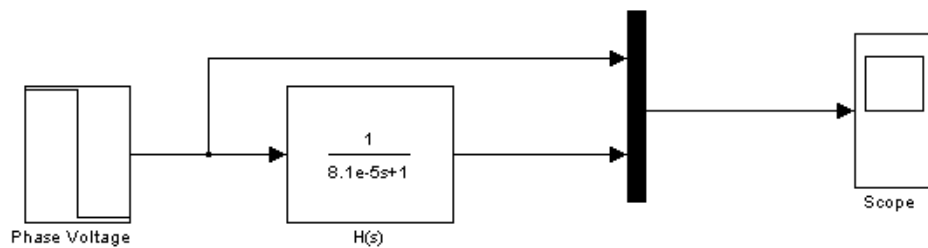


Figure 3. 7 – Setup used in the Simulink to simulate the transfer function characteristic

Input voltage is set to 12 volts which is required to obtain initial rated flux value for test motor #1 (see Figure 3. 9), then it is switched to zero. In Figure 3. 8 it can be observed that the phase voltage drops to zero volt about 300 μ sec.

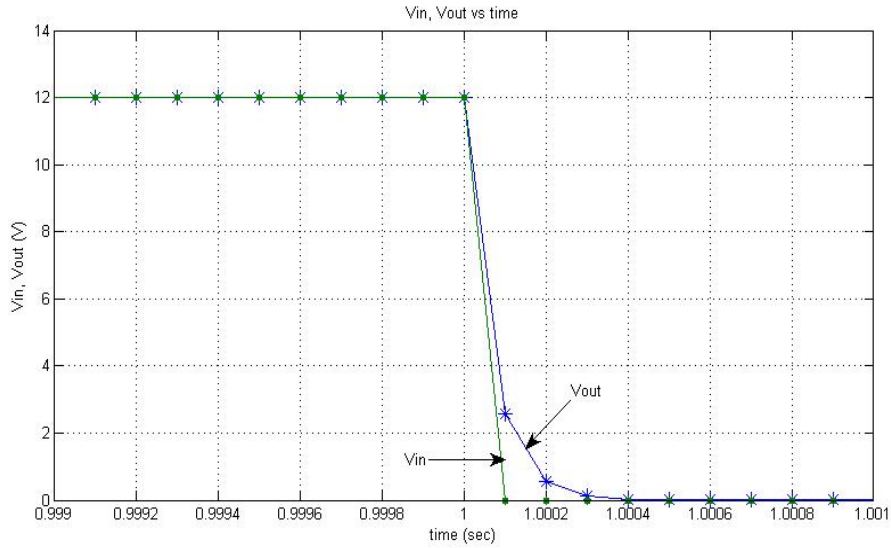


Figure 3. 8 – Step response of low-pass filter used in the measurements

It can be seen from Figure 3. 8, the delay due to low-pass filter is about 300 μ sec. For this reason estimation must start at least after 3 measurement period so that the estimation of leakage inductance is not affected from low-pass filter's delay. The detailed characteristic of this filter was shown in section 2.3.4. of Chapter 2. As discussed there this filter does not have any considerable affect on the signals having fundamental frequency less than 100 Hz. Therefore this delay does not appear in measuring the voltage or current signals under normal operating conditions.

3.3.1. Off Line Leakage Inductance Measurement for Test Motor #1

The recorded phase voltage and current waveforms for test motor #1 are presented in Figure 3. 9. Typically estimation starts when phase voltage V_s falls to negative value and it ends after 10 successive off-line leakage inductance estimations are performed. Note that, the measurement process lasts 1 ms where the rotor time

constant of this motor is 64.3 ms, therefore the rotor flux remains virtually constant during the measurement.

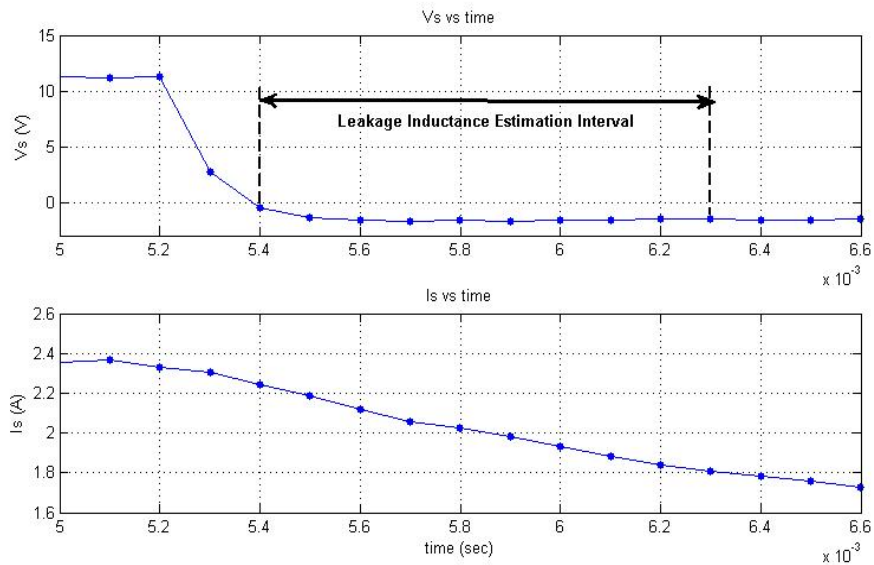


Figure 3. 9 – Measured data for Leakage Inductance Prediction for test motor #1.

Table 3. 2 – Parameters used in the estimation of 1st machine’s leakage Inductance

time(ms)	5,3	5,4	5,5	5,6	5,7	5,8	5,9	6,0	6,1	6,2	6,3	6,4
Vs (V)	11,25	2,72	-0,46	-1,43	-1,62	-1,71	-1,64	-1,76	-1,62	-1,57	-1,49	-1,55
Is (A)	2,33	2,31	2,24	2,19	2,12	2,05	2,03	1,98	1,93	1,88	1,84	1,81
σL_s (mH)			17,19	20,38	15,38	17,13	39,88	23,46	19,96	20,43	24,09	29,26
Lls (mH)			8,59	10,19	7,69	8,56	19,94	11,73	9,98	10,22	12,04	14,63
Average Lls (mH)	11,36											
Measured (Conv.) Lls (mH)	11,70											
Error (%)	2,9											

The measured phase voltage, current and estimated leakage inductance values are presented in Table 3. 2. At the end of the estimation period, the average value of all those 10 estimated leakage inductance values is taken as the final estimation. For this machine average value of the estimated leakage inductance values is 11.36 mH.

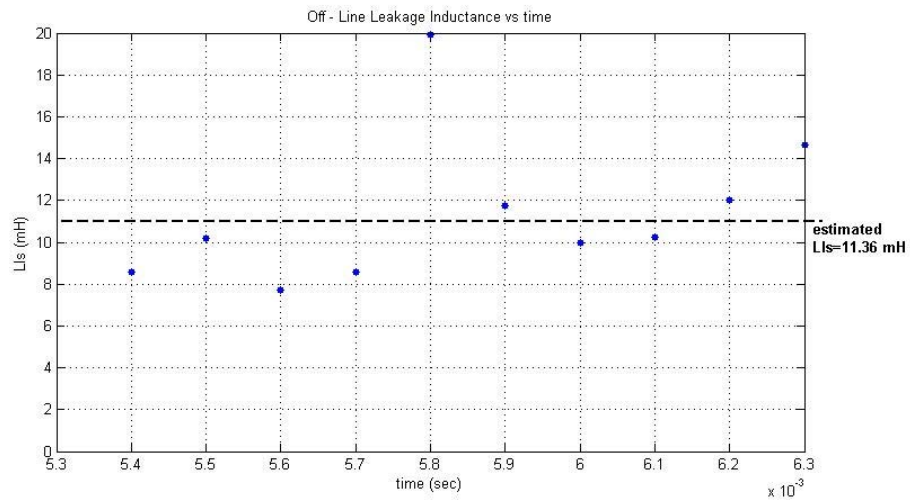


Figure 3. 10 – Estimated leakage inductance in the measurement period for the test motor # 1.

The measured leakage inductance from conventional methods is 11.7 mH. There is an error about 2.9% which is acceptable. As it can be seen in the Figure 3. 10, there is a scattering of the estimated leakage inductances. This is because the time interval in the difference equations is just 100 μ sec. Therefore, measurement errors are magnified. However, by averaging estimated points eliminates the disadvantages of inherent in taking derivative. This is obvious from the very good estimation results for all 3 test motors. (see Table 3. 1)

3.3.2. Off Line Leakage Inductance Measurement for Test Motor #2

In this part the off – line leakage inductance measurement method, described in section 3.3, is applied to test motor #2. Leakage inductance of this test motor was found as 29.75 mH from the conventional methods; no-load test, locked rotor tests.

The recorded phase voltage and current are presented at Figure 3. 11, where the leakage inductance estimation interval is also shown. This estimation interval is taken same for all 3 machines as 10 data points after the phase voltage drops to negative value.

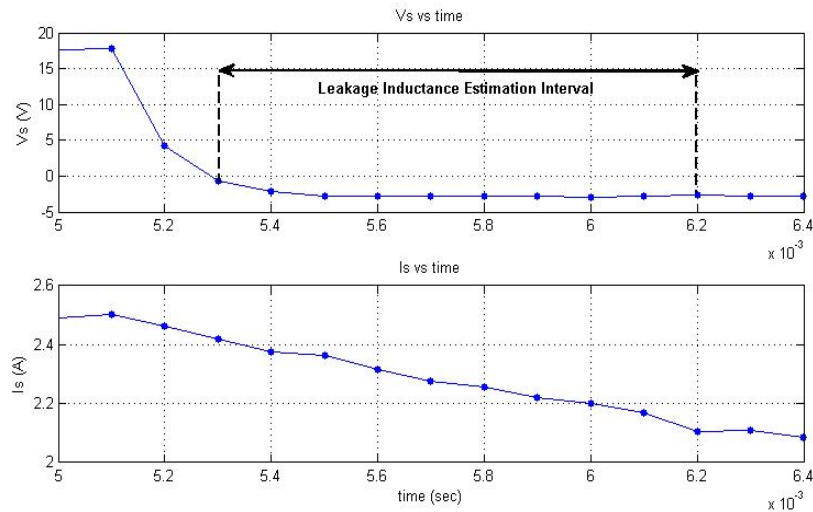


Figure 3. 11 - Measured data for Leakage Inductance Prediction for test motor #2.

Table 3. 3 - Parameters used in the estimation of 2nd machine's leakage Inductance

time(ms)	5,3	5,4	5,5	5,6	5,7	5,8	5,9	6,0	6,1	6,2	6,3	6,4
Vs (V)	17,86	4,29	-0,62	-2,08	-2,74	-2,85	-2,81	-2,85	-2,81	-2,94	-2,80	-2,58
Is (A)	2,50	2,46	2,42	2,37	2,36	2,31	2,28	2,26	2,22	2,20	2,17	2,10
σ Ls (mH)			35,14	38,88	160,5	35,78	43,93	93,44	47,57	72,50	51,97	24,97
Lls (mH)			17,57	19,44	80,27	17,89	21,97	46,72	23,78	36,25	25,98	12,48
Average Lls (mH)	30,24											
Measured (Conv.) Lls (mH)	29,75											
Error (%)	1,65											

The measured phase voltage and related phase current values are presented at Table 3. 3. Besides, all 10 estimated leakage inductances are also listed in the same table for this machine.

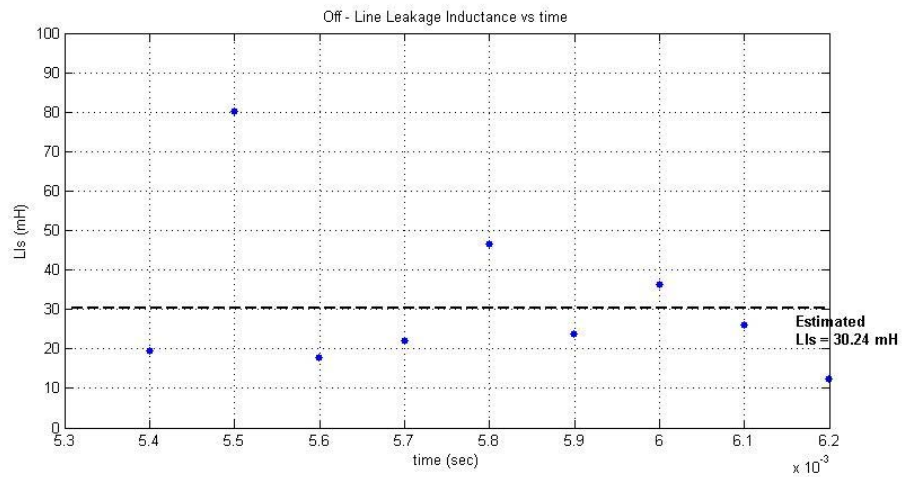


Figure 3. 12 - Estimated leakage inductance in the measurement period for the test motor #

2.

The estimated off-line leakage inductance values are plotted in Figure 3. 12. The average value of estimated leakage inductances for this machine is 30.24 mH where the leakage inductance was found 29.75 mH from conventional methods. Estimation error is under 2% which is in the acceptable region.

3.3.3. Off Line Leakage Inductance Measurement for Test Motor #3

Lastly, off – line leakage inductance estimation algorithm is applied to another machine named here as test motor #3. Typical recorded phase voltage and current values are shown in the Figure 3. 13.

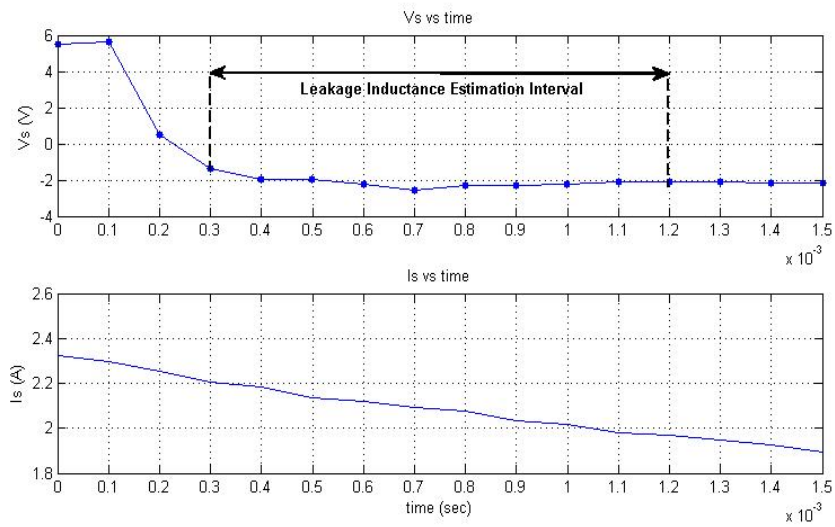


Figure 3. 13 - Measured data for Leakage Inductance Prediction for test motor #3.

Table 3. 4 presents the measured phase voltage, phase current and the estimated leakage inductance values for 3rd machine. The average value of the estimated leakage inductances is taken as a final estimated leakage inductance like at

previous motors. In Figure 3. 14 those 10 estimated off-line leakage inductance values and the average value of those are presented.

Table 3. 4 - Parameters used in the estimation of 3rd machine's leakage Inductance

time(ms)	0,10	0,20	0,30	0,40	0,50	0,60	0,70	0,80	0,90	1,00	1,10	1,20
Vs (V)	5,66	0,47	-1,34	-1,94	-2,00	-2,22	-2,58	-2,29	-2,29	-2,24	-2,09	-2,07
Is (A)	2,30	2,24	2,21	2,19	2,16	2,12	2,09	2,07	2,04	2,01	1,98	1,96
σ Ls(mH)			23,10	24,36	23,82	21,88	24,92	32,68	21,88	26,04	22,64	34,20
Lls(mH)			11,55	12,18	11,91	10,94	12,46	16,34	10,94	13,02	11,32	17,10
Average Lls (mH)	12,78											
Measured (Conv.) Lls(mH)	13,14											
Error (%)	2,74											

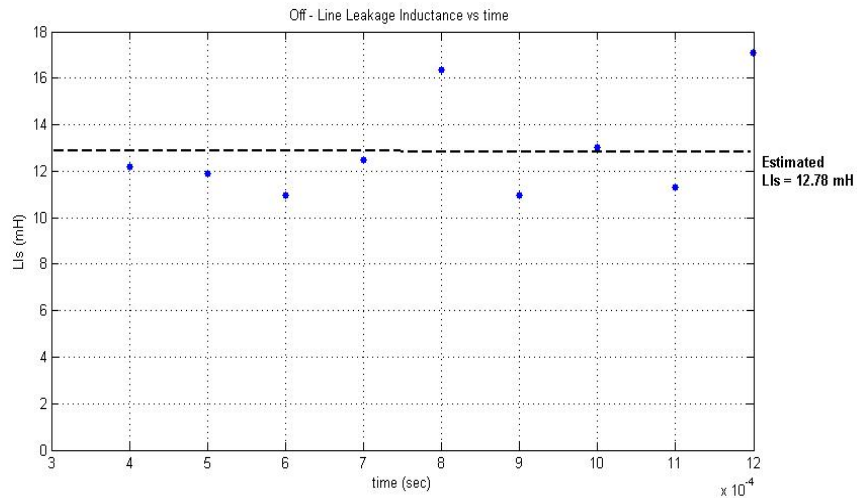


Figure 3. 14 - Estimated leakage inductance in the measurement period for the test motor # 3.

It is seen from Figure 3. 14 the average value of the estimated leakage inductance is 12.78 mH and the leakage inductance found from the conventional methods is

about 13.14 mH. It can be said that the estimated leakage inductance and the measured value from conventional methods are close to each other and the error is less than 3%. Thus, we can use this estimated leakage inductance value in our calculations.

3.4. Conclusion

During the measurement first few data points are not used in the calculation to avoid the delay effect of the filters that could lead to computational errors. The calculations are done for the following 10 measurements. Table 3. 5 shows the comparison of the estimated leakage inductance and measured leakage induction values. The average of the estimated leakage inductance values is assumed to be the predicted value. The scattering in the data points is due to the difference term in Eqn. 3.6. The error is under 3% which is pretty good result. The predicted and measured values for the other two test motors are given also in Table 3. 5. It is obvious that the prediction error can be reduced if the scattering in the calculations can be reduced by filtering the data in some way. Since conventional measurements are also obtained from experiments the results depend on to measurement accuracy.

Table 3. 5 – Comparison of Conventional and Proposed Leakage Inductance Measurement Results

Test motor	Stator leakage inductance(mH)		Error (%)
	Proposed off-line measurement algorithm	Conventional measurement	(Estimated ind. – Conventional ind)x100 / (conventional ind.)
1	11.36	11.70	2.9 %
2	30.24	29.75	1.65 %
3	12.78	13.14	2.74 %

It may be possible to reduce the scattering of the estimate data by extending the period in which the difference equation is calculated. However, even with the raw processing applied here the prediction accuracy is very good.

Since this approach is used for off-line leakage inductance prediction, the duration of 1 msec. is more than acceptable.

The leakage inductance is not load current dependent so normally, it is not necessary to update it for vector controlled applications. If however, it is desired to use leakage inductance values for some other purpose, a faster estimation algorithm is necessary and this requires further research.

CHAPTER 4

ON-LINE STATOR RESISTANCE ESTIMATION METHOD

4.1. Introduction

For both the rotor and stator-flux oriented vector control methods; which are based on the "voltage model", accurate estimation of feedback signals (e.g. flux vector, speed, and frequency) is very important. The variation of the stator resistance with temperature therefore is especially very important in the prediction process. The estimation error becomes even more important near zero speed, where the stator resistance voltage drop tends to be comparable with machine counter-electromotive force (EMF). Therefore, some means of accounting for the resistance variation due to temperature is essential. One method for correctly estimating the resistance value during operation is placing temperature-sensing thermistors in the stator winding in a distributed manner and measuring the average stator winding temperature. Once the temperature of the winding is known, estimating the stator resistance becomes a simple matter, given its value at a known temperature [16]. However, the use of such sensors in a sensorless drive is not acceptable. Another method for online estimation of the stator resistance, based on the zero sequence model is presented in [18]. The proposed method here provides an estimation of the stator resistance that does not require the knowledge of any other parameter and is independent of the drive control strategy. The method requires the measurement of the line voltages and currents. If the neutral wire is available, estimation also can be done by using phase voltages and

currents. Transformations related with line measurements or phase measurements were given in section 2.4.1.6 of Chapter 2.

Ha and Lee proposed a novel online identification method that can be used for estimating both R_s and R_r [19]. In this approach a small magnitude and low frequency AC component is injected to the flux command. Their identification algorithm for R_s is motivated from the steady state power flow between stator and rotor through the air gap. This method can be applied only under steady state conditions. Furthermore the injected low frequency signal may cause problems at low speed. The estimation scheme reported in [20] uses a model reference adaptive approach with proportional-integral controllers. The difference between the measured and observed current is an input for the estimation system. [21] describes also a stator resistance estimation method developed in conjunction with the rotor – flux based MRAS (Model Reference Adaptive System) speed estimator and it operates in the stationary reference frame. Moreover, the error quantity is formed on the basis of differences in rotor flux component values, obtained at the output of the reference and the adjustable model.

Another method for stator resistance estimation is utilizing artificial neural networks [22]. The error between the measured stator current and the estimated stator current using neural network is back propagated to adjust the weights of the neural network.

The method proposed here is simple and promises to eliminate the disadvantages of available resistance estimation methods.

4.2. The Field Orientation Control Method

The stator resistance estimation algorithm in this thesis is developed for a drive using "voltage model" for vector control. As it is well known the "voltage model" approach requires the stator resistance and leakage inductance to be estimated

accurately. This section briefly describes the vector control method used in this thesis. However, on-line stator resistance estimation method developed here works also under scalar control (V/f method). In an induction machine the torque is a function of both the stator and rotor currents, also when stator current is controlled both the rotor flux and torque values are affected. Hence, a direct control of torque with stator currents becomes impossible [23]. However, by transforming the three phase system (a-b-c) into stationary (α - β) and synchronously rotating (d-q) reference frames by using Clarke and Park transformations respectively and coinciding the d-axis and rotor flux (ψ_r); the electrical torque equation becomes as follows:

$$T_e = \frac{3}{2} \frac{p}{2} \frac{L_m}{L_r} \psi_{rd} I_{sq} \quad (4.1)$$

where p is the number of poles, ψ_{rd} is the d-axis component of the rotor flux and I_{sq} is the q-axis component of the stator current at synchronously rotating (d-q) frame.

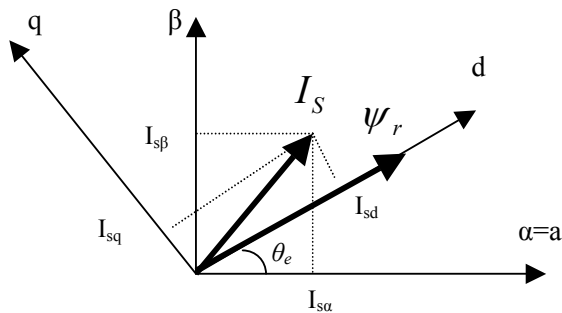


Figure 4. 1- Vector Diagram for Field Orientation of Induction Motor

Figure 4. 1 shows the vector diagram of the reference frames, the projections of stator current and rotor flux, and the rotor flux position with respect to α -axis (θ_e).

In the steady state, namely if the derivative of ψ_{rd} is zero, ψ_{rd} can be expressed as follows:

$$\psi_{rd} = L_m I_{sd} \quad (4.2)$$

Therefore, equation (4.1) can be rewritten as in (4.3); which means that when the rotor flux is maintained constant, the torque of the motor can be controlled through I_{sd} and I_{sq} ,

$$T_e = \frac{3}{2} \frac{p}{2} \frac{L_m^2}{L_r} I_{sd} I_{sq} \quad (4.3)$$

Figure 4.2 shows the Field Orientation Control (FOC) scheme used in vector control drive of induction machine. The drive utilizes the voltage control method without speed sensors; hence the observed parameters in the drive are the stator voltages (V_s) and the stator currents (I_s). Since it is assumed that the all phases of induction machine are identical, it is enough to measure the two of the currents in the three-phase motor with sensors. After two stator currents and voltages are measured and transformed into d-q components (I_{sd} and I_{sq}), these values are compared with the reference values, which are calculated from the reference torque and flux values using (4.2) and (4.3). The error is inserted into a PI regulator in order to generate the voltage references for the PWM generator, which utilizes SVPWM technique.

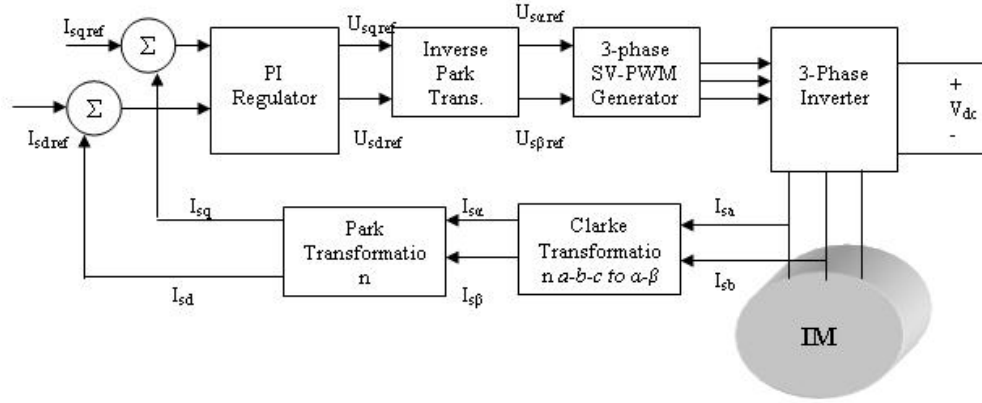


Figure 4. 2- Field Oriented Control (FOC) Scheme for the Motor Drive under Test

The actual stator (ψ_s) and rotor flux (ψ_r) are given by the following equations:

$$\psi_s = \int (V_s - R_s I_s) dt \quad (4.4)$$

$$\psi_r = \frac{L_r}{L_m} (\psi_s - \sigma L_s I_s) \quad (4.5)$$

$$\sigma = 1 - \frac{L_m^2}{L_s \cdot L_r} \quad (4.6)$$

The synchronous speed (ω_s), which is the derivative of the flux position with respect to α -axis (θ_e), is calculated with the following equation:

$$\psi_{r\alpha} = \frac{L_r}{L_m} (\psi_{s\alpha} - \sigma L_s i_{s\alpha}) \quad \psi_{r\beta} = \frac{L_r}{L_m} (\psi_{s\beta} - \sigma L_s i_{s\beta}) \quad \psi_r = \sqrt{\psi_{r\alpha}^2 + \psi_{r\beta}^2} \quad (4.7)$$

$$\cos \theta = \frac{\psi_{r\alpha}}{\psi_r} \quad \sin \theta = \frac{\psi_{r\beta}}{\psi_r} \quad \theta = \tan^{-1} \left(\frac{\psi_{r\beta}}{\psi_{r\alpha}} \right) \quad (4.8)$$

$$\omega_s = \frac{d\theta}{dt} = \dot{\theta} = \frac{(\psi_{r\alpha} \cdot \dot{\psi}_{r\beta} - \psi_{r\beta} \cdot \dot{\psi}_{r\alpha})}{\psi_r^2} \quad (4.9)$$

The dotted terms indicate the derivative of the variables involved. The detailed explanation about finding ω_s is given in section 2.4.1.12

4.3. Online Stator Resistance Estimation Method

The stator voltage vector magnitude at the α - β reference frame ($V_{s\alpha}$ and $V_{s\beta}$) is given by [1]:

$$V_s = \sqrt{V_{s\alpha}^2 + V_{s\beta}^2} \quad (4.10)$$

$$V_{s\alpha} = R_s I_{s\alpha} - \omega_s \psi_{s\beta} \quad (4.11)$$

$$V_{s\beta} = R_s I_{s\beta} + \omega_s \psi_{s\alpha} \quad (4.12)$$

$$\psi_{s\alpha} = \int (V_{s\alpha} - R_s I_{s\alpha}) dt \quad (4.13)$$

$$\psi_{s\beta} = \int (V_{s\beta} - R_s I_{s\beta}) dt \quad (4.14)$$

From the above equations the stator resistance is given by:

$$R_s = \frac{V_{s\beta} - \omega_s \psi_{s\alpha}}{I_{s\beta}} \quad (4.15)$$

In equation (4.15) $V_{s\alpha}$, $I_{s\beta}$ are calculated from measurements and $\psi_{s\alpha}$ can be determined as explained below. The algorithm introduced here relies on measurements of stator voltage and current at the zero crossing instant of $\psi_{s\alpha}$; $\psi_{s\alpha}=0$. The reason why this point is selected to estimate the R_s is that when the $\psi_{s\alpha}$ is near to zero, back emf component ($\omega_s \psi_{s\alpha}$) will be minimum. As a result of this, the errors in calculating the flux and electrical speed have minimum effect on

the stator resistance estimation. Here it is very important to predict the flux variable at the correct instant, since if there is an error about 1% in calculating the flux variable for a motor rated flux is about 1 Wb means for 50 Hz stator frequency ($\omega=314$ rad/sec) that there will be error about 3.14 V at back emf. Consider test machine #1, used in this thesis work, which has a rated stator current of about 2.7 A and cold stator resistance of 4.5 ohms. When we substitute those values in equation (4.15) the voltage drop on stator resistance ($= V_{s\beta} - \omega_s \cdot \psi_{s\alpha}$) is expected about 12.15 volts. Since in the estimation method, the estimation is performed in an interval where the flux $\psi_{s\alpha}$ crosses zero. However, in practice there is no instant where the flux is exactly equal to zero. Estimation starts when the flux is in the interval of (-0.05 - 0.05 Wb) where the rated flux level is 0.9 Wb for this test machine.

It may be argued however, that the contribution of the errors in the negative flux interval cancels the errors in the positive flux interval. Note that back emf voltage term ($\omega_s \cdot \psi_{s\alpha}$) becomes more important at high speeds where the ω_s is high. For this reason estimating flux variable is also important. But there may be some offset errors at the flux variable due to measurement errors about 1% and that error results in about 3 volts for that test machine #1. On the other hand the expected voltage drop on the stator resistance was 12.15 volts, so that 1% error in flux variable results in 25% error in the estimated stator resistance. In experimental results, estimated R_s with respect to flux variable with offset error and estimated error with respect to flux variable whose errors are compensated are shown.

How the variables used in the equation (4.15) are obtained in the algorithm is explained at principles of vector control part of chapter 2, section 2.2. While finding the $\psi_{s\alpha}$, two cascade filters are used as an integrator, which is explained in detail in [4] and it is explained in the software modules section 2.4.1.12 in Chapter 2.

Note that a sensorless vector controlled drive algorithm calculates $V_{s\beta}$, $I_{s\beta}$, ω_s and $\psi_{s\alpha}$ therefore the computational burden of the stator resistance prediction method, introduced here, is minimal. On-line stator resistance estimation algorithm uses the variables calculated in the vector control drive algorithm and only equation (4.15) is added to main vector control software so that the additional calculation introduces only a small increase in the computation period of the main program.

4.4. Experimental Results where Sinusoidal Source is used

To verify the algorithm proposed to find R_s on-line, some experiments are performed at different frequencies with a sinusoidal supply in order to verify the algorithm under continuous near to ideal sinusoidal waveforms. The sinusoidal supply with variable frequency is obtained via a synchronous generator. The synchronous machine is driven with a speed controlled dc machine. The magnitude of the output voltage of the synchronous generator is controlled by adjusting the field current of the generator. By adjusting the speed of dc machine output voltage's frequency can be determined and it is controlled by controlling the dc-supply of dc machine.

This test is useful because possible effects of PWM output of an inverter are eliminated and therefore accuracy of the approach can be tested. During tests motor is driven at its rated flux level by adjusting the supply voltage to the desired level. Only measurement stage of the driver is used during those tests. The experimental setup used for this aim is shown below at Figure 4. 3.

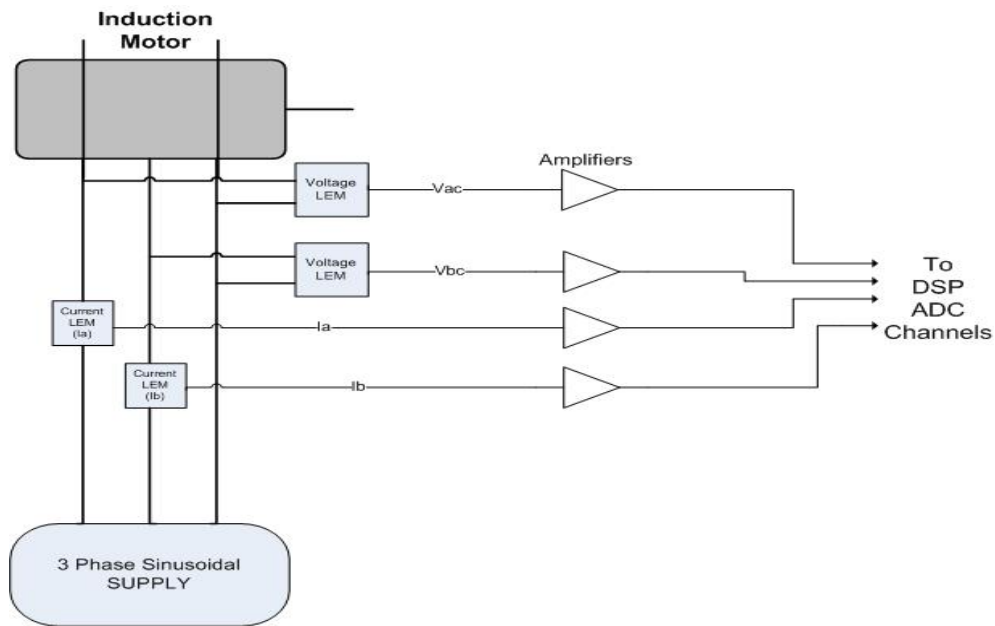


Figure 4. 3 – Experimental setup used for R_s estimation using 3-phase sinusoidal source.

As you see from the Figure 4.3 , motor is driven from sinusoidal source and measurements are taken by the help of voltage and current transducers which are on the drive board. Those taken measurements are used in the R_s estimation algorithm.

The experiments are performed at 30 Hz and 50 Hz where the motor is running under no-load. By using the measurements stator resistance estimation algorithm is performed. In the following sections that experiment results will be examined.

4.4.1. R_s Estimation at 50 Hz Supply Voltage

This experiment is performed at 50 Hz, 380 V_{rms} (line-line) supply voltage with test machine #1 and 2 line voltages (V_{sac} , V_{sbc}) and 2 line currents (I_{sa} , I_{sb}) are measured. That measured signals are transformed to desired variables used in the equation (4.15) to estimate the stator resistance.

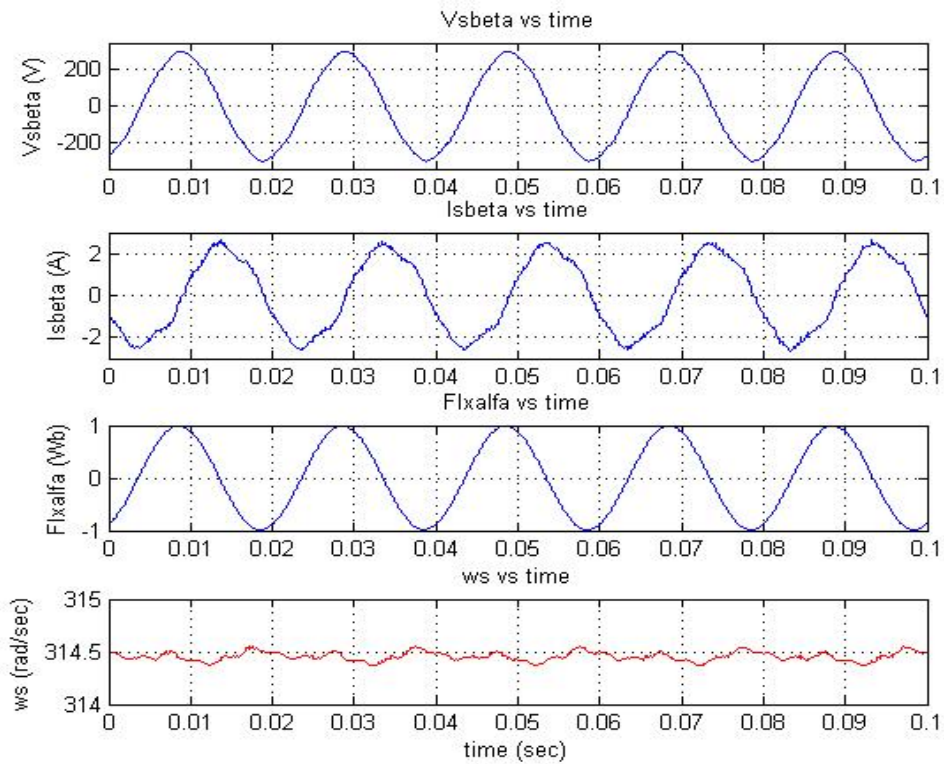


Figure 4. 4 – The variables used in the estimation of R_s at 50 Hz

As you see from the Figure 4. 4, $V_{s\beta}$, ψ_{sa} and w_s seems near to ideal; on the other hand $I_{s\beta}$ waveform is somewhat distorted due to transformations and harmonics effects. Now let's move on to the estimations made by using the above figure at the zero cross of ψ_{sa} , where the back emf is minimum.

Figure 4. 5 presents the estimated stator resistance variation at the zero cross instant of ψ_{sa} . The estimation is made just before ψ_{sa} crosses zero point, is taken as an estimated stator resistance value for related zero cross instant of ψ_{sa} .

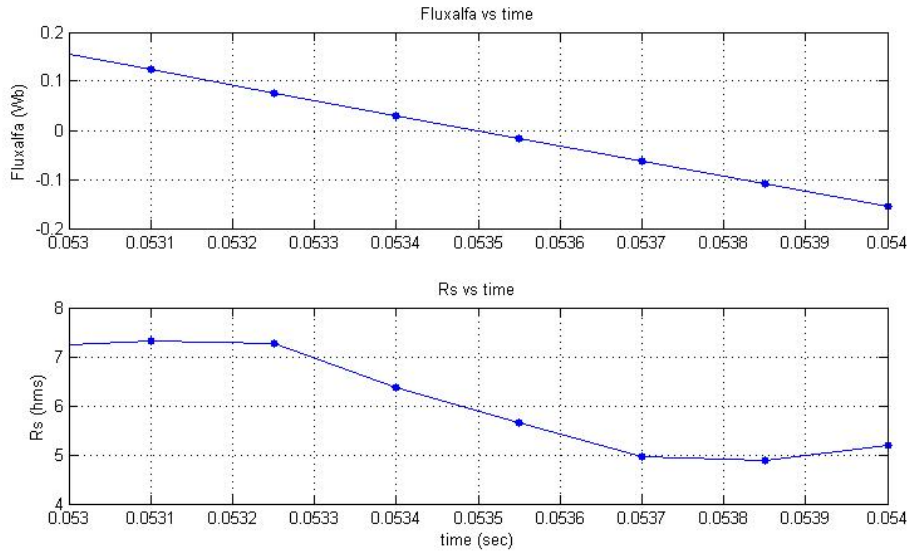


Figure 4. 5 – Stator resistance estimation at zero cross of ψ_{sa} at 50 Hz

It can be seen from the Figure 4. 5, R_s is estimated about 6.36 ohms, where the measured R_s is about 4.5 ohms at this instant. In Table 4. 1, cells around zero crossing region of ψ_{sa} are shaded.

Table 4. 1 - Stator resistance estimation results at the specified interval given at figure 4.5

I_{sa}	-0,03921	-0,19808	-0,23571	-0,35695	-0,44266	-0,56809	-0,62035
I_{sb}	2,213575	2,255299	2,317884	2,330401	2,378384	2,353349	2,334574
V_{sac}	-395,34	-410,639	-425,957	-440,264	-453,601	-466,284	-478,194
V_{sbc}	99,28312	73,24486	44,54187	15,55337	-12,6357	-39,0166	-63,0943
$I_{s\beta}$	2,533381	2,489833	2,540376	2,484828	2,490749	2,389426	2,337573
φ_{sa}	0,123309	0,0769	0,030389	-0,01612	-0,06251	-0,10868	-0,15454
$\varphi_{s\beta}$	0,961369	0,966284	0,969043	0,969602	0,967929	0,964003	0,95783
w_s	314,3935	314,4075	314,4072	314,4218	314,4247	314,4322	314,4319
V_{sa}	-296,654	-298,174	-298,819	-298,694	-298,189	-297,85	-297,764
$V_{s\beta}$	57,32113	42,28794	25,71626	8,979742	-7,29523	-22,5262	-36,4275
R_s	7,3237	7,2735	6,3619	5,6535	4,9624	4,8747	5,2043

If flux variable is examined in detail and it is seen that there is some offset on the flux variable. That offset comes from measurement's errors, and integral error. Effects of errors in flux variable were discussed in section 4.3 of this chapter. To find the offset value at the ψ_{sa} , firstly the difference of absolute values of positive peak and negative peak value is found. If the positive peak value is bigger, half of this difference value is extracted every recorded points of ψ_{sa} . Otherwise, half of this difference value is added to every recorded points of ψ_{sa} . After compensating those errors, ψ_{sa} is calculated again and the estimation is done with respect to that new flux variable. The corrected estimation is seen on the Figure 4. 6 and the corrected estimated stator resistance values are tabulated in the Table 4. 2.

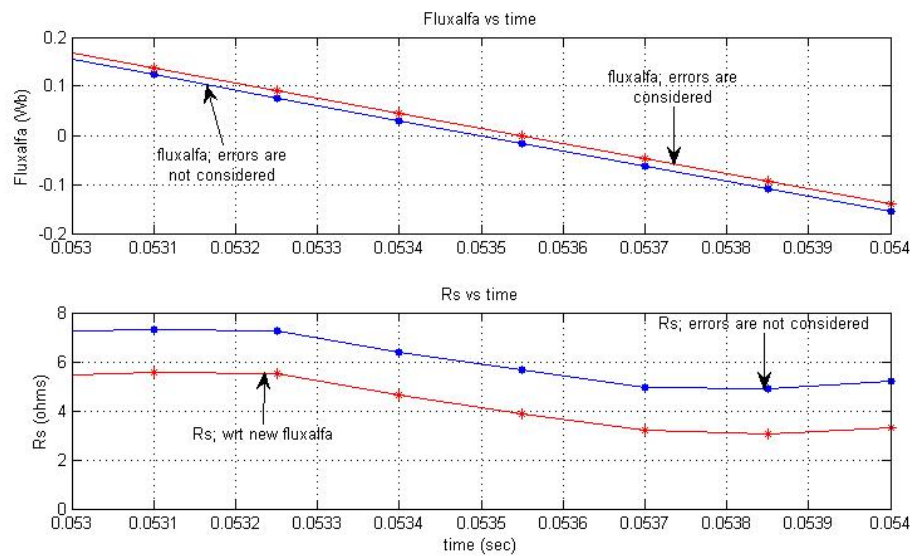


Figure 4. 6 – Stator resistance estimation after compensating the errors in ψ_{sa} calculation.

That R_s estimation is very sensitive to back emf calculation, for this reason zero instant of flux variable is chosen for estimation period. However, errors in measurements, integral errors and residual flux bring some offset on ψ_{sa} . If the R_s estimation is made by correcting for the offset in the flux component, as you see

from the Figure 4. 6 and Table 4. 2, R_s is found about 4.63 ohms where the measured R_s was 4.5 ohms during this experiment. Stator resistance estimation is improved from 6.36 ohms to 4.63 ohms by using the corrected ψ_{sa} . As a result, estimation error is decreased from 41% to 2.9% which is pretty good result.

Table 4. 2 - Stator resistance estimation results after compensating the errors in ψ_{sa} calculation.

I_{sa}	-0,03921	-0,19808	-0,23571	-0,35695	-0,44266	-0,56809	-0,62035
I_{sb}	2,213575	2,255299	2,317884	2,330401	2,378384	2,353349	2,334574
V_{sac}	-395,34	-410,639	-425,957	-440,264	-453,601	-466,284	-478,194
V_{sbc}	99,28312	73,24486	44,54187	15,55337	-12,6357	-39,0166	-63,0943
$I_{s\beta}$	2,533381	2,489833	2,540376	2,484828	2,490749	2,389426	2,337573
ψ_{sa}	0,137309	0,0909	0,044389	-0,00212	-0,04851	-0,09468	-0,14054
$\psi_{s\beta}$	0,961369	0,966284	0,969043	0,969602	0,967929	0,964003	0,95783
w_s	314,3935	314,4075	314,4072	314,4218	314,4247	314,4322	314,4319
V_{sa}	-296,654	-298,174	-298,819	-298,694	-298,189	-297,85	-297,764
$V_{s\beta}$	57,32113	42,28794	25,71626	8,979742	-7,29523	-22,5262	-36,4275
R_s	5,586297	5,505671	4,629243	3,881978	3,195082	3,032395	3,321154

To see the performance of stator resistance estimation algorithm at different frequencies, in the following section another experiment performed at 30 Hz will be explained.

4.4.2. R_s Estimation at 30 Hz Supply Voltage

In this experiment synchronous generator is used as a 30 Hz continuous sinusoidal source to drive the test motor #1 at its rated flux. Similar to experiments done at 50 Hz, 2 line voltages (V_{sac} , V_{sbc}) and 2 line currents (I_{sa} , I_{sb}) are measured. That measured signals are transformed to desired variables to estimate the stator resistance. Applied supply voltage level is about 230 V_{rms} (line-line).

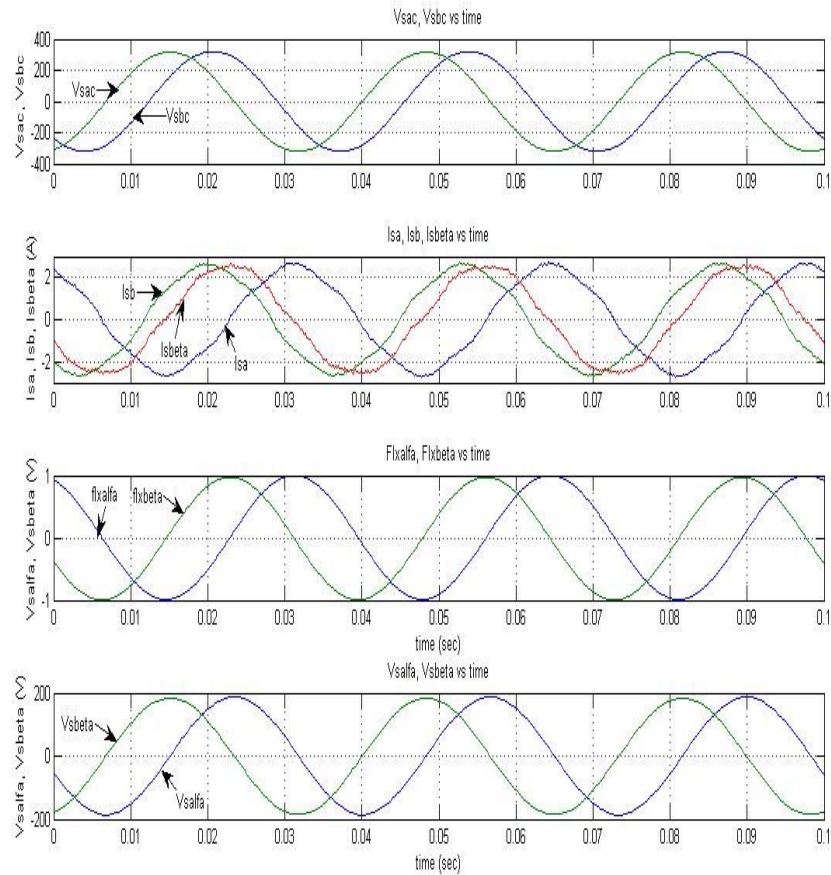


Figure 4. 7 - Measured Variables; V_{sac} , V_{sbc} , I_{sa} , I_{sb} and transformed variables V_{sa} , V_{sb} , I_{sa} , I_{sb} , ψ_{sa} , ψ_{sb} at 30 Hz.

In Figure 4. 7 measured and transformed variables are shown. Voltage and flux variables seem sinusoidal but on the current variables there is small distortion which is in acceptable range.

Now let's look at the variables that are used in the R_s estimation where the frequency is 30 Hz.

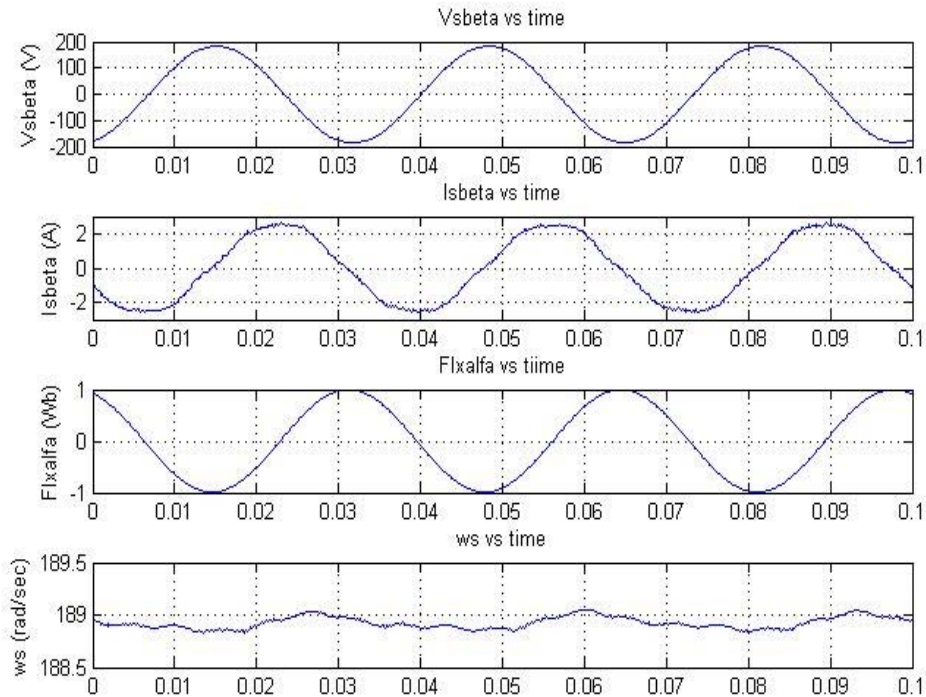


Figure 4. 8 – Variables that are used in the R_s estimation at 30 Hz.

It can be seen from the Figure 4. 8, the variables used in the R_s estimation are so smooth. $I_{s\beta}$ looks like better than the one at 50 Hz. Here also same algorithm is applied and stator resistance is estimated at the zero cross sections of the $\psi_{s\alpha}$.

It is seen from Table 4. 3, estimated stator resistance is 5.12 ohms where the measured resistance is 4.5 ohms. Here, there are also some offset errors in the flux component; however effects of those errors are less important at 30 Hz compared to 50 Hz, since the $(w_s \cdot \psi_{s\alpha})$ term in the equation (4.15) becomes less important. Figure 4. 10 presents the stator resistance estimation after $\psi_{s\alpha}$ is corrected.

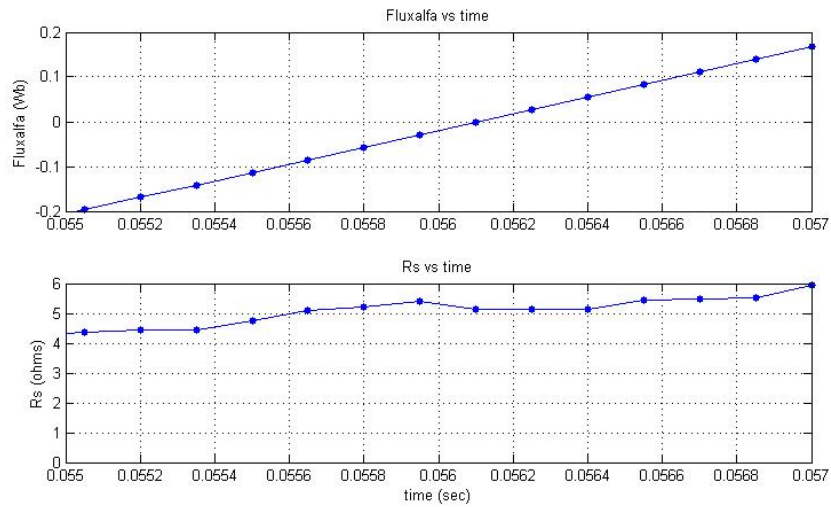


Figure 4.9 - Stator resistance estimation at zero cross of ψ_{su} at 30 Hz

Table 4.3 – Stator resistance estimation results related with figure 4.9

time (sec)	0,05565	0,0558	0,05595	0,0561	0,05625	0,0564	0,05655	0,0567
I_{sa}	-0,24198	-0,1061	-0,04548	0,073679	0,165659	0,268091	0,30781	0,456232
I_{sb}	2,244868	2,213575	2,140559	2,125956	2,050853	2,01956	1,959061	1,906907
V_{sac}	302,3062	299,4922	296,916	293,1311	289,1876	285,5016	281,4194	276,6634
V_{sbc}	49,47135	41,1155	32,30285	22,34816	12,85029	3,828259	-4,50855	-13,3212
$I_{sb\beta}$	2,452443	2,494759	2,445448	2,49738	2,463764	2,486769	2,439843	2,465311
ψ_{su}	-0,08512	-0,05699	-0,02881	-0,00059	0,027654	0,055892	0,084105	0,11227
$\psi_{s\beta}$	0,969214	0,971337	0,972674	0,973225	0,972984	0,971949	0,970121	0,967506
w_s	-188,972	-188,975	-188,97	-188,974	-188,972	-188,973	-188,973	-188,979
V_{su}	185,047	185,9563	187,1764	187,9713	188,5083	189,0583	189,1158	188,8826
$V_{s\beta}$	28,56229	23,73804	18,65005	12,90272	7,419116	2,210246	-2,60301	-7,691
R_s	5,087846	5,197978	5,400047	5,12198	5,132341	5,136089	5,447265	5,486424

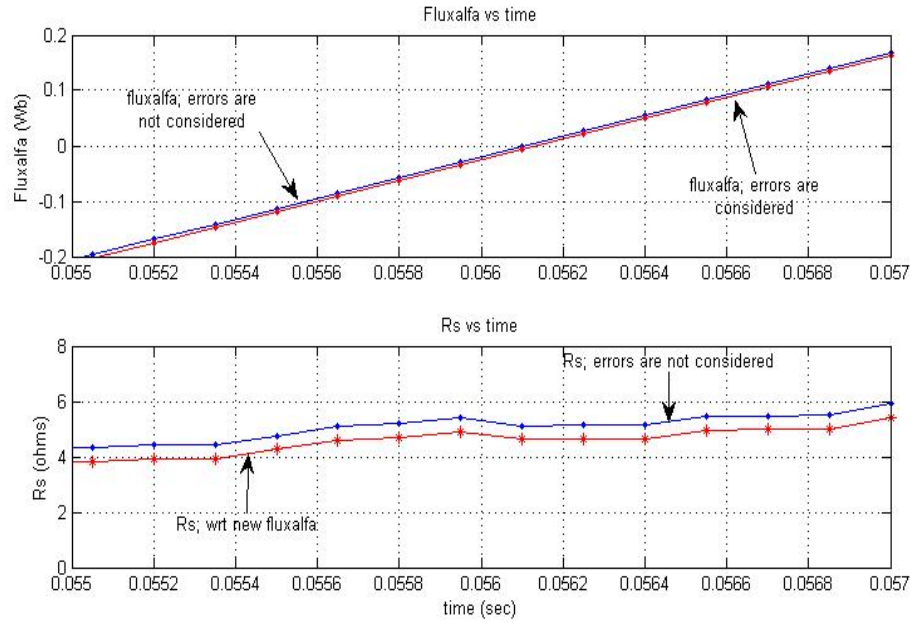


Figure 4. 10 - Stator resistance estimation where the ψ_{sa} is corrected at 30 Hz

Table 4. 4 - Stator resistance estimation results wrt corrected ψ_{sa}

time (sec)	0,05565	0,0558	0,05595	0,0561	0,05625	0,0564	0,05655	0,0567
I_{sa}	-0,24198	-0,1061	-0,04548	0,073679	0,165659	0,268091	0,30781	0,456232
I_{sb}	2,244868	2,213575	2,140559	2,125956	2,050853	2,01956	1,959061	1,906907
V_{sac}	302,3062	299,4922	296,916	293,1311	289,1876	285,5016	281,4194	276,6634
V_{sbc}	49,47135	41,1155	32,30285	22,34816	12,85029	3,828259	-4,50855	-13,3212
$I_{s\beta}$	2,452443	2,494759	2,445448	2,49738	2,463764	2,486769	2,439843	2,465311
ψ_{sa}	-0,09177	-0,06364	-0,03546	-0,00724	0,021004	0,049242	0,077455	0,10562
$\psi_{s\beta}$	0,969214	0,971337	0,972674	0,973225	0,972984	0,971949	0,970121	0,967506
w_s	-188,972	-188,975	-188,97	-188,974	-188,972	-188,973	-188,973	-188,979
V_{sa}	185,047	185,9563	187,1764	187,9713	188,5083	189,0583	189,1158	188,8826
$V_{s\beta}$	28,56229	23,73804	18,65005	12,90272	7,419116	2,210246	-2,60301	-7,691
R_s	4,575433	4,69425	4,886174	4,618782	4,622283	4,630747	4,932205	4,976666

After correcting the offset error in the $\psi_{s\alpha}$ component stator resistance estimation becomes 4.62 ohms. Table 4. 4 shows the tabulated estimation results after correcting the offset error in flux component. Since the measured stator resistance was 4.5 ohms, it is easily seen that the stator resistance estimation becomes better after considering the errors in the flux component.

Estimated stator resistance value changed from 5.12 ohms to 4.62 ohms by compensating the offset error in $\psi_{s\alpha}$. As a result of this, estimation error decreases from 13.8% to 2.7%.

Now let's look at another zero cross instant where the stator resistance estimation is performed. Figure 4. 11 presents the estimated stator resistance points with related zero cross instant of $\psi_{s\alpha}$.

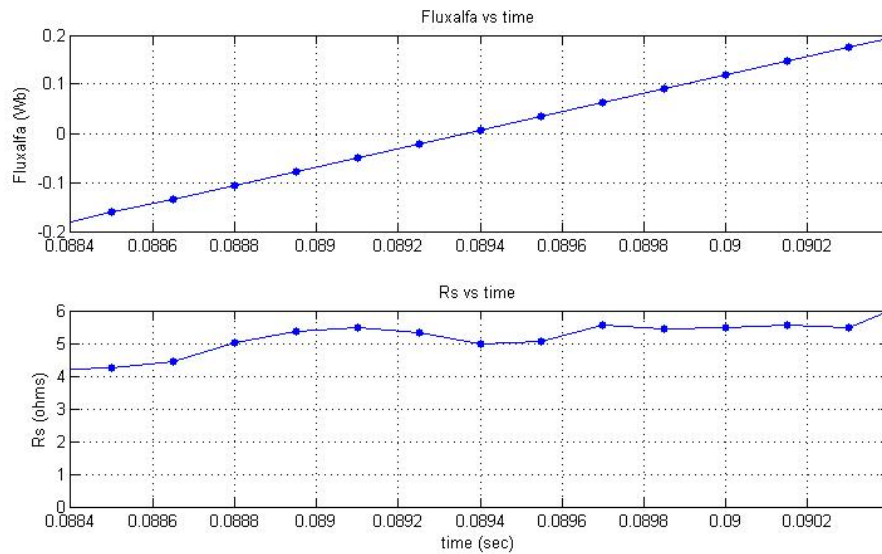


Figure 4. 11 – Stator resistance estimation at another zero cross instant of $\psi_{s\alpha}$ at 30 Hz

Estimated stator resistance values related with Figure 4. 11 are tabulated in Table 4. 5.

Table 4. 5 - Stator resistance estimation results related with figure 4.11

time	0,0888	0,08895	0,0891	0,08925	0,0894	0,08955	0,0897	0,08985
I_{sa}	-0,30887	-0,23571	-0,11237	0,048593	0,197015	0,270181	0,282724	0,389337
I_{sb}	2,244868	2,217748	2,173938	2,167679	2,182283	2,088404	1,967406	1,940286
V_{sac}	304,1888	302,0486	299,6111	296,7575	292,3979	288,2562	284,6891	279,7548
V_{sbc}	55,5241	47,81541	39,42149	30,30429	20,36864	10,96594	2,743332	-6,69744
I_{sb}	2,413821	2,424748	2,445369	2,531075	2,63363	2,567471	2,434995	2,465232
ψ_{sa}	-0,10551	-0,07747	-0,04935	-0,02117	0,00704	0,035264	0,063474	0,091653
ψ_{sb}	0,967578	0,970266	0,972172	0,973296	0,973633	0,973175	0,971922	0,969884
w_s	-188,966	-188,97	-188,973	-188,969	-188,961	-188,956	-188,959	-188,968
V_{sa}	184,2845	185,4272	186,6002	187,7369	188,1423	188,5155	188,8783	188,7357
V_{sb}	32,05685	27,60624	22,76001	17,49619	11,75984	6,331188	1,583863	-3,86677
R_s	5,021077	5,347825	5,493732	5,331763	4,97039	5,061194	5,576163	5,457004

It is seen from Table 4. 5, at zero cross instant of ψ_{sa} stator resistance is estimated about 5.33 ohms where the offset error in ψ_{sa} is not considered. Stator resistance estimation variation with respect to the corrected ψ_{sa} is shown in Figure 4. 12 and the corrected estimation values are tabulated in Table 4. 6.

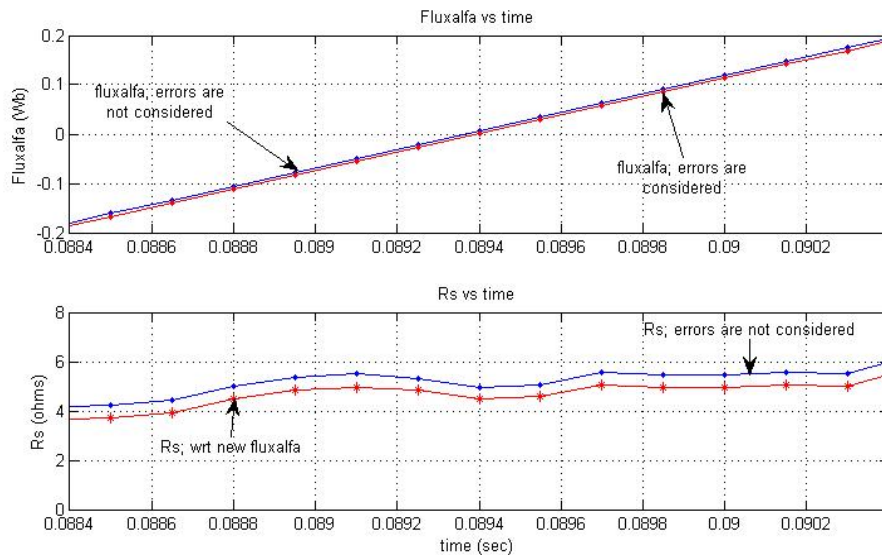


Figure 4. 12 - Stator resistance estimation where the ψ_{sa} is corrected at 30 Hz for another zero cross instant of ψ_{sa}

Table 4. 6 - Stator resistance estimation results wrt corrected $\psi_{s\alpha}$

time	0,0888	0,08895	0,0891	0,08925	0,0894	0,08955	0,0897	0,08985
$I_{s\alpha}$	-0,30887	-0,23571	-0,11237	0,048593	0,197015	0,270181	0,282724	0,389337
$I_{s\beta}$	2,244868	2,217748	2,173938	2,167679	2,182283	2,088404	1,967406	1,940286
$V_{s\alpha}$	304,1888	302,0486	299,6111	296,7575	292,3979	288,2562	284,6891	279,7548
$V_{s\beta}$	55,5241	47,81541	39,42149	30,30429	20,36864	10,96594	2,743332	-6,69744
$I_{s\beta}$	2,413821	2,424748	2,445369	2,531075	2,63363	2,567471	2,434995	2,465232
$\psi_{s\alpha}$	-0,11226	-0,08422	-0,0561	-0,02792	0,00029	0,028514	0,056724	0,084903
$\psi_{s\beta}$	0,967578	0,970266	0,972172	0,973296	0,973633	0,973175	0,971922	0,969884
w_s	-188,966	-188,97	-188,973	-188,969	-188,961	-188,956	-188,959	-188,968
$V_{s\alpha}$	184,2845	185,4272	186,6002	187,7369	188,1423	188,5155	188,8783	188,7357
$V_{s\beta}$	32,05685	27,60624	22,76001	17,49619	11,75984	6,331188	1,583863	-3,86677
R_s	4,492654	4,821771	4,972106	4,82781	4,486081	4,56442	5,052353	4,939594

Note that stator resistance estimation becomes 4.83 ohms after correcting the offset error in flux component where the old estimation was 5.33 ohms and the measured resistance was 4.5 ohms. Estimation error decreases by using the corrected $\psi_{s\alpha}$ from 18.4% to 7.3%.

As a result, it can be concluded that stator resistance estimation algorithm proposed here is robust since the estimations at different zero cross instants are nearly same.

Note that as expected the proposed approach appears to work better at low speeds where “ $w_s \cdot \psi_{s\alpha}$ ” term becomes less important.

4.5. Experimental Results with a PWM Drive

In this section, stator resistance estimation algorithm is applied on the motor drive that we designed, and the results of this estimation will be presented. The R_s prediction approach is tested on 3 different induction machines. Experiments are performed at 10 Hz for all 3 test machines and at 30 Hz for test machine #1.

In Figure 4. 13, you see the block diagram of the drive system where the experimental setup is shown. The switching frequency is about 6.67 kHz and PM25RLA120 is used as IGBT package. The hardware of the drive is explained in detail at section 2.3 of Chapter 2.

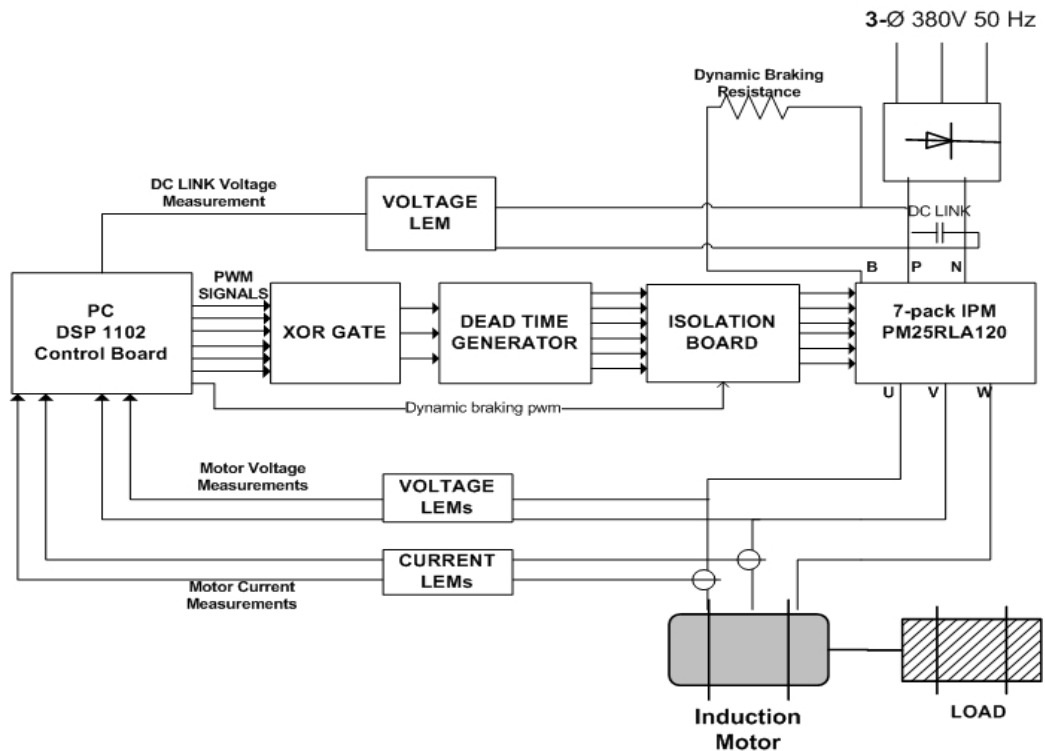


Figure 4. 13 – Experimental setup of stator resistance estimation with driver.

In those experiments, there will be online R_s estimation results will be examined at different frequencies while the test motors are running at steady state.

4.5.1. R_s Estimation at 30 Hz, with a PWM Drive

This experiment is also same as the one done by steady state AC source. Test machine #1 is used in this experiment. The parameters of test machine #1 are listed in Table 4. 7. Here, the main difference is that the reference voltage is determined in the algorithm with respect to the motor ratings. At 30 Hz, test motor #1 is driven at 228 rms (Volts/line-line) at steady state.

Table 4. 7 - Parameters of 1st motor used in the on- line R_s estimation

Parameters of (1 kW, 2-pole, Y-connected, $I_{s,rated}=2.7$ A, $V_{s,rated}=220$ V_(phase)) Induction machine	
R_s	4,50 ohm
R_r	6,01 ohm
L_{ls}	11,7 mH
L_{lr}	11,7 mH
L_s	386,7 mH ($=L_{ls}+L_m$)
L_r	386,7 mH ($=L_{lr}+L_m$)
L_m	375 mH

Figure 4. 14 shows the recorded variables used in predicting the R_s for this machine at 30 Hz.

As you see from Figure 4. 14, $V_{s\beta}$ is not perfectly sinusoidal as in the previous experiments done with ideal sources (see Figure 4. 8). In experiments performed with PWM driver the output voltages are produced by sampling the dc-link voltage with respect to the reference voltage. As a modulation technique SVPWM technique which is explained at section 2.4.1.9 of chapter 2 is applied. As a result, due to switching losses, dead time and pulse skipping; our voltage can somewhat differ from the sinusoidal waveform. The measurements are done via voltage transducers and they are filtered by a low-pass filter which is described in section 2.3.4. of chapter 2. However it can be easily seen that fundamental waveform of

$V_{s\beta}$, in Figure 4. 14, is so close to a sinusoidal waveform. $I_{s\beta}$ seems good and $\psi_{s\alpha}$ waveform is so sinusoidal. Electrical speed, w_s can be assumed constant since the variation is about 0.2 rad/sec around 187.8 rad/sec.

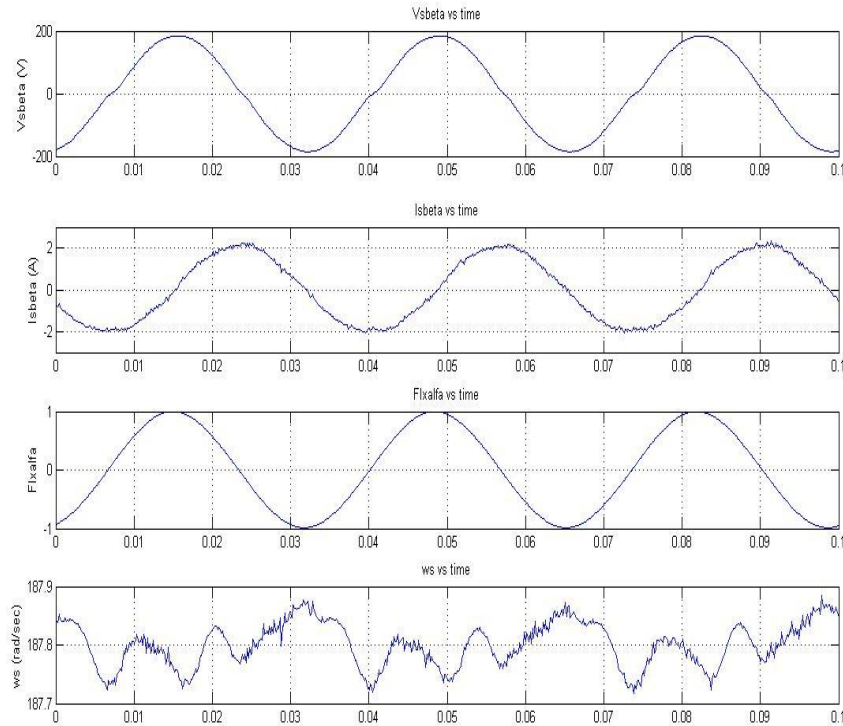


Figure 4. 14 - Variables that are used in the R_s estimation at 30 Hz with driver.

In the experiments done with the PWM driver, the same stator resistance prediction algorithm, utilized for the sinusoidal supply case is used. For this reason, the variables used in equation (4.15) are recorded to estimate the stator resistance. Here also we concentrate on the zero cross instant of the $\psi_{s\alpha}$ to estimate the stator resistance as online.

Figure 4. 15 presents the variables used to estimate stator resistance for one zero cross instant of ψ_{sa} . Following that figure, Table 4. 8 shows the recorded variables for the zero cross instant of ψ_{sa} shown in Figure 4. 15.

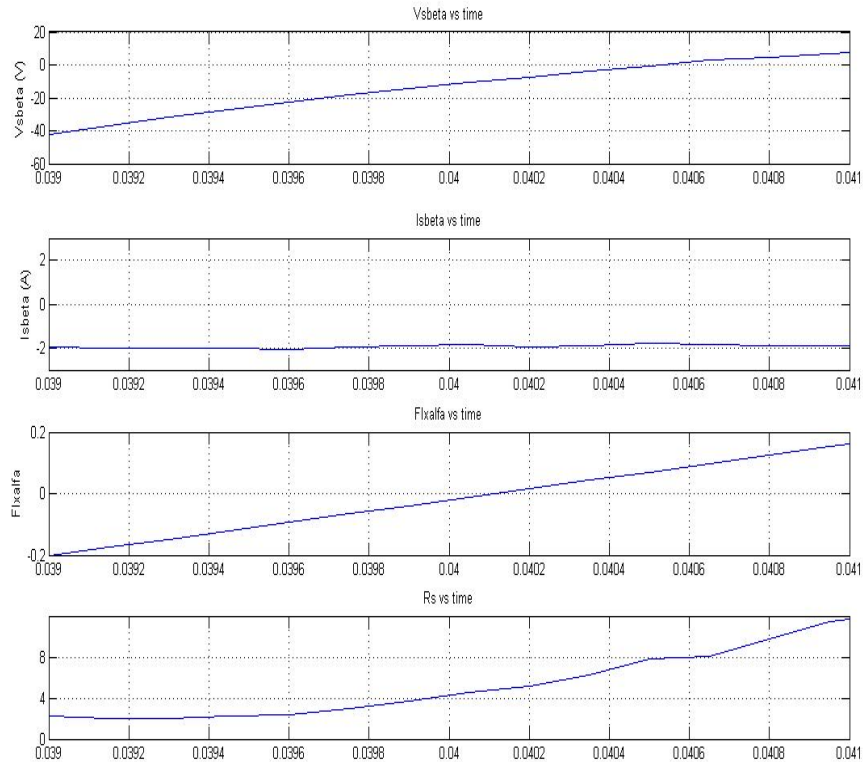


Figure 4. 15 - Stator resistance estimation at zero cross of ψ_{sa} at 30 Hz with driver.

In Table 4. 8, it is seen that when ψ_{sa} zero cross section R_s is estimated about 4.95 ohms where the measured R_s is about 4.5 ohms while doing this experiment. As mentioned before there are some offset errors and integral errors, so those errors effect the calculation of flux variables. In Table 4. 9 stator estimation results are presented where the offset error on ψ_{sa} component is corrected.

Table 4. 8 – Stator resistance estimation results at the specified interval given at figure 4.15

I_{sa}	0,2137	0,1259	0,082	0,0172	-0,0099	-0,0894	-0,1437	-0,1145
I_{sb}	1,7317	1,7442	1,8005	1,836	1,8422	1,8631	1,8756	1,9716
V_{sac}	-231,99	-238,55	-244,63	-249,27	-254,5	-261,85	-267,82	-274,02
V_{sbc}	59,3118	49,9662	40,0496	32,2267	25,051	16,9806	10,6043	3,6379
$I_{s\beta}$	2,123	2,0867	2,1264	2,13	2,1215	2,0997	2,0828	2,2105
ψ_{sa}	0,1291	0,1022	0,0752	0,0482	0,0211	-0,006	-0,0332	-0,0603
$\psi_{s\beta}$	0,9733	0,9762	0,9784	0,9797	0,9802	0,9798	0,9787	0,9769
w_s	187,784	187,778	187,777	187,773	187,775	187,769	187,768	187,778
V_{sa}	-174,43	-175,69	-176,44	-176,92	-178,02	-180,23	-182,08	-183,89
$V_{s\beta}$	34,2437	28,848	23,1227	18,6061	14,4632	9,8038	6,1224	2,1004
R_s	4,710661	4,627909	4,233392	4,486116	4,949874	5,205704	5,932535	6,072572

After compensating the errors and if we consider the R_s estimation interval just as before where the ψ_{sa} crosses zero, it is seen from Table 4. 9 R_s is estimated as 4.58 ohms where the measured was 4.5 ohms. By correcting the ψ_{sa} estimation error decreased from 10% to 1.8% which is pretty good result.

Table 4. 9 – Updated version of table 4.7 after compensating the errors in calculating the ψ_{sa}

I_{sa}	0,2137	0,1259	0,082	0,0172	-0,0099	-0,0894	-0,1437	-0,1145
I_{sb}	1,7317	1,7442	1,8005	1,836	1,8422	1,8631	1,8756	1,9716
V_{sac}	-231,99	-238,55	-244,63	-249,27	-254,5	-261,85	-267,82	-274,02
V_{sbc}	59,3118	49,9662	40,0496	32,2267	25,051	16,9806	10,6043	3,6379
$I_{s\beta}$	2,123	2,0867	2,1264	2,13	2,1215	2,0997	2,0828	2,2105
ψ_{sa}	0,1361	0,1092	0,0822	0,0552	0,0281	0,001	-0,0262	-0,0533
$\psi_{s\beta}$	0,9733	0,9762	0,9784	0,9797	0,9802	0,9798	0,9787	0,9769
w_s	187,784	187,778	187,777	187,773	187,775	187,769	187,768	187,778
V_{sa}	-174,43	-175,69	-176,44	-176,92	-178,02	-180,23	-182,08	-183,89
$V_{s\beta}$	34,2437	28,848	23,1227	18,6061	14,4632	9,8038	6,1224	2,1004
R_s	4,0914	3,9979	3,6152	3,8690	4,3303	4,5797	5,3014	5,4779

To verify the R_s estimation is working properly another zero cross instant of ψ_{sa} is taken into account. The results are shown in Figure 4. 16 and the recorded variables are tabulated in Table 4. 10 for the related zero cross instant of ψ_{sa} .

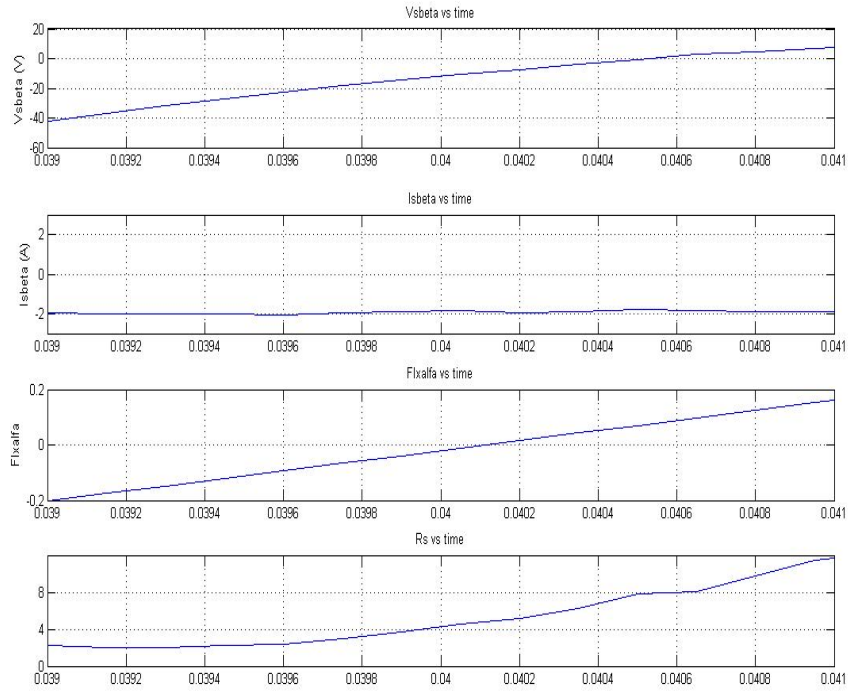


Figure 4. 16 - Stator resistance estimation at another zero cross of ψ_{sa} at 30 Hz with driver.

Table 4. 10 - Stator resistance estimation results at the specified interval given at figure 4.14

I_{sa}	0,174	0,2305	0,1907	0,2869	0,3977
I_{sb}	-1,7126	-1,723	-1,7961	-1,8002	-1,723
V_{sac}	257,421	262,158	267,112	272,145	276,465
V_{sbc}	-24,894	-18,479	-12,56	-6,9829	-0,9112
$I_{s\beta}$	-1,8771	-1,8565	-1,9638	-1,9131	-1,76
ψ_{sa}	-0,0394	-0,0121	0,0153	0,0426	0,07
$\psi_{s\beta}$	-0,9823	-0,9817	-0,9803	-0,9781	-0,9752
w_s	187,726	187,723	187,734	187,728	187,719
V_{sa}	179,912	180,932	182,261	183,758	184,614
$V_{s\beta}$	-14,372	-10,669	-7,2514	-4,0316	-0,5261
R_s	3,716373	4,523376	5,155173	6,287596	7,765005

As you notice that for higher frequencies number of samples decrease since $\psi_{s\alpha}$ changing rate increases. It is easily seen that estimated R_s before $\psi_{s\alpha}$ crosses zero is 4,52 ohms which is very near to measured R_s . For this zero cross instant, the offset on $\psi_{s\alpha}$ is in negligible level so the estimation shown on Table 4. 10 can be taken as a final estimated stator resistance value. Estimation error is here equal to 0.44% which means R_s estimation algorithm is working very well.

4.5.2. R_s Estimation at 10 Hz with a PWM Drive

Test motor #1 is driven with vector control driver, explained in chapter 2, at no-load, where the steady state frequency is 10 Hz. While the motor is running at steady state stator resistance estimation is performed on-line. Measured line-line voltage applied to motor is about 75 V_{rms} .

Estimating the stator resistance at low speeds accurately makes our method favored, since voltage drop on the stator resistance at low speeds is so important at vector control method. At low speeds voltage drop on the R_s becomes comparable with the back emf voltage and it can not be neglected, however at high frequencies where the impedance's of inductances are directly proportional to the frequency get higher but stator resistance doesn't change with the frequency. In some applications, stator resistance can be neglected at high frequencies but in low frequencies like lower than 10 Hz it is impossible to neglect stator resistance. In this view of point, our on-line R_s estimation method will be very useful to update the R_s data on the program as online so makes the vector control to work at low speeds properly. In the experiments performed at 10 Hz offset on the $\psi_{s\alpha}$ is in negligible range, therefore offset error is neglected to estimate the stator resistance.

Similarly 30 Hz, the waveforms, used in the stator estimation at 10 Hz, are given in the Figure 4. 17.

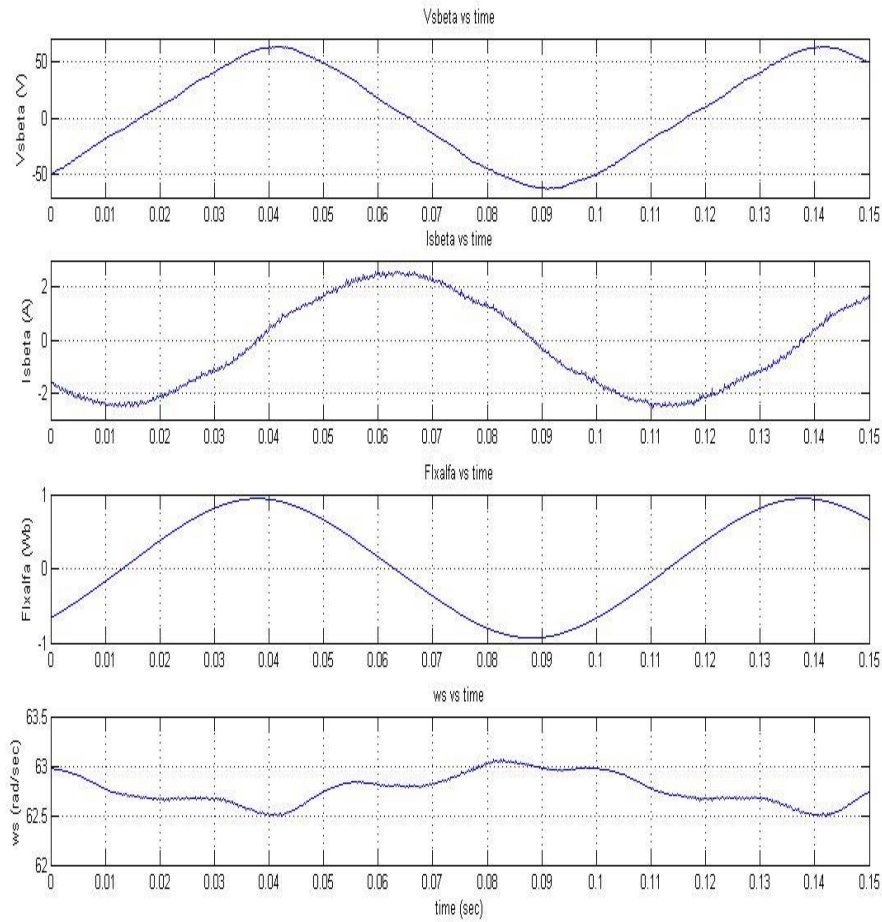


Figure 4. 17 - Variables that are used in the R_s estimation at 10 Hz with PWM drive.

It is seen from Figure 4. 17, voltage and current waveforms in β axis seem sinusoidal. Flux variable in α axis look pretty good and electrical speed w_s can be assumed at steady state since it is varying between 62.5-63 rad/sec. Now let's concentrate on the period where the estimation is done at zero cross of the $\psi_{s\alpha}$.

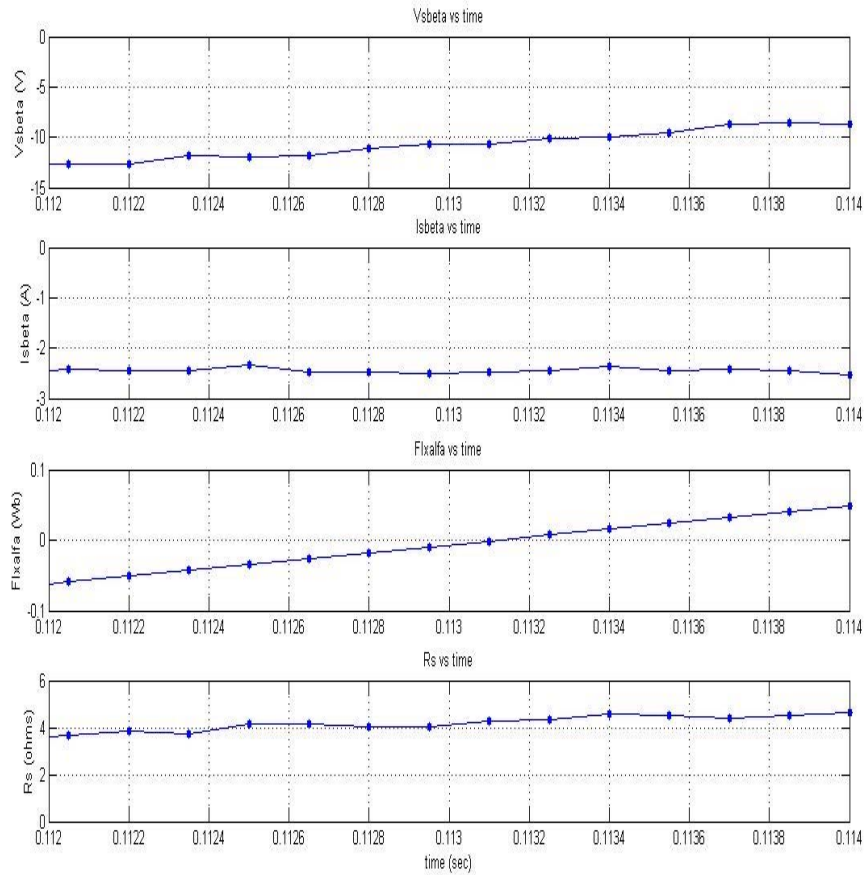


Figure 4. 18 - Stator resistance estimation at zero cross of ψ_{sa} at 10 Hz with PWM drive.

Table 4. 11 - Stator resistance estimation results at 10 Hz, experiment is done with PWM drive

I_{sa}	0,1134	0,0507	0,0611	0,1322	0,1385	0,1176	0,2054	0,1301
I_{sb}	-2,1069	-2,1695	-2,1924	-2,1883	-2,182	-2,2029	-2,1486	-2,2237
V_{sac}	73,0668	73,4235	75,2863	75,1079	76,6338	76,4753	76,4158	76,7924
V_{sbc}	-19,9259	-19,754	-18,27	-18,346	-16,747	-16,442	-16,138	-15,129
I_{sb}	-2,3674	-2,4759	-2,4763	-2,4505	-2,4396	-2,4758	-2,3625	-2,4926
ψ_{sa}	-0,0267	-0,0184	-0,0101	-0,0018	0,0065	0,0148	0,0231	0,0315
ψ_{sb}	-0,9402	-0,9399	-0,9395	-0,939	-0,9384	-0,9378	-0,9371	-0,9363
w_s	62,7141	62,7219	62,7205	62,7112	62,7105	62,7135	62,7019	62,7126
V_{sa}	55,3532	55,5339	56,2809	56,1873	56,6716	56,4644	56,3233	56,238
V_{sb}	-11,5042	-11,405	-10,9482	-10,592	-9,6691	-9,4932	-9,3174	-8,735
R_s	4,152122	4,1404	4,165377	4,27636	4,13048	4,20929	4,556958	4,296898

Shaded variables in the table are represents the zero cross of the ψ_{sa} . As you see from Table 4. 11, at zero cross of ψ_{sa} estimated R_s is predicted to be about 4.2 ohms and the measured resistance at this instant was about 4.4 ohms. Estimation of R_s is made for several other zero crossing of ψ_{sa} . An example measurement is given in Figure 4. 19. The corresponding R_s prediction is tabulated in Note that the estimated resistance value at 10 Hz comes out to be smaller than the value predicted at 30 Hz. this may be because the experiments are not performed on the same day, therefore the ambient temperatures may be different or the motor may have been operated a while before the tests are done.

Table 4. 12.

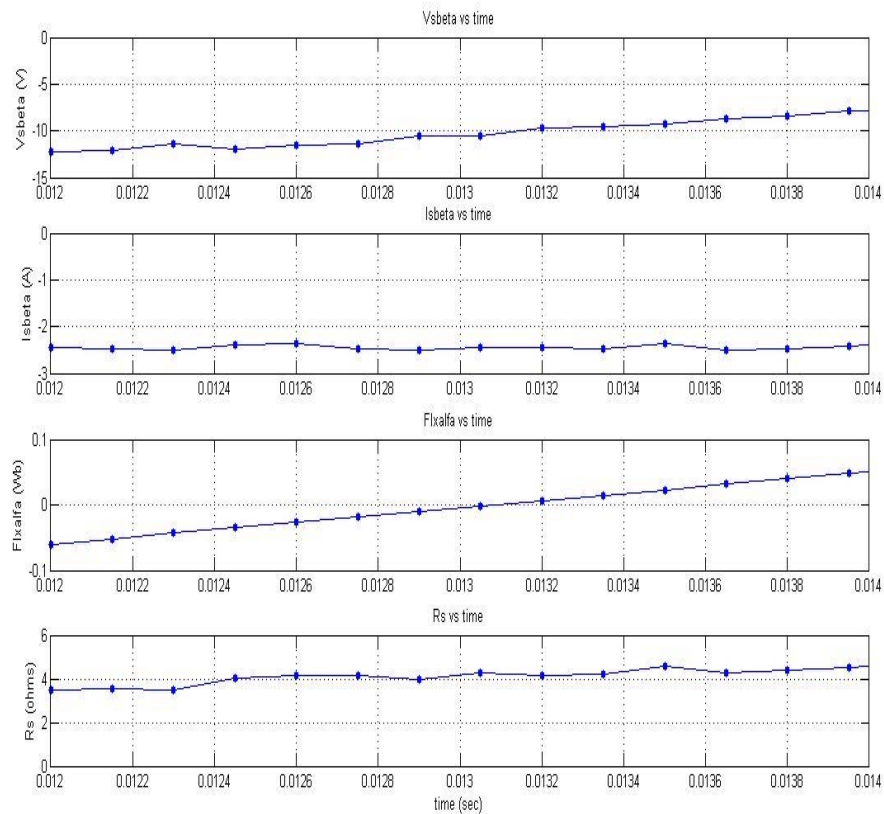


Figure 4. 19 – Another stator resistance estimation interval at 10 Hz with driver.

Note that the estimated resistance value at 10 Hz comes out to be smaller than the value predicted at 30 Hz. this may be because the experiments are not performed on the same day, therefore the ambient temperatures may be different or the motor may have been operated a while before the tests are done.

Table 4. 12 – Another stator resistance estimation results at 10 Hz, experiment is done with driver

I_{sa}	0,055	0,055	0,057	0,070	0,136	0,178	0,159	0,172
I_{sb}	-2,165	-2,165	-2,197	-2,184	-2,184	-2,142	-2,195	-2,182
V_{sac}	72,393	74,078	74,731	75,128	75,524	75,108	76,852	77,823
V_{sbc}	-20,535	-19,165	-18,460	-18,403	-17,623	-17,185	-16,595	-14,977
$I_{s\beta}$	-2,469	-2,469	-2,504	-2,482	-2,443	-2,371	-2,442	-2,420
$\psi_{s\alpha}$	-0,026	-0,018	-0,009	-0,001	0,007	0,016	0,024	0,032
$\psi_{s\beta}$	-0,940	-0,939	-0,939	-0,938	-0,938	-0,937	-0,936	-0,936
w_s	62,725	62,725	62,725	62,723	62,715	62,709	62,712	62,711
$V_{s\alpha}$	55,107	55,773	55,974	56,220	56,224	55,800	56,766	56,874
$V_{s\beta}$	-11,856	-11,065	-10,658	-10,625	-10,175	-9,922	-9,581	-8,647
R_s	4,142	4,032	4,022	4,253	4,349	4,595	4,535	4,404

In this interval, if we look at Note that the estimated resistance value at 10 Hz comes out to be smaller than the value predicted at 30 Hz. this may be because the experiments are not performed on the same day, therefore the ambient temperatures may be different or the motor may have been operated a while before the tests are done.

Table 4. 12, R_s is estimated about 4.25 ohms where the measured R_s was 4.4 ohms. As you see, estimated and measured stator resistances are very near, so we can say that this on-line R_s estimation can be used in the vector control algorithm to update stator resistance R_s as on-line.

Up to here all experimental results are related with test motor #1. In the following sections, results of on-line stator resistance estimation experiments performed on test machines #2 and #3 at 10 Hz will be presented.

4.5.3. R_s Estimation at 10 Hz with 2nd Test Motor

Another method to verify the algorithm is testing the algorithm on different induction machines. For this reason, same algorithm is applied to another machine whose parameters shown at Table 4. 13. Measured line-line voltage applied to test machine #2 at 10 Hz is about 65 V_{rms} .

Table 4. 13 - Parameters of 2nd motor used in the on- line R_s estimation

Parameters of (1.1 kW, 6-pole, Y-connected, $I_{s, rated} = 3.1$ A, $V_{s, rated} = 220$ V_(phase)) Induction machine	
R_s	6,50 ohm
R_r	7,667 ohm
L_{ls}	29,75 mH
L_{lr}	29,75 mH
L_s	338,55 mH (= $L_{ls} + L_m$)
L_r	338,55 mH (= $L_{ls} + L_m$)
L_m	308,8 mH

Now let's look at the parameters that will be used to estimate the stator resistance for this machine.

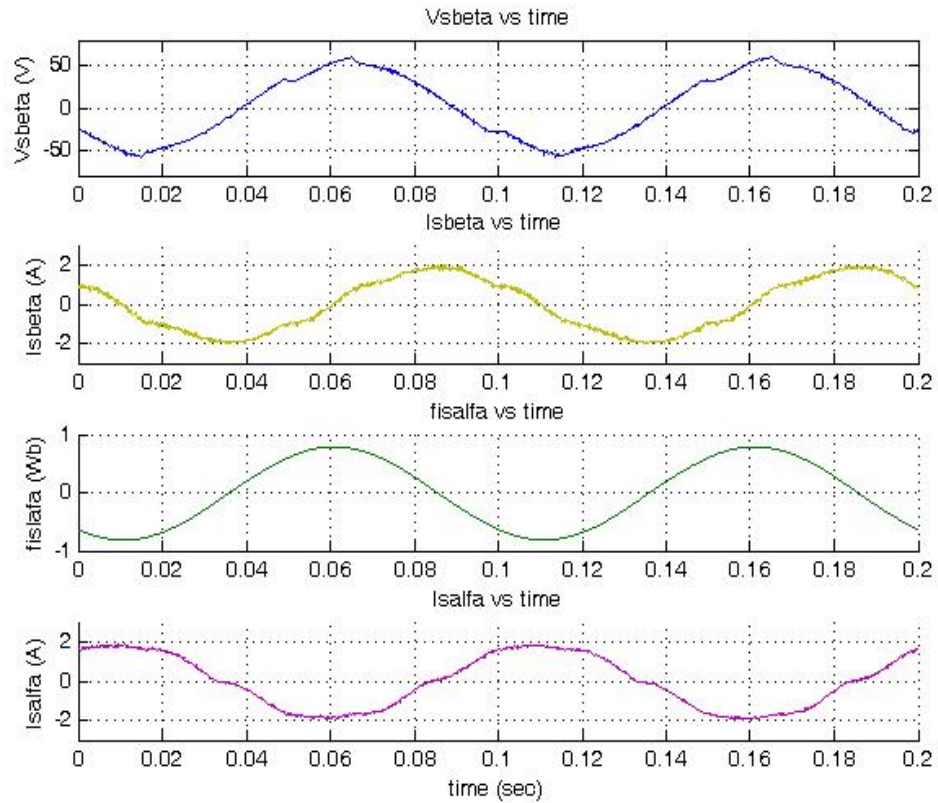


Figure 4. 20 – Variables of 2nd machine which will be used to estimate the R_s at 10 Hz.

Since motor is running at steady state, ω_s is taken as 62.8 rad/sec for 10 Hz. Similarly same algorithm is applied here to estimate the stator resistance, so again the zero cross instant of $\psi_{s\alpha}$ is taken as an estimation interval. In Figure 4. 20 computed $V_{s\beta}$ and $I_{s\beta}$ variables are given. Both have some distortion due to switching and harmonic effects. However flux variable seems sinusoidal since it is calculated as an output of two cascade filters explained in software part of chapter 2 (see section 2.3.1.12.).

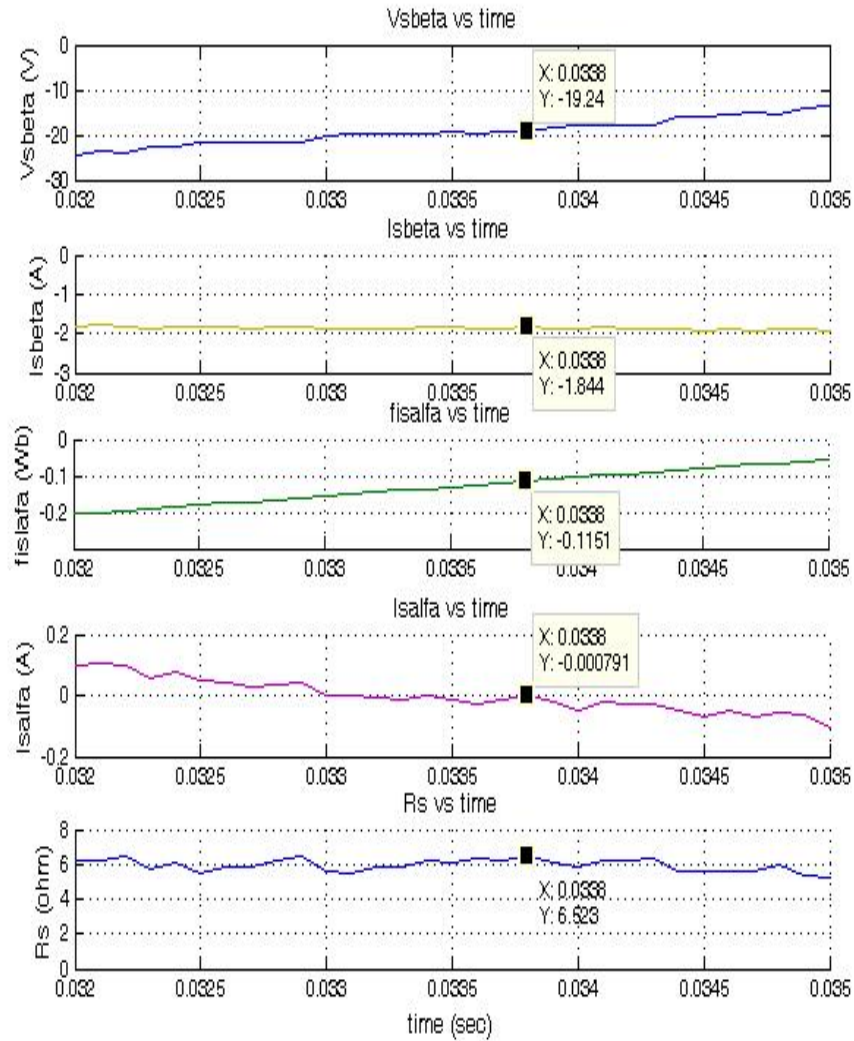


Figure 4. 21 – Stator resistance estimation at zero cross of ψ_{sa} at 10 Hz with PWM drive, for 2nd machine.

It is seen that in this interval stator resistance is estimated as 6.52 ohms where the measured resistance is about 6.50 ohms. Since the offset at the flux variable is very small in this experiment, effect of offset is neglected in stator resistance estimation here. Estimations are made in several other intervals. The result of another interval to estimate the stator resistance is given in Figure 4. 22.

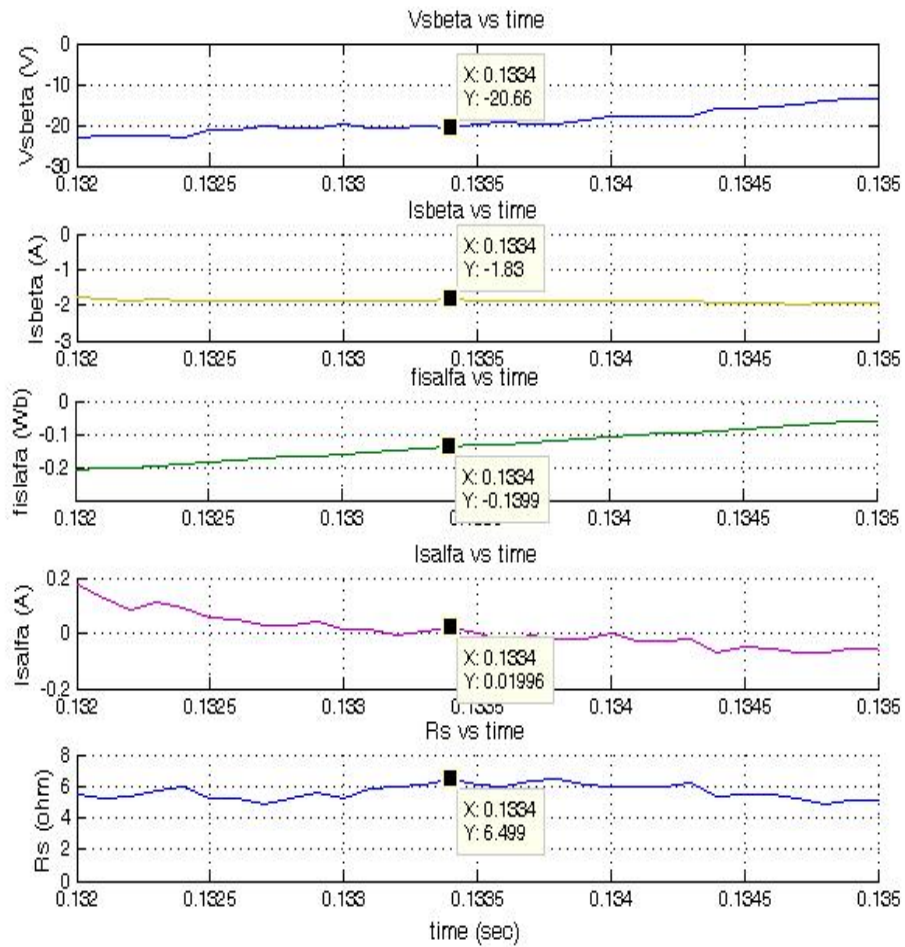


Figure 4. 22 – Another interval for 2nd machine to estimate the Rs at 10 Hz.

From Figure 4. 21 and Figure 4. 22, it can be said that, online R_s estimation method is working very well; since estimated resistance is about 6.499 ohms and the measured resistance is about 6.5 ohms when this experiment is done. Again the off set is found to be very small for this measurement and is neglected. Estimated stator resistance is nearly same with the measured resistance.

4.5.4. R_s Estimation at 10 Hz with 3rd Test Motor

Same on-line stator resistance estimation algorithm is lastly applied to another machine which is 3rd induction machine used in this method. The parameters of that machine are listed at Table 4. 14. Measured line-line voltage applied to test machine #3 at 10 Hz is about 65 V_{rms} .

Table 4. 14 - Parameters of 3rd motor used in the on- line R_s estimation

Parameters of (2.2 kW, 2-pole, Y-connected, $I_{s,rated}=4.8$ A, $V_{s,rated}=220$ V_(phase)) Induction machine	
R_s	2,65 ohm
R_r	3,065 ohm
L_{ls}	13,14 mH
L_{lr}	13,14 mH
L_s	397,41 mH (= $L_{ls}+L_m$)
L_r	397,41 mH (= $L_{lr}+L_m$)
L_m	384,27 mH

Similar to on-line stator resistance estimation process applied on 1st and 2nd machines, firstly the parameters used in estimating the stator resistance are presented in Figure 4. 23.

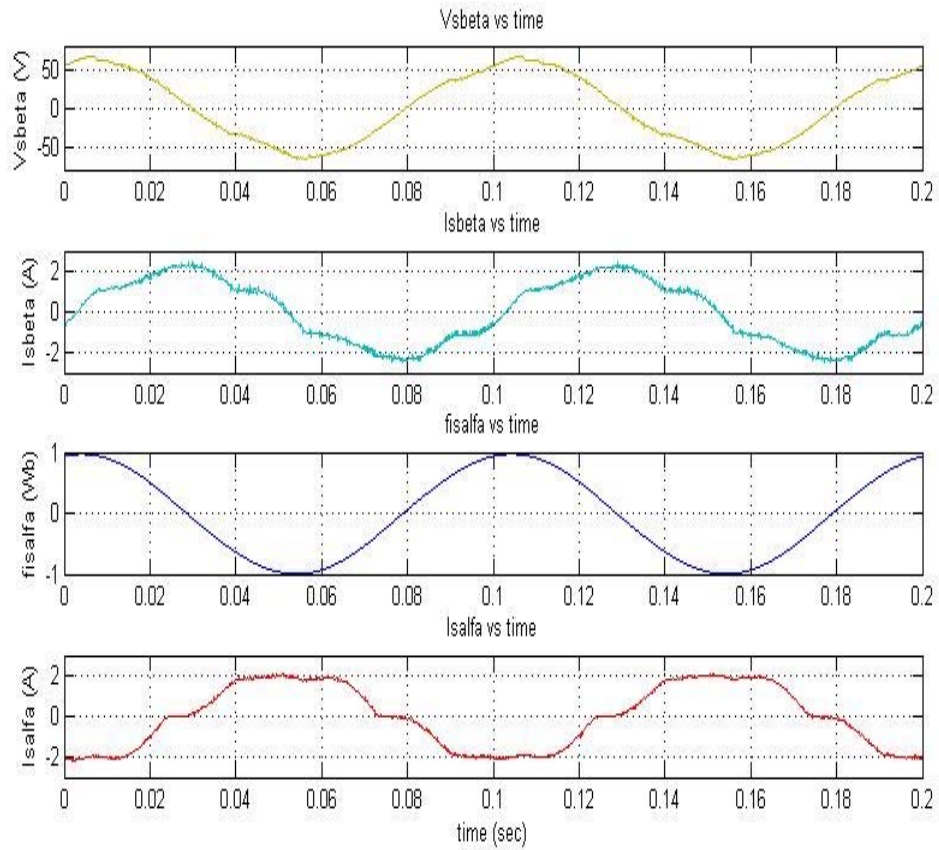


Figure 4. 23 - Variables of 3rd machine which will be used to estimate the R_s at 10 Hz.

Since motor is running at steady state, ω_s is taken 62.8 rad/sec for 10 Hz which was the same situation at the 2nd machine. Similarly same logic is applied here to estimate the stator resistance, so the zero cross of $\psi_{s\alpha}$ is taken as an estimation interval. Waveforms are similar to 2nd motor's waveforms. Here also, offset at the flux variable is very small; it is neglected in stator resistance estimation for this experiment.

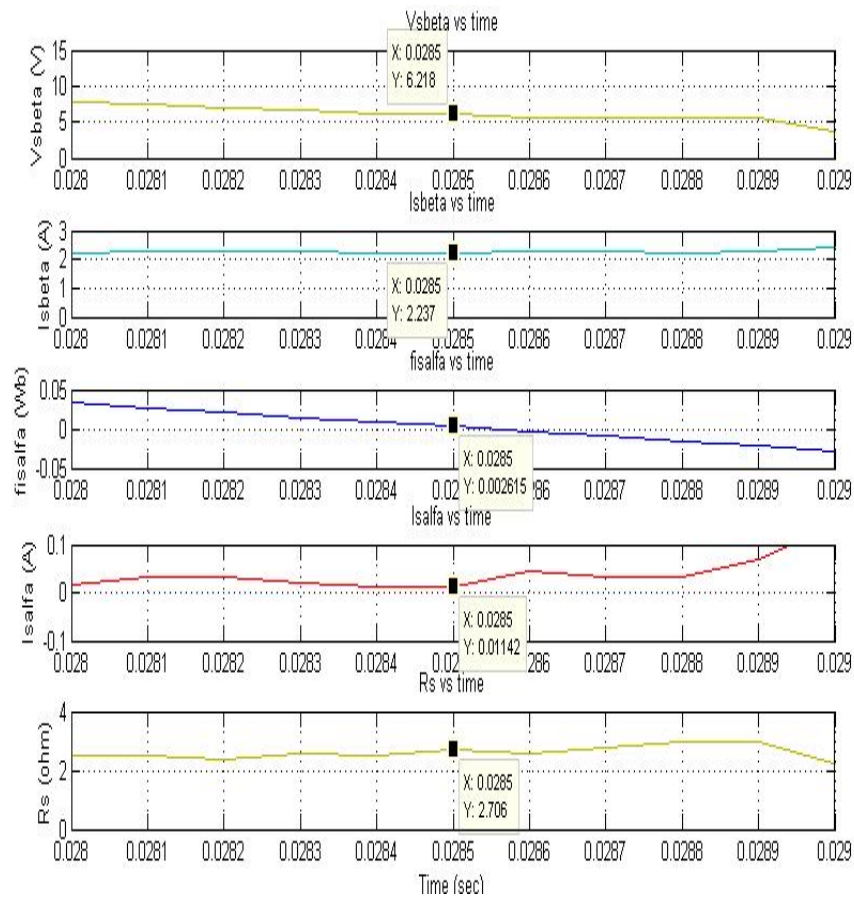


Figure 4. 24 - Stator resistance estimation at zero cross of ψ_{sa} at 10 Hz with driver, for 3rd machine.

As you see from Figure 4. 24, stator resistance is estimated as about 2.7 ohms when the ψ_{sa} crosses zero, and the measured resistance was 2.74 ohms while doing this experiment. Estimation error is about 1.5% which is very good result.

The same algorithm is repeated in another interval where the stator resistance estimation is performed. Again the offset is found to be very small for this measurement and is neglected. Stator estimation result for this interval is presented in Figure 4. 25.

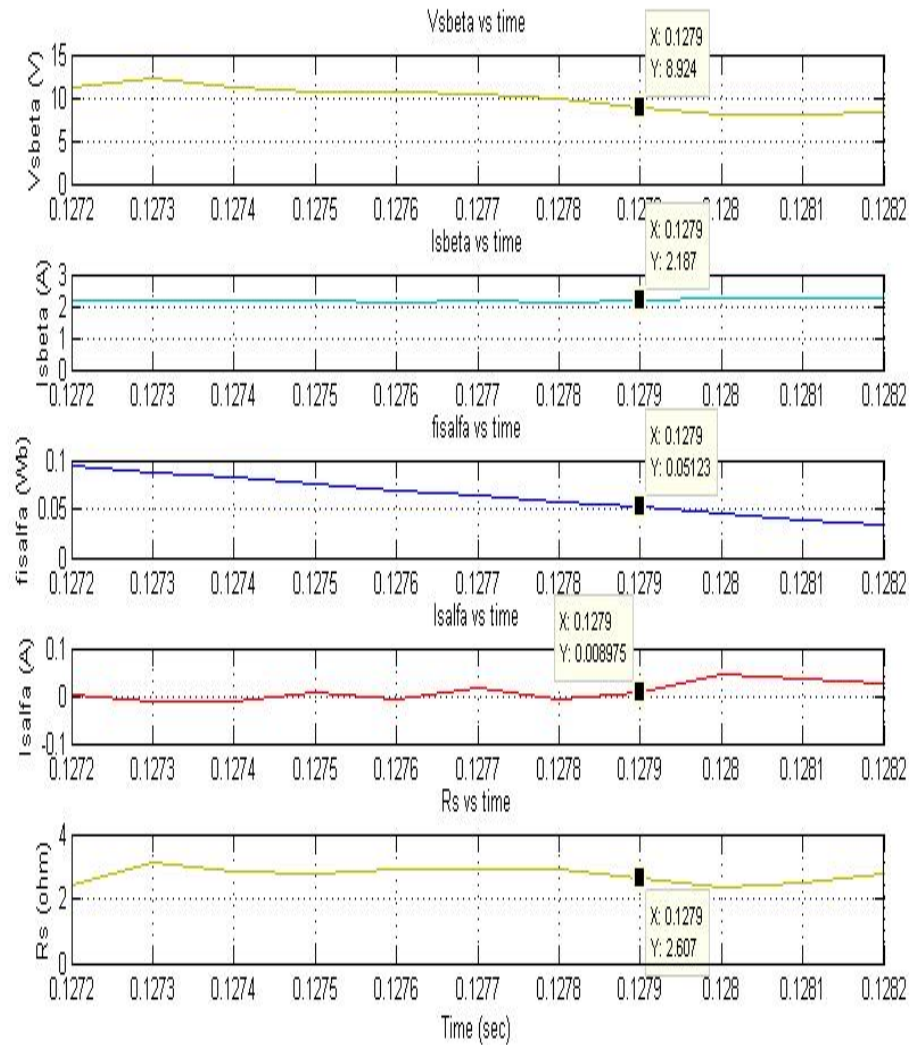


Figure 4. 25 – Another interval to estimate the stator resistance for 3rd machine at 10 Hz.

In this interval R_s is estimated as 2.6 ohms where the measured one was 2.74 ohms. Estimation error here is about 5.1% which is acceptable range.

From Figure 4. 24 and Figure 4. 25, estimated stator resistance values of this machine are close to measured resistance at the instant $\psi_{s\alpha}$ is near to zero.

The proposed method is applied to 3 different induction machines and it is seen that the on-line stator estimation is working pretty well for all those motors at low frequencies where the stator resistance data is very important.

4.6. Stator Resistance Variation with Temperature under Load

The aim of estimating the stator resistance on-line is to update the stator resistance data in the vector control software to estimate the flux vector correctly. However, the algorithm can also be used to estimate the temperature rise of given motor. The resistance changes with temperature and the motor's temperature changes while motor is running under load. To verify the resistance measurement algorithm; 2nd test motor is coupled to a magnetic powder brake which is used as a load. The load torque is set to 3.5 Nm, which is about 33% of the rated torque for this machine. Experimental setup is shown in Figure 4. 26. The motor is operated about 1 hour and the stator resistance is estimated and measured in 15 minutes periods. During the measurements, vector control drive is stopped and inverter side is decoupled from induction machine by means of 3 phase mechanical switch and micro-ohmmeter (Agilent 34420A) is used to measure the stator resistance. Micro-ohmmeter readings are recorded in a very short time. Then the inverter side is coupled again to the machine and driving the machine at the same load condition is continued. The cold resistance of the machine was measured as 6.35 ohms where the medium temperature is 22^o. Then the first measurement is taken a while later and this instant is taken as a starting time as shown in Table 4. 15.

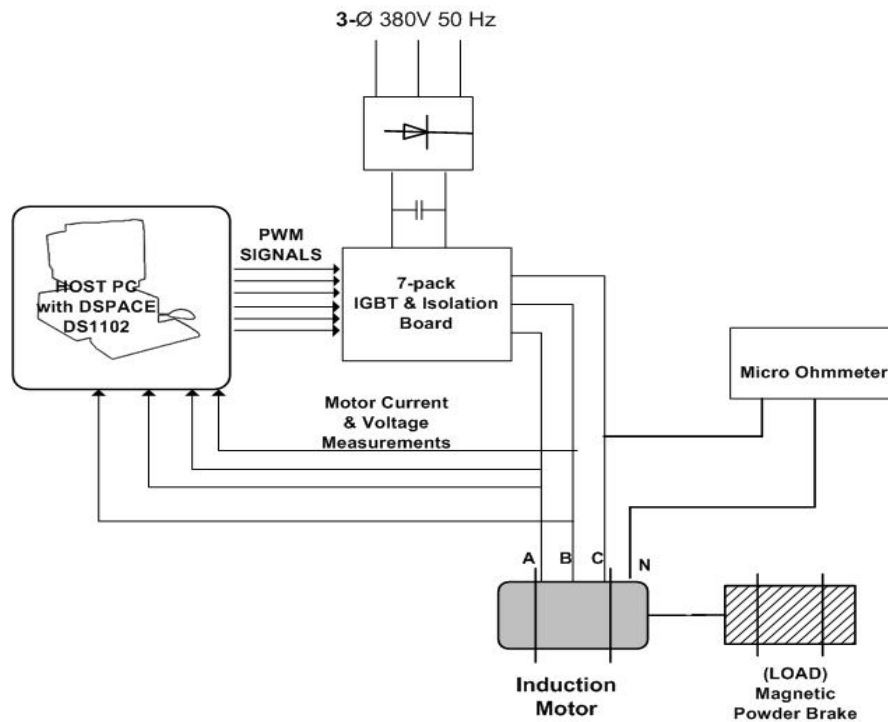


Figure 4. 26 – Experimental setup used to observe stator resistance change under load

In Table 4. 15, the recorded measurements and estimations of stator resistance is given. It seems that our proposed on-line stator resistance estimation algorithm is working very well under load conditions.

Table 4. 15 – Measured and Estimated R_s and temperature, while the motor is running under load

<i>Time (minutes)</i>	<i>Measured R_s (ohm)</i>	<i>Estimated R_s (ohm)</i>	<i>Estimated temperature wrt Measured R_s ($^{\circ}$)</i>	<i>Estimated temperature wrt Estimated R_s ($^{\circ}$)</i>
0	6,40	6,45	24,02	26,04
15	6,59	6,65	31,69	34,12
30	6,75	6,8	38,16	40,18
45	6,87	6,92	43,00	45,02
60	6,93	6,98	45,43	47,45

In Figure 4. 27, the measured and estimated stator resistances listed in table 4.9 are presented.

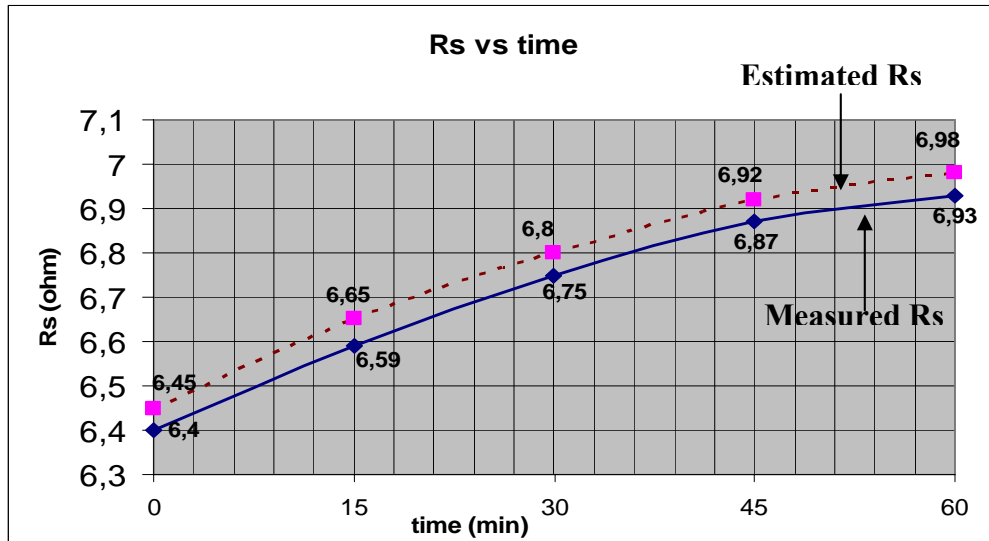


Figure 4. 27 – Measured and estimated Rs variation while motor is running under load.

After measured and estimated stator resistance values are obtained, now let's look at the temperature change relation with rising resistance. Relation between temperature and resistance is given below in equation (4.16);

$$\frac{234,5 + T_0}{234,5 + T_f} = \frac{R_{initial}}{R_{final}} \quad (4.16)$$

Since initial laboratory temperature was 22⁰, the initial temperature of the induction machine is taken as 22⁰, too. Now let's calculate the motor's temperature by using the equation (4.16) with respect to measured stator resistance. Initial temperature of the machine is 22⁰.

$$T_0 = 22^0$$

$$R_{\text{initial}} = 6,35 \text{ ohms}$$

$$R_{\text{final}} = 6,93 \text{ ohms}$$

Substitute these values in equation 4.16;

$$\frac{234,5 + T_0}{234,5 + T_f} = \frac{R_{\text{initial}}}{R_{\text{final}}} \Rightarrow \frac{234,5 + 22}{234,5 + T_f} = \frac{6,35}{6,98} \Rightarrow T_f = 45,43^\circ$$

Final motor temperature is found as 45.43^0 with respect to the micro-ohmmeter readings of stator resistance.

Now let's calculate the motor's average temperature with respect to the estimated stator resistance values by using the initial conditions.

$$T_0 = 22^0$$

$$R_{\text{initial}} = 6,35 \text{ ohms}$$

$$R_{\text{final}} = 6,98 \text{ ohms}$$

$$\frac{234,5 + T_0}{234,5 + T_f} = \frac{R_{\text{initial}}}{R_{\text{final}}} \Rightarrow \frac{234,5 + 22}{234,5 + T_f} = \frac{6,35}{6,98} \Rightarrow T_f = 47,45^\circ$$

Final motor temperature with respect to the estimated stator resistance is found as 47.45^0 . On the other hand motor's average temperature is calculated as 45.43^0 by using the measured resistance values. Estimation error is about 4.45% with respect to the temperature found by using measured resistance values.

As you see from Table 4. 15 and Figure 4. 27, estimated and measured stator resistance is so close to each other. The resistance changes about 8% under 33%

of rated torque in about 1 hour, that means motor resistance changes are important under load conditions. It is obvious that for good position estimation it is important to update the resistance in the vector control method, and this algorithm is well suited for the purpose.

The final motor temperatures are nearly same, so we can use this temperature change data to update the all other resistance variables in the induction machine by using the equation (4.16). This temperature data can also be used as a protection variable without using any temperature sensor.

4.7. Conclusion

In this chapter, a novel approach to on-line stator resistance estimation is examined. The theory is explained in first parts and then some experiments are performed to verify the method. Experiments are done at different frequencies with different voltage sources. Firstly, sinusoidal voltage supplies are used and then the PWM driver that we designed is used to drive the motor at different frequencies at steady state. For both cases our on – line method has worked properly.

It is very important to know stator resistance exactly at low frequencies, since the voltage drop on the stator resistance becomes comparable with the voltage drops on the inductances and the most useful side of our method is that, it is pretty good working at low speeds. As a result of this, this method gives so advantage at sensorless vector control of induction machines where the stator resistance is very important especially at low speeds.

On the other hand, when motor is running under load, its' temperature gets higher so its resistance parameters increase. Since the stator resistance measurement algorithm here works on-line we can obtain the motor's average temperature change instantly. Therefore if the phase resistance is known at a certain temperature, the average temperature of stator windings can be calculated. This

average temperature data gives an idea about temperature change in other parts of the induction motor, as well. Knowing the temperature of the motor is very important at emergency situations. By checking the temperature, for pre-determined limit, it becomes possible to stop the motor's operation without using any temperature sensors.

CHAPTER 5

CONCLUSION

5.1. General

In this thesis work, it is aimed to improve the previously developed vector control drive studies as hardware and software environments. In the hardware, new intelligent power module (IPM, 7-pack inverter), which has dynamic braking capability, is integrated to the existing vector control drive. Besides, dead time generator module is improved by using new IC, which is explained in Chapter 2. In the software, dynamic braking and dc-link compensation modules are constructed. Software is built up in modules so it became easy to control and change the software program. In previous studies, only phase voltages and currents could be measured. If the machine is Y-connected the previous drive requires star point to make measurements. However, in newly developed vector control drive it is possible to take measurements both from phase and line voltages. Therefore it became possible to control Δ -connected motors.

Another purpose of this thesis work was to develop off-line leakage inductance and on-line stator resistance estimation methods that can be integrated to the drive. Theory and algorithm of a new off-line leakage inductance prediction algorithm is explained in detail in Chapter 3. Experiments are performed with 3 different test machines to verify the developed off-line leakage inductance estimation algorithm. As shown in Table 3.5 predicted and measured leakage inductances match very well for all of the test machines and the estimation error is under 3%.

On the other hand, in Chapter 4, theory behind the on-line stator resistance estimation method developed in this work is explained. When the motor is

running at steady state 2 line or phase voltages and currents are measured via voltage and current transducers on developed driver. These measurements are used in the prediction of stator resistance while the motor is running at steady state. On-line stator resistance experiments are performed at different supply frequencies with various induction machines. Experimental results related with on-line stator resistance estimation are shown in Chapter 4. Experiments, performed on various test machines for predicting the stator resistance, are compared with the measured stator resistance. It is shown that the proposed algorithm work well and the prediction accuracy is better than 8% irrespective of supply frequency or motor type. It is also shown that since the stator resistance can be well predicted under operation. It is possible to predict the motor average temperature using the proposed algorithm. The only requirement for this approach to work well is to know the phase resistance at a known temperature. This can be easily done by the user during commissioning and entered as data to the drive. An experiment is performed to investigate how well the temperature prediction algorithm works. It is shown that the approach works well, too.

5.2. Future Work

The performance vector control drive relies on accurate knowledge of motor parameters. In this thesis work just leakage inductance is estimated as offline and stator resistance is estimated online. In future work;

- Off-line stator leakage estimation and on-line stator resistance estimation algorithms developed here should be embedded to the main software.
- Estimated points in stator leakage inductance prediction are scattered. To minimize that scattering of estimated points, filtering techniques like Extended Kalman Filter should be utilized.
- In verification of stator resistance estimation algorithm, there should be more experiments performed on several induction motors at different frequencies.

- Since knowing stator resistance value accurately is very important at low frequencies, on-line stator resistance estimation algorithm introduced in this thesis should be performed at frequencies less than 10 Hz.
- In this thesis work, dynamic tests are not performed, so there should be some dynamic tests to examine the dynamic performance of the drive as a future work.

REFERENCES

- [1] Bose, Bimal K. , “Modern Power Electronics and AC Drives” , Prentice Hall PTR, 2002.
- [2] Novotny, D. W. , Lipo, T.A. , “Vector Control And Dynamics Of AC Drives, Oxford University Press, 1998
- [3] DS1102 Software Environment dSPACE, 1996
- [4] Acar, A. “Implementation of a Vector Controlled Induction Motor Drive” , Msc. Thesis, METU, 2004.
- [5] Murat, İ. E. , “Self Commissioning And Online Parameter Identification of Induction Motors”, Msc. Thesis METU, 2002.
- [6] Akın, M. , “Bir Vektör Kontrol Yönteminin Uygulama Hız Sınırlarının Genişletilmesi İçin Yöntem Geliştirme”, Msc. Thesis, Hacettepe University, 2002.
- [7] Özyurt, Ç. H. , “ Parameter and Speed estimation of Induction Motors from Manufacturers Data and Measurements” , Msc Thesis, METU, 2005.
- [8] “Field Oriented Control of 3-Phase AC Motors”, Texas Instruments Europe Application Note, Literature Number: BPRA073, 1998.
- [9] “Implementing Space Vector Modulation with ADMC401”, Analog Devices, AN401-18, January 2000.

- [10] A. M. Khambadkone, J. Holtz, "Vector Controlled Induction Motor Drive With a Self Commissioning Scheme", IEEE Transactions on Industrial Electronics, Vol. 38 No 5, pp. 322-327, Oct. 1991.
- [11] P. Vas, Sensorless Vector and Direct Torque Control, Oxford University Press, 1998.
- [12] H. Can, "Implementation of Vector Control for Induction Motors", MSc. Thesis, Middle East Technical University, Ankara, Turkey, 1999.
- [13] P. Vas, Parameter Estimation, Condition Monitoring, and Diagnosis of Electrical Machines, Clarendon Press, Oxford 1993.
- [14] C.B. Jacobina, J.E.C. Filho, A.M.N. Lima, "Online Estimation of the Stator Resistance of Induction Machines Based on Zero Sequence Model", IEEE Transactions on Power Electronics, Vol. 15, No.2, pp. 346-353, March 2000.
- [15] J.L. Silvino, B.C. Rabelo, "An Improved Estimation of The Induction Machine Leakage Inductances", IEEE Transactions on Industrial Electronics, Letter to the Editor, Vol 46, No.5, pp. 1040-1042, Oct. 1999.
- [16] Y. Lai, J. Lin, J. Wang, "Direct Torque Control Induction Motor Drives with Self Commissioning Based on Taguchi Methodology", IEEE Transactions on Power Electronics, Vol 15, No 6, pp. 1065-1071, Nov. 2000.
- [17] H. B. Ertan, E. Murat, B. Colak, "A Novel Approach to Detection of Some Parameters of Induction Motors" , IEEE - IEMDC'07 May 3-5, 2007, Antalya Turkey, AF 012327.

- [18] Y. Lin, C. Chen, "Automatic IM Parameter Measurement under Sensorless Field-Oriented Control", IEEE Transactions on Industrial Electronics, Vol. 46, No 1, pp. 111-127, Feb. 1999.
- [19] B. K. Bose, N. Patel, "Quasi-Fuzzy Estimation of Stator Resistance Estimation of Induction Motor", IEEE Transactions On Power Electronics, Vol. 13, No. 3, pp. 401-409, May 1998.
- [20] G. Guidi, H. Umida, "A novel stator resistance estimation method for speed sensorless induction motor drives," IEEE Trans. Ind. Appl., vol. 36, pp. 1619-1627, Nov./Dec. 2000.
- [21] V. Vasic, S. N. Vukosavic, E. Levi, "A Stator Resistance Estimation Scheme for Speed Sensorless Rotor Flux Oriented Induction Motor Drives", IEEE Trans On Energy Conversion, Vol. 18, No.4, pp. 476-483, Dec 2003.
- [22] B. Karanayil, M.F.Rahman, C. Grantham, "Online Stator and Rotor Resistance Estimation Scheme Using Artificial Neural Networks for Vector Controlled Speed Sensorless Induction Motor Drive", IEEE Transactions on Industrial Electronics, Vol. 54, No. 1, pp. 167-146, Feb 2007.
- [23] H. B. Ertan, Q. H. Ozyurt "Prediction of Induction motor Parameters From Manufacturer's Data" SIELA 2005, Plovdiv, Bulgaria, 2-3 June 2005.
- [24] Lai Yen-Shin, Chang Ye-Then "Design And Implementation Of Vector Controlled Induction Motor Drives Using Random Switching Technique With Constant Sampling Frequency", IEEE Transactions on Power Electronics, Vol.16, No.3, May 2001.

- [25] K. Rajashekara, A. Kawamura and K. Matsuse (Ed.), “Sensorless Control of AC Drives”, IEEE Press, NY, 1996.

APPENDIX A

Calculation of PI Controller Parameters

The controller design under consideration of high dynamic performance induction motor drive is based on [24].

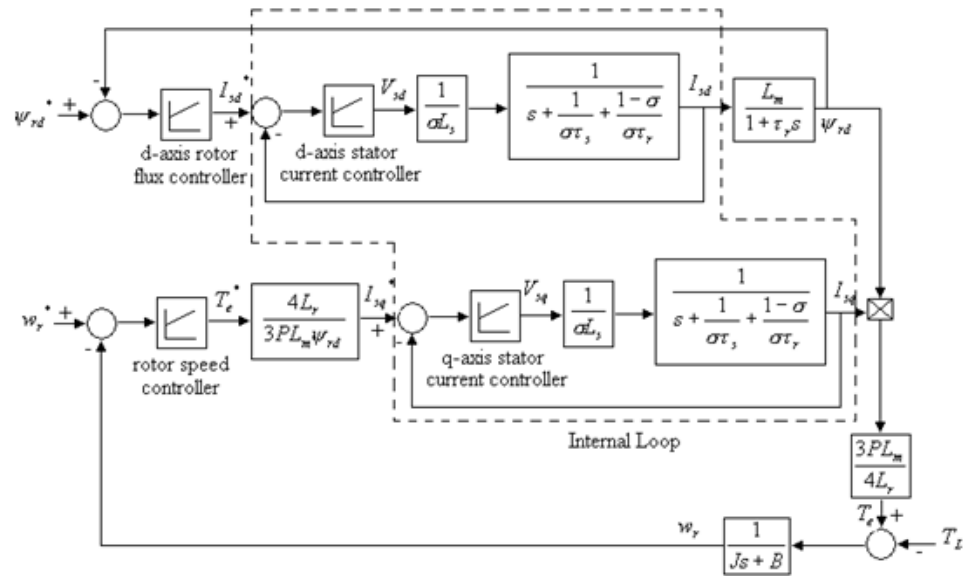


Figure A. 1 – Control system of vector controlled induction motor drives

The dynamic model of induction motors for rotor flux oriented vector control applications can be written as follows [4];

$$p \begin{bmatrix} I_{ds} \\ I_{qs} \\ \psi_{rd} \\ \psi_{rq} \end{bmatrix} = \begin{bmatrix} -\frac{1}{\sigma\tau_s} - \frac{1-\sigma}{\sigma\tau_r} & w_e & \frac{L_m}{\sigma L_s \tau_r L_r} & \frac{L_m w_r}{\sigma L_s L_r} \\ -w_e & -\frac{1}{\sigma\tau_s} - \frac{1-\sigma}{\sigma\tau_r} & -\frac{L_m w_r}{\sigma L_s L_r} & \frac{L_m}{\sigma L_s \tau_r L_r} \\ \frac{L_m}{\tau_r} & 0 & -\frac{1}{\tau_r} & w_s \\ 0 & \frac{L_m}{\tau_r} & -w_s & -\frac{1}{\tau_r} \end{bmatrix} \begin{bmatrix} I_{ds} \\ I_{qs} \\ \psi_{rd} \\ \psi_{rq} \end{bmatrix} + \frac{1}{\sigma L_s} \begin{bmatrix} V_{sd} \\ V_{sq} \\ 0 \\ 0 \end{bmatrix} \quad (\text{A.1})$$

Substituting the condition of rotor flux oriented vector control

$$\psi_r = \psi_{rd} + j\psi_{rq} = \psi_{rd} \quad (\text{A.2})$$

$$\psi_{rq} = 0 \quad (\text{A.3})$$

into (A.1) yields;

$$p \begin{bmatrix} I_{sd} \\ I_{sq} \\ \psi_{rd} \end{bmatrix} = \begin{bmatrix} -\frac{1}{\sigma\tau_s} - \frac{1-\sigma}{\sigma\tau_r} & w_e & \frac{L_m}{\sigma L_s \tau_r L_r} \\ -w_e & -\frac{1}{\sigma\tau_s} - \frac{1-\sigma}{\sigma\tau_r} & -\frac{L_m w_r}{\sigma L_s L_r} \\ \frac{L_m}{\tau_r} & 0 & -\frac{1}{\tau_r} \end{bmatrix} \begin{bmatrix} I_{sd} \\ I_{sq} \\ \psi_{rd} \end{bmatrix} + \frac{1}{\sigma L_s} \begin{bmatrix} V_{sd} \\ V_{sq} \\ 0 \end{bmatrix} \quad (\text{A.4})$$

and the torque equation becomes

$$T_e = \frac{3}{2} \frac{P}{2} \frac{L_m}{L_r} I_{sq} \psi_{rd} \quad (\text{A.5})$$

Rewriting the Equation (A.1) in the form of decoupling as shown in Equation (A.6), the nonlinearity can be separated from the consideration of controller design.

$$p \begin{bmatrix} I_{sd} \\ I_{sq} \\ \psi_{rd} \end{bmatrix} = \begin{bmatrix} -\frac{1}{\sigma\tau_s} - \frac{1-\sigma}{\sigma\tau_r} & 0 & 0 \\ 0 & -\frac{1}{\sigma\tau_s} - \frac{1-\sigma}{\sigma\tau_r} & 0 \\ \frac{L_m}{\tau_r} & 0 & -\frac{1}{\tau_r} \end{bmatrix} \begin{bmatrix} I_{sd} \\ I_{sq} \\ \psi_{rd} \end{bmatrix} + \frac{1}{\sigma L_s} \begin{bmatrix} V_{sd}^* \\ V_{sq}^* \\ 0 \end{bmatrix} \quad (\text{A.6})$$

where

$$\begin{bmatrix} V_{sddecoup} \\ V_{sqdecoup} \end{bmatrix} = \begin{bmatrix} \omega_e I_{sq} + \frac{L_m}{\sigma L_s \tau_r L_r} \psi_{rd} \\ -\omega_e I_{sd} - \frac{L_m}{\sigma L_s \tau_r L_r} \psi_{rd} \end{bmatrix} \quad (\text{A.7})$$

The transfer function of the plant for the controllers of the vector controlled induction motor drives can be derived and shown as follows

d-Axis Current Controller:

$$G_{Id}(s) = \frac{I_{sd}}{V_{sd}} = \frac{\frac{1}{\sigma L_s}}{s + \frac{1}{\sigma L_s} + \frac{1-\sigma}{\sigma\tau_r}} = \frac{\frac{1}{\sigma L_s}}{s + \frac{\tau_r + \tau_s - \sigma\tau_s}{\sigma\tau_s\tau_r}} \quad (\text{A.8})$$

q-Axis Current Controller:

$$G_{Iq}(s) = \frac{I_{sq}}{V_{sq}} = \frac{\frac{1}{\sigma L_s}}{s + \frac{1}{\sigma L_s} + \frac{1-\sigma}{\sigma\tau_r}} = \frac{\frac{1}{\sigma L_s}}{s + \frac{\tau_r + \tau_s - \sigma\tau_s}{\sigma\tau_s\tau_r}} \quad (\text{A.9})$$

Flux Controller:

$$G_{\psi}(s) = \frac{\Psi_{rd}}{I_{sd}} = \frac{\frac{L_m}{s + \frac{1}{\tau_r}}}{I_{sd}} \quad (\text{A.10})$$

Speed Controller:

$$G_s(s) = \frac{w_r}{T_e} = \frac{\frac{1}{J_m}}{s + \frac{B}{J_m}} \quad (\text{A.11})$$

Since the motor plants of q-axis current control, d-axis current control, flux control, and speed control are all first order systems, the design process for these four controllers are similar.

Transfer function of current control system is given below

$$G_I(s) = \frac{I_s}{V_s} = \frac{\frac{1}{\sigma L_s}}{s + \frac{\tau_r + \tau_s - \sigma \tau_s}{\sigma \tau_s \tau_r}} \quad (\text{A.12})$$

For a proportional-integral controller, the controller, C(s), is

$$C(s) = \frac{k_p \left(s + \frac{k_i}{k_p} \right)}{s} \quad (\text{A.13})$$

By using the pole-zero cancellation method, the parameters of the controller are derived and shown as follows

$$k_p = BW \cdot \sigma L_s \quad (\text{A.14})$$

$$k_i = \frac{\tau_r + \tau_s - \sigma \tau_s}{\sigma \tau_s \tau_r} \cdot BW \cdot \sigma L_s \quad (\text{A.15})$$

where BW=bandwidth of the controller.

Calculations performed up to now are valid in continuous time domain. But in real time applications, system is controlled in discrete time domain, so parameters of the controller must be calculated in discrete time domain also. Block diagram of the current controller in discrete time domain is shown in Figure A.2.

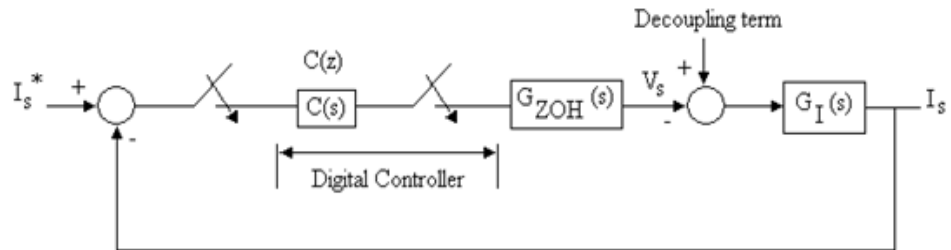


Figure A. 2 – Block diagram of the current control system in discrete time domain

The proportional-integral controller in terms of “Z” transforms in the discrete time domain can be derived as shown

$$C(z) = \frac{(k_p + k_i T)z - k_p}{z - 1} \quad (\text{A.16})$$

The controller design in discrete time domain includes the following steps:

- 1) Calculating the open loop transfer function of the plant
- 2) Deriving the loop gain of the control system using a pole-zero cancellation method.
- 3) Deducing the parameters of the controller for the specified bandwidth.

Step 1- Calculating the open loop transfer function of the plant:

The open loop transfer function of the plant in discrete time domain can be derived as

$$\begin{aligned} \frac{I_s(z)}{\Delta I_s(z)} &= C(z) \cdot Z[G_{ZOH}(s) \cdot G_I(s)] \\ &= \frac{(k_p + k_i T) \tau_r \tau_s}{L_s(\tau_r + \tau_s - \sigma \tau_s)} \cdot \frac{\left(z - \frac{k_p}{k_p + k_i T} \right) \left[1 - \exp\left(-\frac{\tau_r + \tau_s - \sigma \tau_s}{\sigma \tau_r \sigma_s} T \right) \right]}{(z-1) \left[z - \exp\left(-\frac{\tau_r + \tau_s - \sigma \tau_s}{\sigma \tau_r \tau_s} \right) \right]} \end{aligned} \quad (\text{A.17})$$

Step 2- Deriving the loop gain of the control system using a pole-zero cancellation method:

The relationship between the proportional and integral constants for pole-zero cancellation can be derived as

$$k_p = \frac{\exp\left(-\frac{\tau_r + \tau_s - \sigma \tau_s}{\sigma \tau_r \sigma_s} T \right) \cdot k_i T}{1 - \exp\left(-\frac{\tau_r + \tau_s - \sigma \tau_s}{\sigma \tau_r \sigma_s} T \right)} \quad (\text{A.18})$$

Substituting Equation (A.18) into Equation (A.17), the transfer function shown in Equation (A.17) becomes

$$\frac{I_s(z)}{\Delta I_s(z)} = \frac{(k_p + k_i T)\tau_r \tau_s}{L_s(\tau_r + \tau_s - \sigma\tau_s)} \cdot \frac{\left[1 - \exp\left(-\frac{\tau_r + \tau_s - \sigma\tau_s}{\sigma\tau_r \sigma_s} T\right)\right]}{(z-1)} \quad (\text{A.19})$$

Step 3- Deducing the parameters of the controller for the specified bandwidth:

The closed loop transfer function of the system can be derived as

$$\frac{I_s(z)}{I_s^*(z)} = \frac{\frac{(k_p + k_i T)\tau_r \tau_s \left[1 - \exp\left(-\frac{\tau_r + \tau_s - \sigma\tau_s}{\sigma\tau_r \sigma_s} T\right)\right]}{L_s(\tau_r + \tau_s - \sigma\tau_s)}}{z - 1 + \frac{(k_p + k_i T)\tau_r \tau_s \left[1 - \exp\left(-\frac{\tau_r + \tau_s - \sigma\tau_s}{\sigma\tau_r \sigma_s} T\right)\right]}{L_s(\tau_r + \tau_s - \sigma\tau_s)}} \quad (\text{A.20})$$

By specifying the bandwidth of the first order system, the corresponding representation in discrete time-domain is

$$Z\left[G_{zOH}(s) \frac{BW}{s + BW}\right] = \frac{1 - \exp(-BW \cdot T)}{z - \exp(-BW \cdot T)} \quad (\text{A.21})$$

Comparing Equation (A.20) and Equation (A.21) yields

$$k_p + k_i T = \frac{[1 - \exp(-BW \cdot T)]L_s(\tau_r + \tau_s - \sigma\tau_s)}{\tau_r \tau_s \left[1 - \exp\left(-\frac{\tau_r + \tau_s - \sigma\tau_s}{\sigma\tau_r \sigma_s} T\right) \right]} \quad (\text{A.22})$$

$$k_i = \frac{[1 - \exp(-BW \cdot T)]L_s(\tau_r + \tau_s - \sigma\tau_s)}{\tau_r \tau_s T} \quad (\text{A.23})$$

$$k_p = \frac{\exp\left(-\frac{\tau_r + \tau_s - \sigma\tau_s}{\sigma\tau_r \sigma_s} T\right) [1 - \exp(-BW \cdot T)]L_s(\tau_r + \tau_s - \sigma\tau_s)}{\tau_r \tau_s \left[1 - \exp\left(-\frac{\tau_r + \tau_s - \sigma\tau_s}{\sigma\tau_r \sigma_s} T\right) \right]} \quad (\text{A.24})$$

Flux Controller:

$$k_i = \frac{[1 - \exp(-BW \cdot T)]}{L_m T} \quad (\text{A.25})$$

$$k_p = \frac{\exp\left(-\frac{1}{\tau_r} T\right) [1 - \exp(-BW \cdot T)]}{\left[1 - \exp\left(-\frac{1}{\tau_r} T\right) \right] L_m} \quad (\text{A.26})$$

Speed Controller:

$$k_i = \frac{[1 - \exp(-BW \cdot T)]B_m}{T} \quad (\text{A.27})$$

$$k_p = \frac{\exp\left(-\frac{B_m}{J_m} T\right) [1 - \exp(-BW \cdot T)] B_m}{\left[1 - \exp\left(-\frac{B_m}{J_m} T\right)\right]} \quad (\text{A.28})$$

PI controller parameters of the vector controlled system for different bandwidth values are given in Table A.1. In the application, PI controller parameters calculated for 314 rad/sec are used.

Table A. 1 – PI controller parameters for different bandwidth values

Bandwidth of PI controller parameters (rad/sec)	k_i	k_p
314	3195	6,97
500	5041	10,99
1000	9837	21,45

APPENDIX B

DATASHEET of IPM

MITSUBISHI <INTELLIGENT POWER MODULES>

PM25RLA120

FLAT-BASE TYPE
INSULATED PACKAGE

PM25RLA120

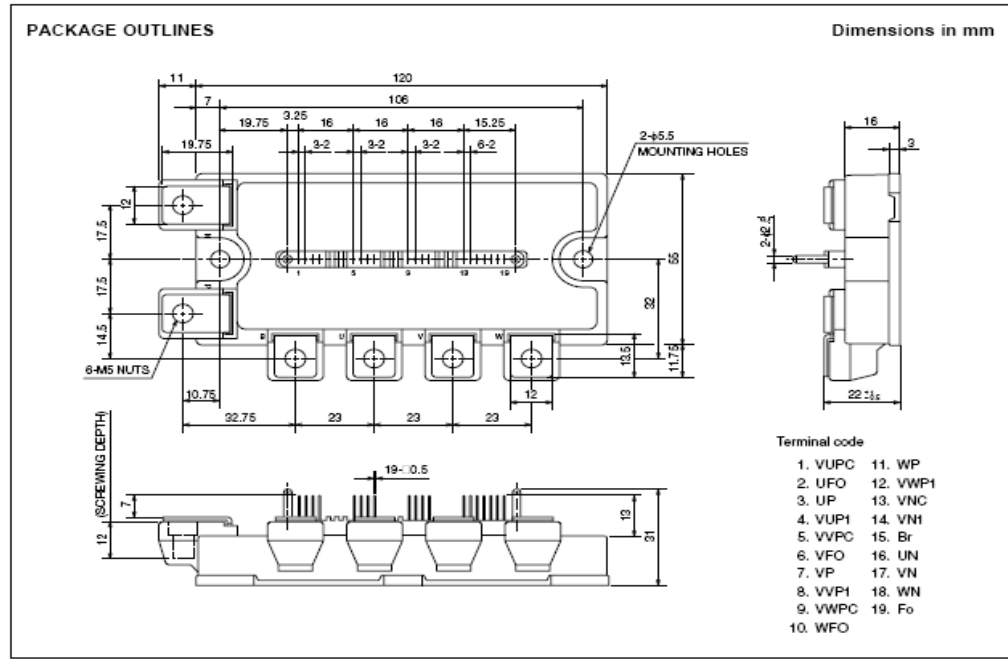


FEATURE

- a) Adopting new 5th generation IGBT (CSTBT) chip, which performance is improved by 1 μ m fine rule process.
For example, typical $V_{ce(sat)}=1.9V$ @ $T_J=125^{\circ}C$
- b) I adopt the over-temperature conservation by T_J detection of CSTBT chip, and error output is possible from all each conservation upper and lower arm of IPM.
- c) Current rating of brake part increased.
60% for the current rating of inverter part.
 - 3 ϕ 25A, 1200V Current-sense IGBT type inverter
 - 15A, 1200V Current-sense regenerative brake IGBT
 - Monolithic gate drive & protection logic
 - Detection, protection & status indication circuits for, short-circuit, over-temperature & under-voltage (P-F ϕ available from upper arm devices)
 - Acoustic noise-less 3.7kW class inverter application
 - UL Recognized Yellow Card No.E80276(N)
File No.E80271

APPLICATION

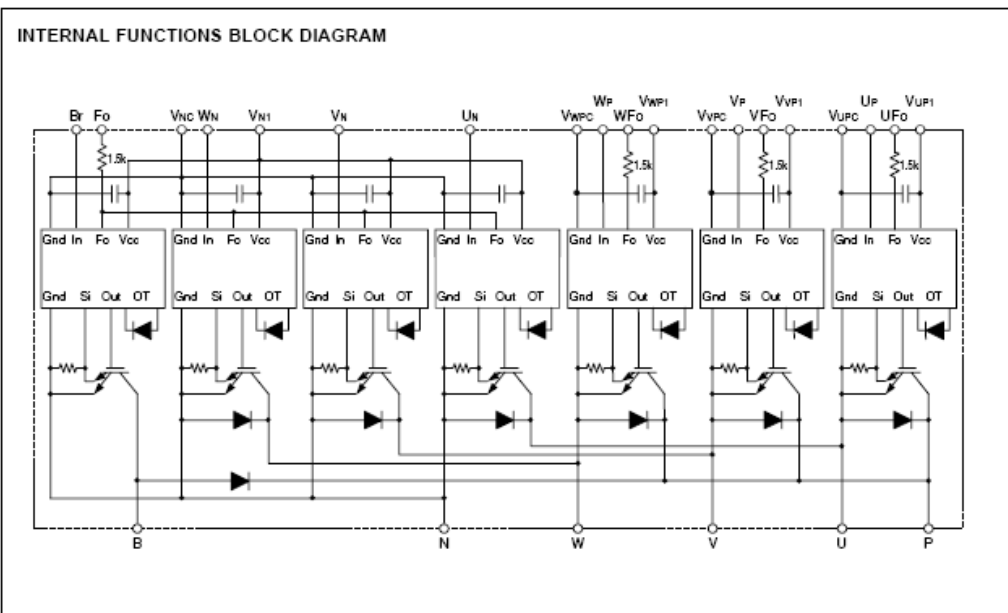
General purpose inverter, servo drives and other motor controls



MITSUBISHI <INTELLIGENT POWER MODULES>

PM25RLA120

FLAT-BASE TYPE
INSULATED PACKAGE



MAXIMUM RATINGS (T_J = 25°C, unless otherwise noted)

INVERTER PART

Symbol	Parameter	Condition	Ratings	Unit
V _{CEs}	Collector-Emitter Voltage	V _D = 15V, V _{CIN} = 15V	1200	V
I _c	Collector Current	T _c = 25°C	25	A
I _{cP}	Collector Current (Peak)	T _c = 25°C	50	A
P _c	Collector Dissipation	T _c = 25°C (Note-1)	150	W
T _J	Junction Temperature		-20 ~ +150	°C

BRAKE PART

Symbol	Parameter	Condition	Ratings	Unit
V _{CEs}	Collector-Emitter Voltage	V _D = 15V, V _{CIN} = 15V	1200	V
I _c	Collector Current	T _c = 25°C	15	A
I _{cP}	Collector Current (Peak)	T _c = 25°C	30	A
P _c	Collector Dissipation	T _c = 25°C (Note-1)	130	W
V _{R(DC)}	FWDi Rated DC Reverse Voltage	T _c = 25°C	1200	V
I _F	FWDi Forward Current	T _c = 25°C	15	A
T _J	Junction Temperature		-20 ~ +150	°C

CONTROL PART

Symbol	Parameter	Condition	Ratings	Unit
V _D	Supply Voltage	Applied between : V _{UP1} -V _{UPC} V _{VP1} -V _{VPc} , V _{WP1} -V _{WPc} , V _{N1} -V _{Nc}	20	V
V _{CIN}	Input Voltage	Applied between : U _P -V _{UPc} , V _P -V _{VPc} W _P -V _{WPc} , U _N - V _N - W _N - Br-V _{Nc}	20	V
V _{FO}	Fault Output Supply Voltage	Applied between : U _{FO} -V _{UPc} , V _{FO} -V _{VPc} , W _{FO} -V _{WPc} Fo-V _{Nc}	20	V
I _{FO}	Fault Output Current	Sink current at U _{FO} , V _{FO} , W _{FO} , Fo terminals	20	mA

TOTAL SYSTEM

Symbol	Parameter	Condition	Ratings	Unit
V _{CC(PROT)}	Supply Voltage Protected by SC	V _D = 13.5 ~ 16.5V, Inverter Part, T _J = +125°C Start	800	V
V _{CC(surge)}	Supply Voltage (Surge)	Applied between : P-N, Surge value	1000	V
T _{stg}	Storage Temperature		-40 ~ +125	°C
V _{iso}	Isolation Voltage	60Hz, Sinusoidal, Charged part to Base, AC 1 min.	2500	V _{rms}

THERMAL RESISTANCES

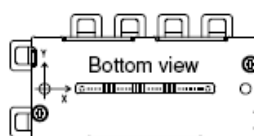
Symbol	Parameter	Condition	Limits			Unit
			Min.	Typ.	Max.	
R _{th(j-c)}	Junction to case Thermal Resistances	Inverter IGBT (per 1 element) (Note-1)	—	—	0.83*	°C/W
R _{th(j-f)}		Inverter FWDi (per 1 element) (Note-1)	—	—	1.36*	
R _{th(j-c)}		Brake IGBT (Note-1)	—	—	0.96*	
R _{th(j-f)}		Brake FWDi (Note-1)	—	—	1.82*	
R _{th(c-f)}	Contact Thermal Resistance	Case to fin, (per 1 module) Thermal grease applied (Note-1)	—	—	0.038	

* If you use this value, R_{th(f-a)} should be measured just under the chips.

(Note-1) T_c (under the chip) measurement point is below.

(Unit : mm)

axis	arm		UP		VP		WP		UN		VN		WN		Br	
	IGBT	FWDi	IGBT	FWDi	IGBT	FWDi	IGBT	FWDi	IGBT	FWDi	IGBT	FWDi	IGBT	FWDi	IGBT	FWDi
X	29.0	29.3	65.0	65.5	85.6	85.9	37.8	37.5	55.2	55.7	75.8	75.3	19.0	22.3		
Y	-7.1	1.5	-7.1	2.0	-7.1	2.0	5.1	-4.5	5.1	-4.5	5.1	-4.5	-7.3	6.6		



ELECTRICAL CHARACTERISTICS ($T_j = 25^\circ\text{C}$, unless otherwise noted)

INVERTER PART

Symbol	Parameter	Condition	Limits			Unit	
			Min.	Typ.	Max.		
$V_{CE(sat)}$	Collector-Emitter Saturation Voltage	$V_D = 15\text{V}$, $I_C = 25\text{A}$ $V_{CIN} = 0\text{V}$ (Fig. 1)	$T_j = 25^\circ\text{C}$	—	1.8	2.3	V
			$T_j = 125^\circ\text{C}$	—	1.9	2.4	
V_{EC}	FWDi Forward Voltage	$-I_C = 25\text{A}$, $V_D = 15\text{V}$, $V_{CIN} = 15\text{V}$ (Fig. 2)	—	2.5	3.5	V	
t_{on}	Switching Time	$V_D = 15\text{V}$, $V_{CIN} = 0\text{V} \leftrightarrow 15\text{V}$ $V_{CC} = 600\text{V}$, $I_C = 25\text{A}$ $T_j = 125^\circ\text{C}$ Inductive Load (Fig. 3,4)	—	0.5	1.0	2.5	μs
t_r			—	—	0.5	0.8	
$t_{c(on)}$			—	—	0.4	1.0	
t_{off}			—	—	2.0	3.0	
$t_{c(off)}$			—	—	0.7	1.2	
I_{CES}	Collector-Emitter Cutoff Current	$V_{CE} = V_{CES}$, $V_{CIN} = 15\text{V}$ (Fig. 5)	$T_j = 25^\circ\text{C}$	—	—	1	mA
			$T_j = 125^\circ\text{C}$	—	—	10	

BRAKE PART

Symbol	Parameter	Condition	Limits			Unit	
			Min.	Typ.	Max.		
$V_{CE(sat)}$	Collector-Emitter Saturation Voltage	$V_D = 15\text{V}$, $I_C = 15\text{A}$ $V_{CIN} = 0\text{V}$ (Fig. 1)	$T_j = 25^\circ\text{C}$	—	1.8	2.3	V
			$T_j = 125^\circ\text{C}$	—	1.9	2.4	
V_{FM}	FWDi Forward Voltage	$I_F = 15\text{A}$ (Fig. 2)	—	2.5	3.5	V	
I_{CES}	Collector-Emitter Cutoff Current	$V_{CE} = V_{CES}$, $V_{CIN} = 15\text{V}$ (Fig. 5)	$T_j = 25^\circ\text{C}$	—	—	1	mA
			$T_j = 125^\circ\text{C}$	—	—	10	

CONTROL PART

Symbol	Parameter	Condition	Limits			Unit	
			Min.	Typ.	Max.		
I _D	Circuit Current	V _D = 15V, V _{CIN} = 15V	V _{N1} -V _{NC}	—	20	30	mA
			V _{P1} -V _{PC}	—	5	10	
V _{IN(ON)}	Input ON Threshold Voltage	Applied between : U _P -V _{UPC} , V _P -V _{VPC} , W _P -V _{WPC} U _N • V _N • W _N • B _r -V _{NC}		1.2	1.5	1.8	V
V _{IN(OFF)}	Input OFF Threshold Voltage			1.7	2.0	2.3	
SC	Short Circuit Trip Level	-20 ≤ T _J ≤ 125°C, V _D = 15V (Fig. 3,6)	Inverter part	50	—	—	A
			Brake part	30	—	—	
t _{off(SC)}	Short Circuit Current Delay Time	V _D = 15V (Fig. 3,6)	—	0.2	—	μs	
OT	Over Temperature Protection	V _D = 15V Detect T _J of IGBT chip	Trip level	135	145	—	°C
			Reset level	—	125	—	
UV	Supply Circuit Under-Voltage Protection	-20 ≤ T _J ≤ 125°C	Trip level	11.5	12.0	12.5	V
			Reset level	—	12.5	—	
I _{FO(H)}	Fault Output Current	V _D = 15V, V _{FO} = 15V (Note-2)		—	—	0.01	mA
				—	10	15	
t _{FO}	Minimum Fault Output Pulse Width	V _D = 15V (Note-2)	1.0	1.8	—	ms	

(Note-2) Fault output is given only when the internal SC, OT & UV protections schemes of either upper or lower arm device operate to protect it.

MECHANICAL RATINGS AND CHARACTERISTICS

Symbol	Parameter	Condition	Limits			Unit
			Min.	Typ.	Max.	
—	Mounting torque	Mounting part screw : M5	2.5	3.0	3.5	N • m
—	Mounting torque	Mounting part screw : M5	2.5	3.0	3.5	N • m
—	Weight	—	—	380	—	g

RECOMMENDED CONDITIONS FOR USE

Symbol	Parameter	Condition	Recommended value	Unit
V _{CC}	Supply Voltage	Applied across P-N terminals	≤ 800	V
V _D	Control Supply Voltage	Applied between : V _{UP1} -V _{UPC} , V _{VP1} -V _{VPC} V _{WP1} -V _{WPC} , V _{N1} -V _{NC} (Note-3)	15.0 ± 1.5	V
V _{CIN(ON)}	Input ON Voltage	Applied between : U _P -V _{UPC} , V _P -V _{VPC} , W _P -V _{WPC} U _N • V _N • W _N • B _r -V _{NC}	≤ 0.8	V
V _{CIN(OFF)}	Input OFF Voltage		≥ 9.0	
f _{PWM}	PWM Input Frequency	Using Application Circuit of Fig. 8	≤ 20	kHz
t _{dead}	Arm Shoot-through Blocking Time	For IPM's each input signals (Fig. 7)	≥ 2.5	μs

(Note-3) With ripple satisfying the following conditions: dv/dt swing ≤ ±5V/μs, Variation ≤ 2V peak to peak

PRECAUTIONS FOR TESTING

- Before applying any control supply voltage (V_D), the input terminals should be pulled up by resistors, etc. to their corresponding supply voltage and each input signal should be kept off state.
After this, the specified ON and OFF level setting for each input signal should be done.
- When performing "SC" tests, the turn-off surge voltage spike at the corresponding protection operation should not be allowed to rise above V_{CES} rating of the device.
(These test should not be done by using a curve tracer or its equivalent.)

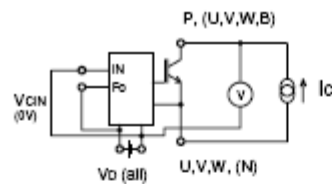


Fig. 1 $V_{CE(sat)}$ Test

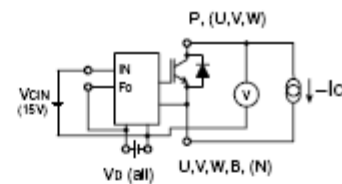
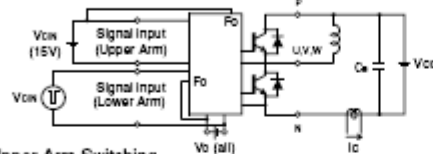


Fig. 2 V_{EC} , (V_{FM}) Test

a) Lower Arm Switching



b) Upper Arm Switching

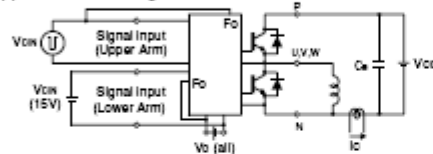


Fig. 3 Switching time and SC test circuit

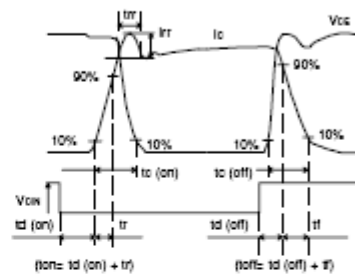


Fig. 4 Switching time test waveform

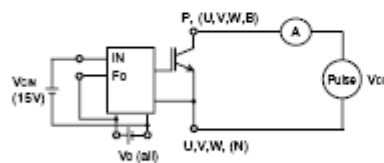


Fig. 5 I_{CES} Test

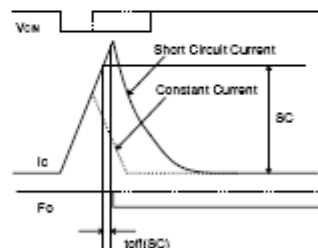
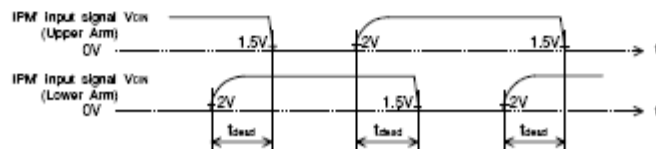


Fig. 6 SC test waveform



1.5V: Input on threshold voltage $V_{th(on)}$ typical value, 2V: Input off threshold voltage $V_{th(off)}$ typical value

Fig. 7 Dead time measurement point example

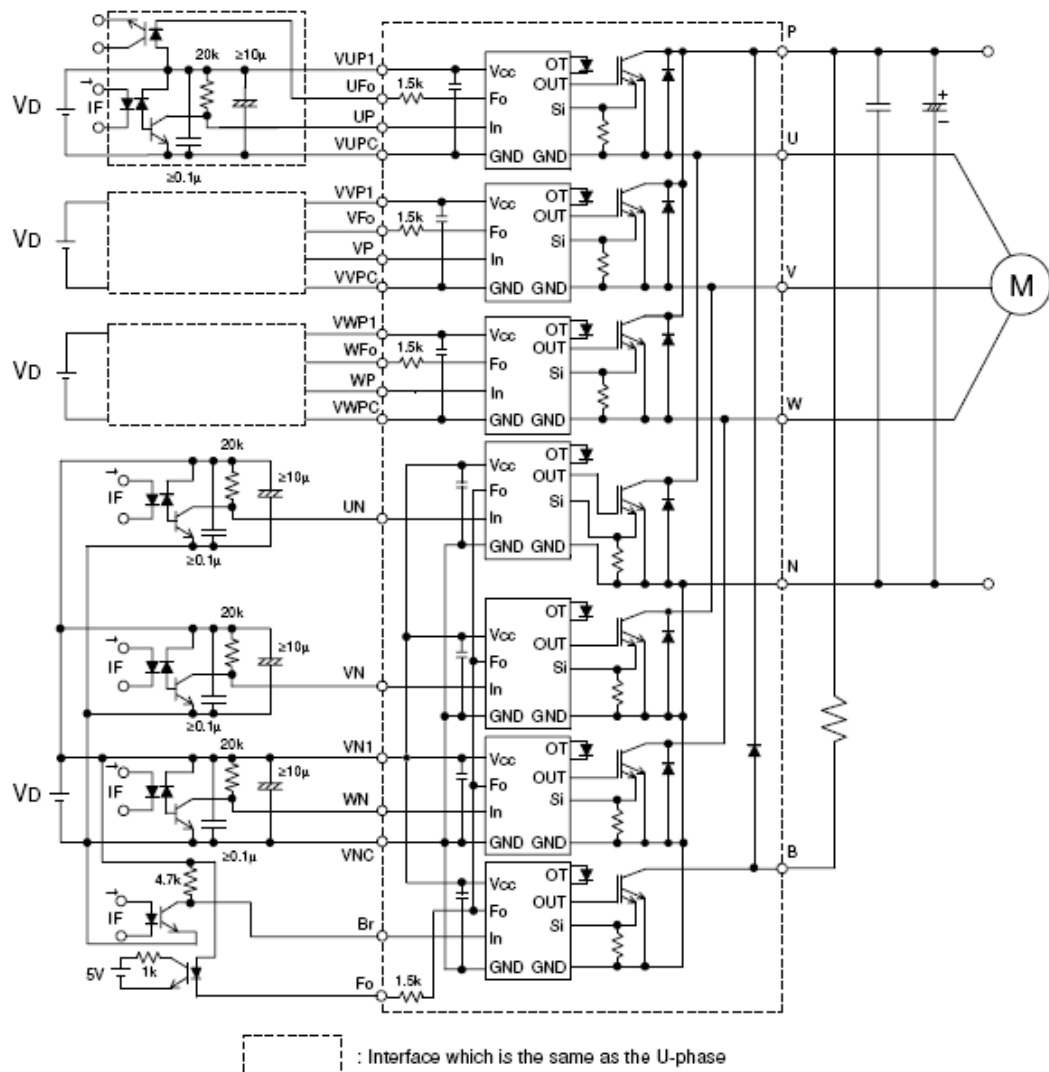
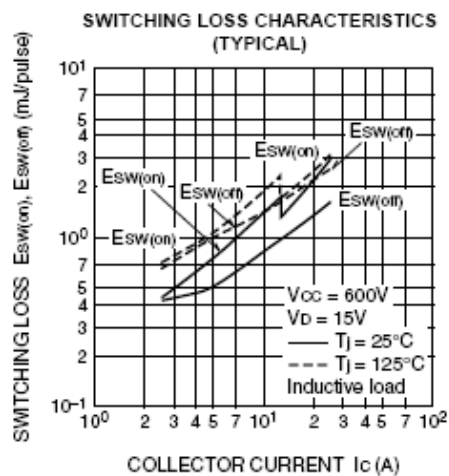
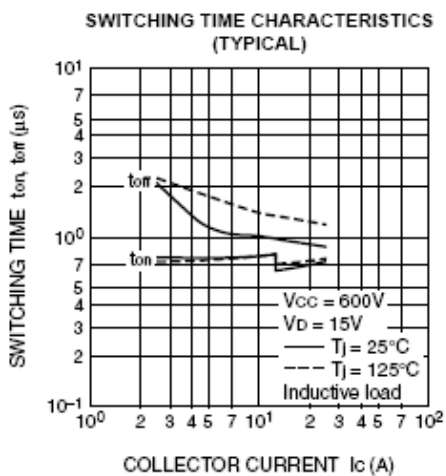
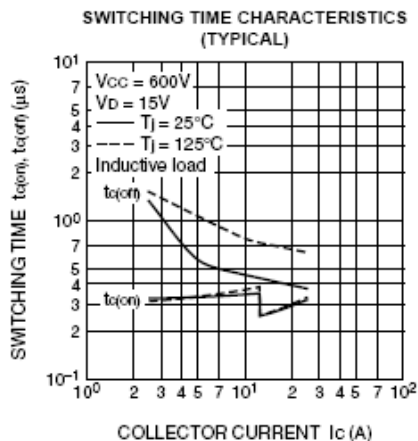
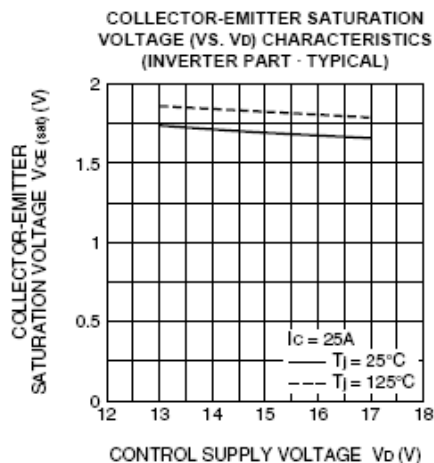
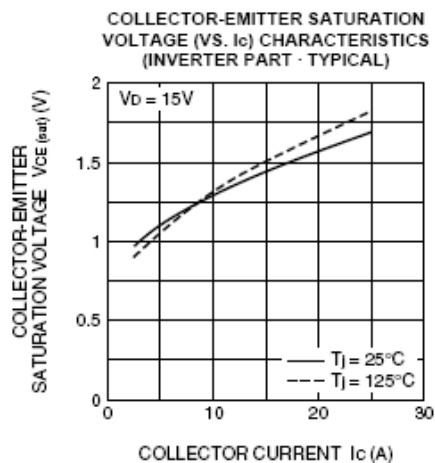
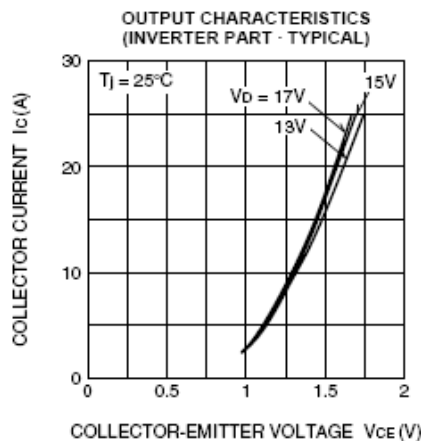


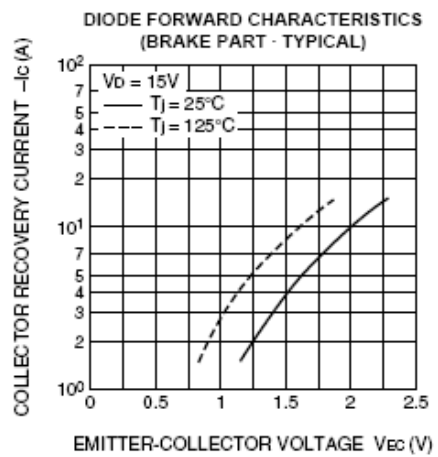
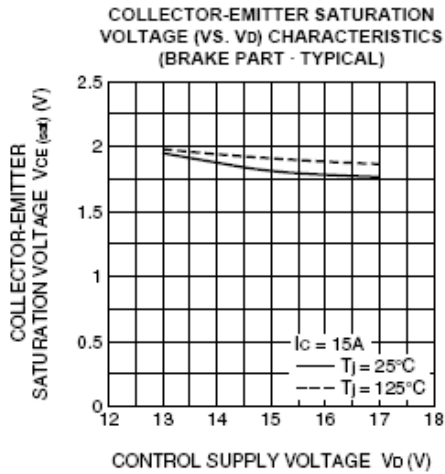
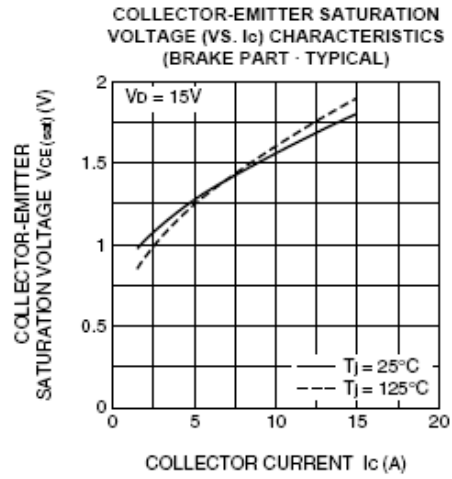
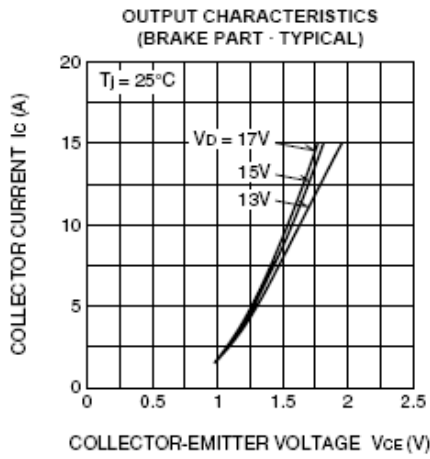
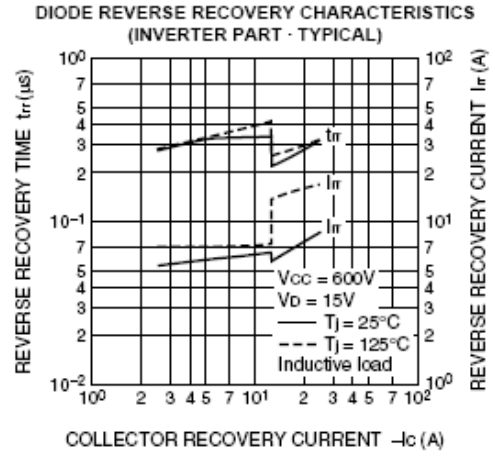
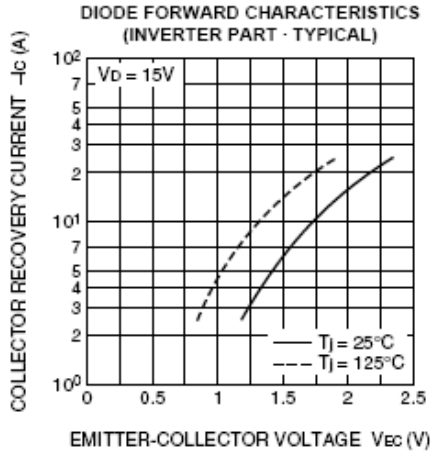
Fig. 8 Application Example Circuit

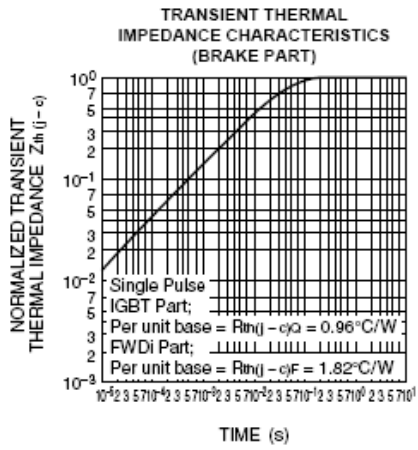
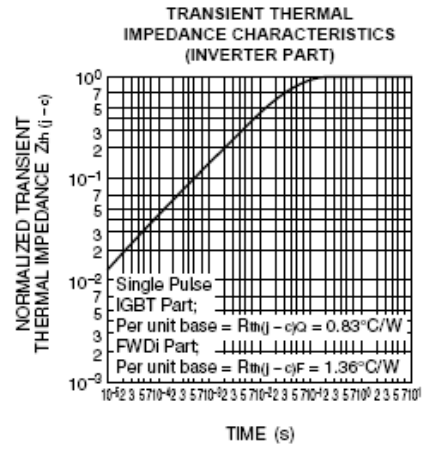
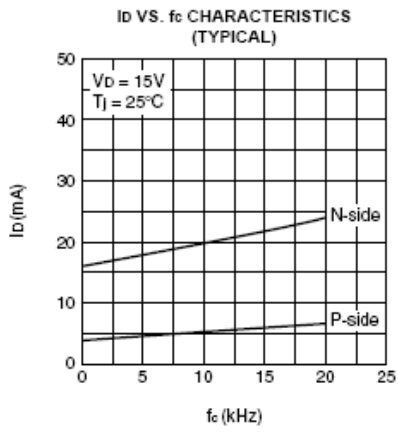
NOTES FOR STABLE AND SAFE OPERATION ;

- Design the PCB pattern to minimize wiring length between opto-coupler and IPM's input terminal, and also to minimize the stray capacity between the input and output wirings of opto-coupler.
- Connect low impedance capacitor between the Vcc and GND terminal of each fast switching opto-coupler.
- Fast switching opto-couplers: $t_{PLH}, t_{PHL} \leq 0.8\mu s$, Use High CMR type.
- Slow switching opto-coupler: $CTR > 100\%$
- Use 4 isolated control power supplies (Vd). Also, care should be taken to minimize the instantaneous voltage charge of the power supply.
- Make inductance of DC bus line as small as possible, and minimize surge voltage using snubber capacitor between P and N terminal.
- Use line noise filter capacitor (ex. 4.7nF) between each input AC line and ground to reject common-mode noise from AC line and improve noise immunity of the system.

PERFORMANCE CURVES







APPENDIX C

PARAMETERS OF TEST MOTORS

C.1. Parameters of Test Motor #1

Parameters of test motor #1 are obtained from conventional methods; no-load test and locked-rotor test. Motor parameters are tabulated in Table C. 1

Table C. 1 - Parameters of test motor #1

Parameters of (1 kW, 2-pole, Y-connected, $I_{s,rated}=2.7$ A, $V_{s,rated}=220$ V_(phase), pf:0.76) Induction machine	
R_s	4,50 ohm
R_r	6,01 ohm
L_{ls}	11,7 mH
L_{lr}	11,7 mH
L_s	386,7 mH (= $L_{ls} + L_m$)
L_r	386,7 mH (= $L_{lr} + L_m$)
L_m	375 mH
τ_r	64,3 msec (= L_r/R_r)
ψ_r	0,9 Wb
σ	$0.0596 (= 1 - \frac{L_m^2}{L_s L_r})$

The rated rotor flux value is found by using the nameplate data of the motor as shown below.

$$E_{lm} = \sqrt{[(V_s \cdot \cos \varphi - R_s I_s)^2 + (V_s \cdot \sin \varphi - w_s \sigma L_s I_s)^2]} \quad (C.1)$$

$$E_{lm} = \sqrt{[(220 \times 0,76 - 4,5 \times 2,7)^2 + (220 \times 0,65 - 314 \times 0,023 \times 2,7)^2]} \cong 198,2V \quad (C.2)$$

$$\psi_r = \frac{E_{lm} \sqrt{2}}{\omega_s} \cong 0,9 \text{ Wb} \quad (\text{C.3})$$

$$I_{sdref} = \frac{\psi_r}{L_m} \cong 2,4 \text{ A} \quad (\text{C.4})$$

C.2. Parameters of Test Motor #2

Similarly, parameters of test motor #2 are obtained from conventional methods; no-load test and locked-rotor test. Motor parameters are tabulated in Table C. 2

Table C. 2 - Parameters of test motor #2

Parameters of (1.1 kW, 6-pole, Y-connected, $I_{s,rated}=3.1 \text{ A}$, $V_{s,rated}=220 \text{ V}_{(phase)}$, pf:0.77) Induction machine	
R_s	6,50 ohm
R_r	7,667 ohm
L_{ls}	29,75 mH
L_{lr}	29,75 mH
L_s	338,55 mH (= $L_{ls}+L_m$)
L_r	338,55 mH (= $L_{lr}+L_m$)
L_m	308,8 mH
τ_r	44,2 msec (= L_r/R_r)
ψ_r	0,77 Wb
σ	$0.168 (= 1 - \frac{L_m^2}{L_s L_r})$

The rated rotor flux value is found by using the nameplate data of the motor as shown below.

$$E_{lm} = \sqrt{[(220 \times 0,77 - 6,5 \times 3,1)^2 + (220 \times 0,64 - 314 \times 0,057 \times 3,1)^2]} \cong 171,9 \text{ V} \quad (\text{C.5})$$

$$\psi_r = \frac{E_{lm} \sqrt{2}}{\omega_s} \cong 0,77 \text{ Wb} \quad (\text{C.6})$$

$$I_{sdref} = \frac{\psi_r}{L_m} \cong 2,5 \text{ A} \quad (\text{C.7})$$

C.3. Parameters of Test Motor #3

Similarly, parameters of test motor #3 are obtained from conventional methods; no-load test and locked-rotor test. Motor parameters are tabulated in Table C. 3

Table C. 3 - Parameters of test motor #3

Parameters of (2.2 kW, 2-pole, Y-connected, $I_{s,rated}=4.8 \text{ A}$, $V_{s,rated}=220 \text{ V}_{(phase)}$, pf:0.89) Induction machine	
R_s	2,65 ohm
R_r	3,065 ohm
L_{ls}	13,14 mH
L_{lr}	13,14 mH
L_s	397,41 mH ($=L_{ls}+L_m$)
L_r	397,41 mH ($=L_{lr}+L_m$)
L_m	384,27 mH
τ_r	129,7 msec ($=L_r/R_r$)
ψ_r	0,87 Wb
σ	$0.065 (=1 - \frac{L_m^2}{L_s L_r})$

The rated rotor flux value is found by using the nameplate data of the motor as shown below.

$$E_{lm} = \sqrt{[(220 \times 0,89 - 2,65 \times 4,8)^2 + (220 \times 0,46 - 314 \times 0,026 \times 4,8)^2]} \cong 193,3 \text{ V} \quad (\text{C.8})$$

$$\psi_r = \frac{E_{lm} \sqrt{2}}{\omega_s} \cong 0,87 Wb \quad (C.9)$$

$$I_{sdref} = \frac{\psi_r}{L_m} \cong 2,26 A \quad (C.10)$$

The variables used in the equations are defined in variables and symbols section.